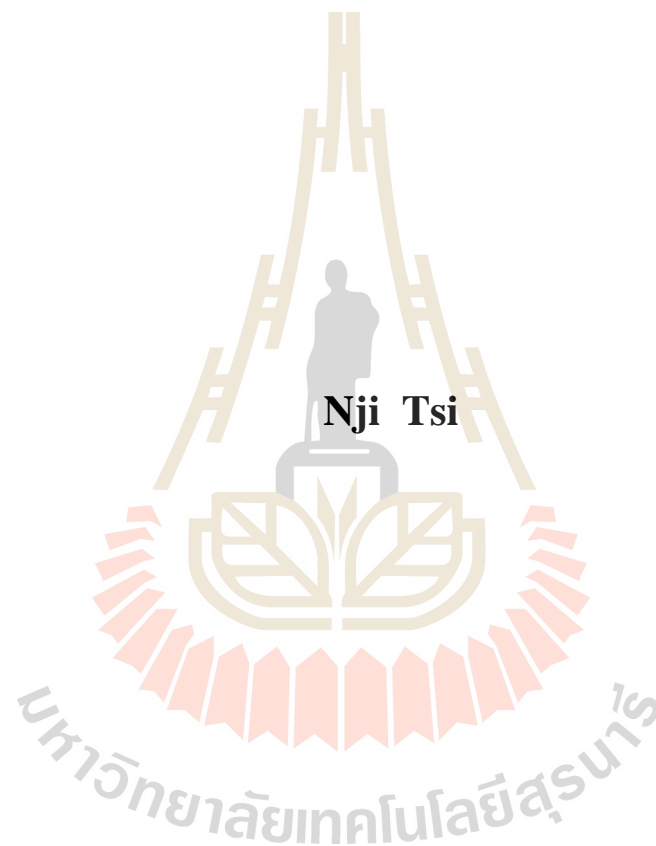


**GOLD NANOPARTICLE EFFECT ON RICE
GERMINATION AND ROOTS**



**A Thesis Submitted in Partial Fulfillment of the Requirement for the
Degree of Master of Science in Environmental Biology
Suranaree University of Technology
Academic Year 2016**

ผลของอนุภาคนาโนของทองคำรองและรากของข้าว



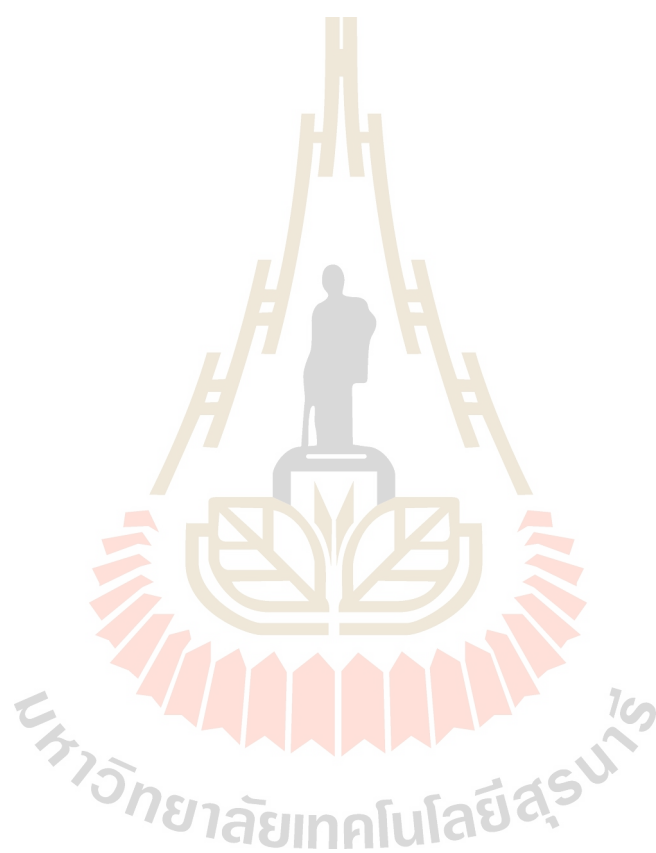
วิทยานิพนธ์นี้เป็นส่วนหนึ่งของการศึกษาตามหลักสูตรปริญญาวิทยาศาสตรมหาบัณฑิต
สาขาวิชาชีววิทยาสังแวดล้อม
มหาวิทยาลัยเทคโนโลยีสุรนารี
ปีการศึกษา 2559

เอ็นจี ที : ผลของอนุภาคนาโนของทองต่อการงอกและรากของข้าว (GOLD
NANOPARTICLE EFFECT ON RICE GERMINATION AND ROOTS)

อาจารย์ที่ปรึกษา : ผู้ช่วยศาสตราจารย์ ดร.ดวงกมล แม้นศิริ, 117 หน้า.

อนุภาคนาโนถูกนำมาประยุกต์ใช้อย่างกว้างขวาง เช่น ทางการแพทย์ เครื่องสำอาง ตลอดจนด้านการเกษตร อนุภาคนาโนของทองเป็นอนุภาคที่มีศักยภาพสำหรับการประยุกต์ใช้ในงานด้านการแพทย์ เทคโนโลยีชีวภาพ และอิเล็กทรอนิกส์ จึงมีความจำเป็นที่ต้องมีการศึกษาเพื่อลดความเสี่ยงที่อาจเกิดขึ้นจากการประยุกต์ใช้ซึ่งเป็นสิ่งที่ควรทำกับเทคโนโลยีที่อยู่ในช่วงของการพัฒนาการสังเคราะห์อนุภาคนาโนโดยใช้สารสกัดจากพืชเป็นทางเลือกที่สอดคล้องกับเป้าหมายในการลดความเสี่ยงดังกล่าว งานวิจัยนี้ทำการศึกษาผลกระทบของอนุภาคนาโนของทองต่อรากของต้นอ่อนที่ความเข้มข้นต่าง ๆ รวมถึงความเป็นพิษต่อพืช ในการศึกษาได้ใช้สารสกัดจาก *Tiliacora triandra* ในการสังเคราะห์อนุภาคนาโนของทองจากสารละลายโกลด์เตตราคลอไรด์ จากนั้นทำการศึกษาคุณสมบัติของอนุภาคนาโนที่ได้จากกระบวนการนี้ โดยใช้กล้องจุลทรรศน์อิเล็กตรอนแบบส่องผ่าน การเลี้ยวเบนรังสีเอ็กซ์ เทคนิคอัลตราไวโอเลตและวิซิเบิลสเปกโทรสโกปี และฟูเรียร์ทรานสฟอร์มอินฟราเรดสเปกโทรสโกปี ทำการเพาะเมล็ดข้าวในอนุภาคนาโนที่สังเคราะห์ได้ที่มีความเข้มข้นต่าง ๆ (0 10 100 500 1000 2000 มิลลิกรัมต่อลิตร) เป็นเวลา 7 วัน ประเมินผลกระทบของอนุภาคนาโนต่อการงอกและรากของข้าวโดยการติดตามการงอก การวัดการตายของเซลล์ การวัดความเป็นพิษต่อพืช การวัดระดับเมลอนไดอัลดีไฮด์ และระดับไฮโดรเจนเปอร์ออกไซด์ในเนื้อเยื่อ พบว่า ข้าวในชุดทดลองมีอัตราการงอกที่สูง (95-98.38%) ถึงแม้จะพบว่ามีความยาวรากและยอดต่ำกว่ากลุ่มควบคุมเล็กน้อย ผลการศึกษาระดับความเป็นพิษต่อพืชแสดงให้เห็นว่าอนุภาคนาโนของทองที่สังเคราะห์โดยใช้สารสกัดจาก *T. triandra* ไม่แสดงความเป็นพิษต่อข้าว พบการตายของเซลล์ที่รากเพิ่มขึ้น ปริมาณไฮโดรเจนเปอร์ออกไซด์ และปริมาณเมลอนไดอัลดีไฮด์เพิ่มขึ้นเมื่อเทียบกับกลุ่มควบคุม อย่างไรก็ตาม ความแตกต่างนี้ไม่มีนัยสำคัญทางสถิติ ($p \leq 0.05$) การทดลองทั้งหมดในการศึกษานี้แสดงให้เห็นอย่างชัดเจนว่า อนุภาคนาโนของทองที่สังเคราะห์โดยใช้สารสกัดจาก *T. triandra* ไม่

เป็นพืชต่อเมล็ดข้าว และผลการทดลองยังแสดงให้เห็นว่าอนุภาคทองคำยังมีความปลอดภัยต่อ
สิ่งแวดล้อม



สาขาวิชาชีววิทยา

ปีการศึกษา 2559

ลายมือชื่อนักศึกษา _____

ลายมือชื่ออาจารย์ที่ปรึกษา _____

NJI TSI : GOLD NANOPARTICLE EFFECT ON RICE GERMINATION AND
ROOTS. THESIS ADVISOR : ASST. PROF. DUANGKAMOL MAENSIRI,
Ph.D. 117 PP.

PHYTOTOXICITY/ PLANT-MEDIATED NANOPARTICLE SYNTHESIS/
TILIACORA TRIANDRA

Nanoparticles are now widely used in a range of applications and in fields such as medicine, cosmetics and in agriculture. Gold nanoparticles, for example, have potential applications in medicine, biotechnology and electronics. Like with every growing technology, there is the need to invest in efforts to cut back associated risk. Plant-mediated synthesis as an alternative, aligns with such a goal. This research seeks to monitor the effect of gold nanoparticles, on the roots of rice seedlings at various concentrations as well as its phytotoxicity. In this study, plant leaf extracts of *Tiliacora triandra* were used to synthesized gold nanoparticles from an aqueous mixture of gold tetrachloride. The nanoparticles particles obtained from this process were characterized by use of transmission electron microscope, X-ray diffraction, UV-vis spectrophotometer and Fourier Transform infrared spectroscopy. The rice grains were exposed to the biosynthesized nanoparticles at different concentration (0, 10, 100, 500, 1000, 2000 mg/L) for a period of seven days. The effects of these nanoparticles on rice germination and roots were assessed by several experiments such as germination measurements, cell death evaluations, phytotoxicity, the extent of the effect of incubation and soaking on root length, Malondialdehyde (MDA) and hydrogen peroxide (H₂O₂) tissue levels. Germination percentages were high (95 to 98.38%), though a slight decrease in root and

shoot lengths relative to the control was observed. Phytotoxicity results proved that *T. triandra* synthesized gold nanoparticles were of minimal toxicity to rice seedlings. Incubation was found to hamper root elongation more than soaking. Increases in root cell mortality, hydrogen peroxide and MDA amounts in root and shoot tissues with respect to the control were observed. These increases were not statistically significant ($p \leq 0.05$). All experiments conducted in this research proves beyond reasonable doubt that *T. triandra* synthesized gold nanoparticles are non-toxic to rice grains. This study suggest that the nanoparticles synthesized are environmentally benign.



School of Biology

Student's Signature _____

Academic Year 2016

Advisor's Signature _____

GOLD NANOPARTICLE EFFECT ON RICE GERMINATION AND ROOTS

Suranaree University of Technology has approved this thesis submitted in partial fulfillment of the requirements for the Master's Degree.

Thesis Examining Committee

(Dr. Pongrit Krubphachaya)

Chairperson

(Asst. Prof. Dr. Duangkamol Maensiri)

Member (Thesis Advisor)

(Prof. Dr. Santi Maensiri)

Member

(Asst. Prof. Dr. Thitiporn Machikowa)

Member

(Prof. Dr. Sukit Limpijumnong)

Vice Rector for Academic Affairs
and Innovation

(Prof. Dr. Santi Maensiri)

Dean of Institute of Science

AKNOWLEDGEMENTS

I would like to express my sincere gratitude and profound appreciation to my advisor, Assistant Professor Dr. Duangkamol Maensiri for her guidance on numerous fronts ranging from her scientific input through guidance to financial support during my study. Our numerous interactions over the years certainly expanded my understanding of life principles with applications that stretch beyond the academic world.

I do extend my gratitude to Professor Santi Maensiri for guiding me through the unknown academic waters of material science. I should have been totally lost at sea had it not been for his wealth of knowledge and willingness to share it in a domain I was totally clueless about.

Heartfelt thanks equally goes to Dr. Pongrit Krubphachaya and Assistant Professor Dr. Thitiporn Machikowa for thoroughly going through this piece of work on such a short notice. Their invaluable tips are very much appreciated.

I would like to also thank all lecturers in the School of Biology and the technical staff of F10 and F2 for giving me access to their knowledge and immense experience. Special thanks equally goes to the members of our lab group and to that of Advance Material Physics. They were ever ready and patient in spite of the occasional language barrier to put me through countless academic related problems and other issues that made my life and stay here much comfortable.

Finally, I would like to thank my parents, siblings, extended family and friends for their love and care, heartfelt prayers and encouragement.

Nji Tsi

CONTENTS

	Page
ABSTRACT IN THAI	I
ABSTRACT IN IN ENGLISH	III
ACKNOWLEDGEMNTS	V
CONTENTS.....	VI
LIST OF TABLES.....	X
LIST OF FIGURES	XI
LIST OF ABBREVITONS AND SYMBOLS	XV
CHAPTER	
I INTRODUCTION.....	1
1.1 Background/Problem	1
1.2 Research objectives	3
1.3 Research hypothesis	3
1.5 Scope and limitations of the study	3
1.6 Expected results	4
II LITERATURE REVIEW	5
2.1 Nanomaterial importance and application	5
2.2 Green synthesis of metal based nanoparticles	6
2.3 Green synthesis of gold nanoparticles using plants	9
2.4 Morphology and importance of the rice plant	12
2.5 The process of germination	14

CONTENTS (Continued)

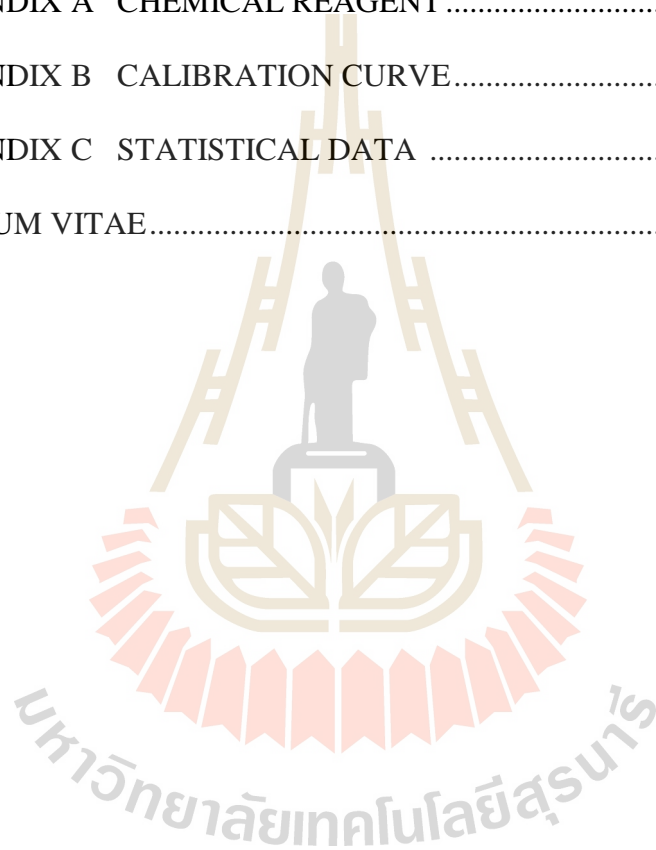
	Page
2.6 Plant root morphology and mechanism of root uptake	17
2.7 Metal nanoparticle effect on germination and uptake	20
2.8 Relationship between plant stress and hydrogen peroxide	23
2.9 The future of nanotechnology and Agriculture	24
III MATERIALS AND METHODS	27
3.1 Synthesis of gold nanoparticles	27
3.1.1 <i>Tiliacora triandra</i> leaf extract aided synthesis	27
3.1.2 Synthesis of gold nanoparticles with gelatin and gelatin-glucose mixtures	28
3.2 Gold nanoparticle characterization	29
3.2.1 Transmission electron microscope	29
3.2.2 UV-vis spectroscopy	29
3.2.3 X-ray diffraction analysis	30
3.2.3 FTIR spectroscopy	30
3.3 Gold nanoparticle effect on rice	31
3.3.1 Seed preparation, germination and root development	31
3.3.2 Determination of germinated seedling relative water content	32
3.3.3 Cell death evaluation	33
3.3.4 Determination of the effects of seed soaking and incubation on root elongation	33
3.3.5 Hydrogen peroxide and Lipid peroxidation estimation	34
3.3.6 Statistical analysis	35

CONTENTS (Continued)

	Page
IV RESULTS AND DISCUSSION	36
4.1 Characterization of gold nanoparticles synthesized from <i>T. triandra</i>	36
4.1.1 TEM studies for <i>T. triandra</i> synthesis of AuNP	36
4.1.2 XRD patterns of gold nanoparticles synthesized with plant extract	47
4.1.3 FTIR spectra for <i>T. triandra</i> extract mediated synthesis	50
4.1.4 UV-vis spectroscopy for <i>T. triandra</i> synthesized gold nanoparticles	52
4.2 Characterization of gold nanoparticles synthesized from gelatin/glucose-gelatin mixture	57
4.2.1 TEM studies for gelatin/gelatin-glucose synthesis of AuNPs	57
4.2.2 FTIR spectra for gelatin/gelatin-glucose synthesized AuNP	62
4.2.3 UV-vis spectroscopy for gelatin/gelatin-glucose synthesized AuNP	64
4.3 Possible mechanism for gold nanoparticle formation	66
4.4 Gold nanoparticle effect on rice seedlings	68
4.4.1 Determination of germinated seedling water content	74
4.4.2 Cell death evaluation	75
4.4.3 Determination of the effects of seed soaking and incubation on root elongation	76
4.4.4 Uptake of gold nanoparticles by seedling roots	79
4.4.5 Hydrogen peroxide and lipid peroxide estimation	82

CONTENTS (Continued)

	Page
IV CONCLUSION	89
REFERENCES	92
APPENDICES	107
APPENDIX A CHEMICAL REAGENT	108
APPENDIX B CALIBRATION CURVE	110
APPENDIX C STATISTICAL DATA	112
CURRICULUM VITAE	117

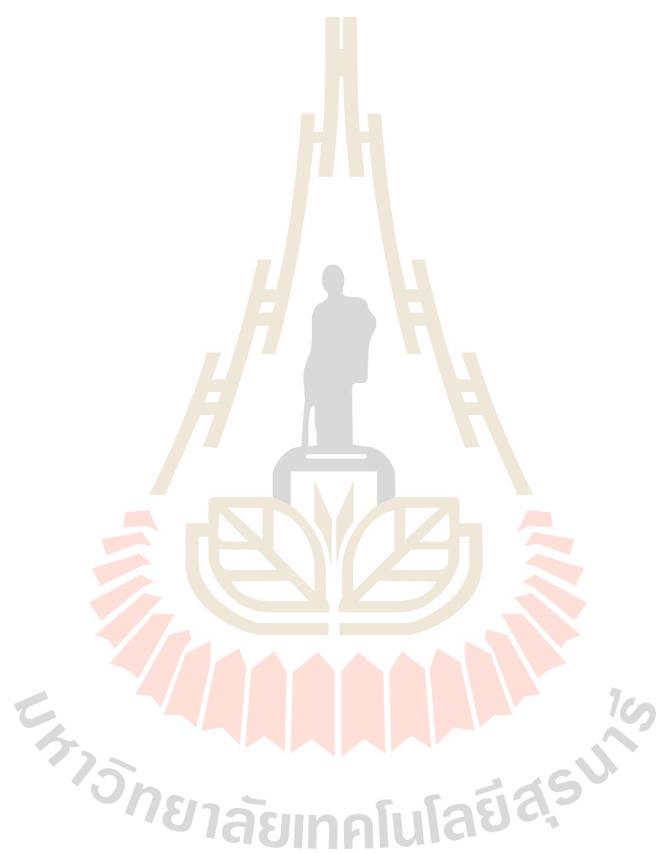


LIST OF TABLES

Table	Page
4.1 Average TEM size of gold nanoparticles synthesized under different conditions.....	46
4.2 Lattice parameter and crystallite size of gold nanoparticles synthesized under different conditions	49
4.3 Average TEM size of gold nanoparticles synthesized from gelatin/gelatin-glucose mixtures at different temperatures	62
4.4 Values are means \pm SD (n=3) of germination percentage, relative root elongation, root length and shoot length of rice seedlings at different concentrations of gold nanoparticles. Mean with the same letter are not significantly different at Tukey's test ($p \leq 0.05$)	73
4.5 Values are means \pm SD (n=3) of hydrogen peroxide and MDA amounts in root and shoot tissue of rice seedlings exposed to different concentrations of gold nanoparticles. H_2O_2 amounts in $\mu\text{g/mL}$ corresponds to absorbance amount in graphs. Mean with the same letter are not significantly different at Tukey's test ($p \leq 0.05$)	88
B.1 Preparation of hydrogen peroxide standards	110
C.1 Relative water content of rice seedlings exposed to gold nanoparticles at different concentrations.....	114
C.2 Cell viability of rice root grains exposed to gold nanoparticles at different concentrations expressed in terms of absorbance ratio.....	115

LIST OF TABLES (Continued)

Table	Page
C.3 Cell viability of rice root grains exposed to gold nanoparticles at concentration of 2000 mg/L under different treatment conditions	116



LIST OF FIGURES

Figure	Page
2.1 Generalized flowchart for nanoparticle syntheses approach with emphasis on nanobiosynthesis	8
2.2 TEM images of gold nanoparticles of varying shapes synthesized using Magnolia leaf broth at temperatures of (A) 25°C (B) 60°C (C) 95°C	12
2.3 Characteristics of rice (<i>O. sativa</i>)	14
2.4 Parts of a germinating rice seedling	17
2.5 Plant root structure	18
2.6 Depiction of pathways of water/substance uptake in plant roots	20
4.1 Size distribution histogram at ambient temperatures	39
4.2 Size distribution histogram of AuNP synthesized at 65°C	39
4.3 Size distribution histogram of AuNP synthesized at 80°C	40
4.4 Size distribution histogram of AuNP synthesized with 50% plant extract	40
4.5 Size distribution histogram of AuNP synthesized with 80% of plant extract.....	41
4.6 Size distribution histogram of AuNP synthesized with 6 mL of plant extract	41
4.7 Size distribution histogram of AuNP synthesized with 8 mL of plant extract.....	42

LIST OF FIGURES (Continued)

Figure	Page
4.8	TEM images of AuNPs of varying shapes synthesized using <i>T. triandra</i> leaf extracts at temperatures of (A) 25°C (B) 65°C (C) 80°C 43
4.9	TEM images of AuNPs of varying shapes synthesized using <i>T. triandra</i> leaf extract concentrations of (A) 50% (B) 80% (C) 100% 44
4.10	TEM images of AuNPs of varying shapes synthesized using <i>T. triandra</i> leaf extract volumes of (A) 6 mL (B) 8 mL (C) 10 mL 45
4.11	SAED pattern of <i>T. triandra</i> synthesized AuNP 46
4.12	XRD patterns at different temperatures of synthesis 48
4.13	XRD patterns at different plant extract concentration 48
4.14	XRD patterns at different plant extract volumes 49
4.15	FTIR spectrum of pure leaf extract of <i>T. triandra</i> and reduced AuNPs 52
4.16	Colour variation of <i>T. triandra</i> synthesized gold nanoparticle solutions at (a) ambient temperature (b) 65°C and (c) 80°C..... 53
4.17	UV-vis spectra of <i>T. triandra</i> synthesized AuNPs at different temperatures .. 54
4.18	UV-vis spectra of <i>T. triandra</i> synthesized AuNPs at different plant concentrations 55
4.19	UV-vis spectra of <i>T. triandra</i> synthesized AuNPs at different volumes of plant extracts 56
4.20	TEM images of AuNPs of varying shapes synthesized using gelatin-glucose (GGR) solution at temperatures of (A) 28°C (B) 40°C (C) 60°C 59

LIST OF FIGURES (Continued)

Figure	Page
4.21	TEM images of AuNPs of varying shapes synthesized using gelatin (GR) solution at temperatures of (A) 28°C (B) 40°C (C) 60°C..... 60
4.22	Size distribution histogram of gelatin-glucose synthesized AuNP at 28°C..... 61
4.23	Size distribution histogram of gelatin synthesized AuNP at 60°C 61
4.24	FTIR spectrum of gelatin reduced (GR) AuNPs at 40°C..... 63
4.25	FTIR spectrum of gelatin-glucose reduced (GGR) AuNPs at 60°C 63
4.26	Colour variation of gelatin/gelatin-glucose synthesized AuNP solutions at temperatures of (a) 28°C (b) 40°C (c) 60°C..... 64
4.27	UV-vis spectra of gelatin/gelatin-glucose synthesized AuNPs..... 65
4.28	Schematic representation of possible mechanism of AuNP synthesis..... 67
4.29	pH values of nano-gold suspensions at different concentrations..... 69
4.30	Seedling root length upon exposure to AuNPs..... 70
4.31	Untreated and treated rice seedlings after seven days of germination..... 70
4.32	Seedling shoot length upon exposure to gold nanoparticles (AuNP) 71
4.33	Percentage germination of AuNP treated seedlings..... 72
4.34	Relative root elongation of AuNP treated seedlings..... 73
4.35	Relative water content of AuNP treated seedlings 75
4.36	Cell viability extent following AuNP treatment 76
4.37	Seed soaking/incubation and phytotoxicity test on rice seedlings (A, B and C represents treatments I, II and III, respectively) 78
4.38	Cell viability of roots of seedlings subjected to soaking/incubation and phytotoxicity treatments..... 79

LIST OF FIGURES (Continued)

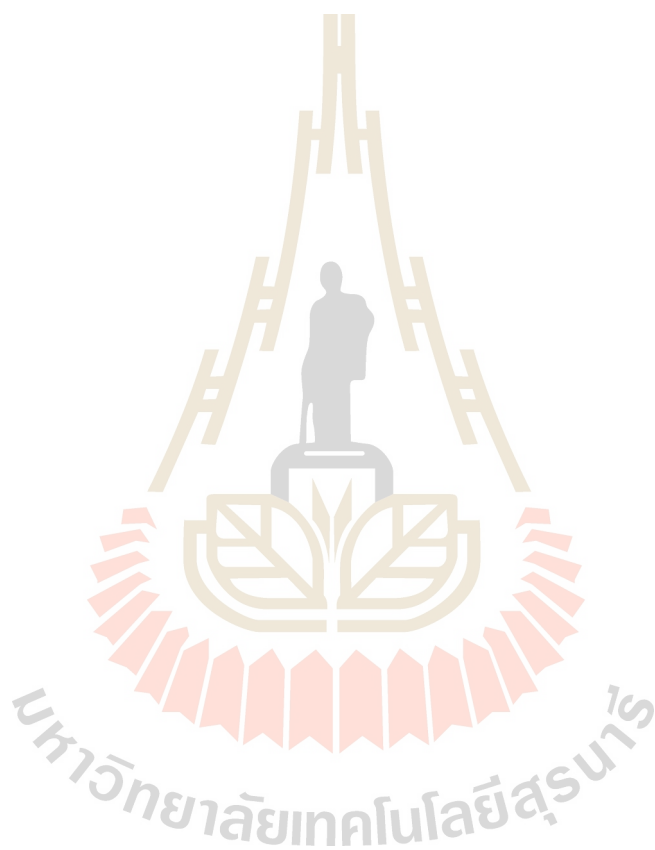
Figure	Page
4.39 Micrograph of (a) Untreated root tissue (x2000) (b) treated root tissue (x2000) (c) treated root tissue (x4000)	81
4.40 Hydrogen peroxide amount in root tissue of seedlings.....	84
4.41 Hydrogen peroxide amount in shoot tissue of seedlings	84
4.42 MDA content in seedling roots exposed to AuNPs	87
4.43 MDA content in seedling shoots exposed to AuNPs.....	87
B.2 Standard curve of hydrogen peroxide content	111
C.1 Size distribution histogram of gelatin-glucose synthesized AuNP at 60°C...	112
C.2 Size distribution histogram of gelatin synthesized AuNP at 40°C	112
C.3 Size distribution histogram of gelatin-glucose synthesized AuNP at 40°C...	113
C.4 Size distribution histogram of gelatin synthesized AuNP at 28°C	113

LIST OF ABBREVIATIONS AND SYMBOLS

%	Percentage
Å	Angstroms
AuNPs	Gold nanoparticles
°C	Degree Celsius
cm	Centimeter
DW	Dry Weight
FTIR	Fourier transforms infra-red
FW	Fresh weight
g	gram
H ₂ O ₂	Hydrogen Peroxide
L	Litre
M	Molar
MDA	Malondialdehyde
mg	Milligram
ml	millilitre
mm	millimeter
nm	nanometer
RRE	relative root elongation
TBA	Thiobarbituric acid
TCA	Trichloroacetic acid
TEM	Transmission electron microscope

LIST OF ABBREVIATIONS AND SYMBOLS (Continued)

TW	turgid weight
XRD	X-ray diffraction



CURRICULUM VITAE

NAME Nji Tsi

DATE OF BIRTH June 27, 1989

PLACE OF BIRTH Bamenda

EDUCATION 2016 M.Sc. in Environmental Biology, School of Biology, Institute of Science, Suranaree University of Technology, Nakhon Ratchasima, Thailand

2011 B.Sc. in Microbiology, Department of Biochemistry and Microbiology, Faculty of Science, University of Buea, Cameroon

PUBLICATION --

มหาวิทยาลัยเทคโนโลยีสุรนารี

GOLD NANOPARTICLE EFFECT ON RICE GERMINATION AND ROOTS

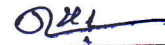
Suranaree University of Technology has approved this thesis submitted in partial fulfillment of the requirements for the Master's Degree.

Thesis Examining Committee



(Dr. Pongrit Krubphachaya)

Chairperson



(Asst. Prof. Dr. Duangkamol Maensiri)

Member (Thesis Advisor)



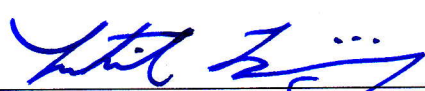
(Prof. Dr. Santi Maensiri)

Member



(Asst. Prof. Dr. Thitiporn Machikowa)

Member



(Prof. Dr. Sukit Limpijunanon)

Vice Rector for Academic Affairs
and Innovation



(Prof. Dr. Santi Maensiri)

Dean of Institute of Science

เอ็นจี ที : ผลของอนุภาคนาโนของทองต่อการงอกและรากของข้าว (GOLD
NANOPARTICLE EFFECT ON RICE GERMINATION AND ROOTS)

อาจารย์ที่ปรึกษา : ผู้ช่วยศาสตราจารย์ ดร.ดวงกมล แม่นศิริ, 117 หน้า.

อนุภาคนาโนถูกนำมาประยุกต์ใช้อย่างกว้างขวาง เช่น ทางการแพทย์ เครื่องสำอาง ตลอดจนด้านการเกษตร อนุภาคนาโนของทองเป็นอนุภาคที่มีศักยภาพสำหรับการประยุกต์ใช้ในงานด้านการแพทย์ เทคโนโลยีชีวภาพ และอิเล็กทรอนิกส์ จึงมีความจำเป็นที่ต้องมีการศึกษาเพื่อลดความเสี่ยงที่อาจเกิดขึ้นจากการประยุกต์ใช้ซึ่งเป็นสิ่งที่ควรทำกับเทคโนโลยีที่อยู่ในช่วงของการพัฒนาการสังเคราะห์อนุภาคนาโนโดยใช้สารสกัดจากพืชเป็นทางเลือกที่สอดคล้องกับเป้าหมายในการลดความเสี่ยงดังกล่าว งานวิจัยนี้ทำการศึกษาผลกระทบของอนุภาคนาโนของทองต่อรากของต้นอ่อนที่ความเข้มข้นต่าง ๆ รวมถึงความเป็นพิษต่อพืช ในการศึกษาได้ใช้สารสกัดจาก *Tiliacora triandra* ในการสังเคราะห์อนุภาคนาโนของทองจากสารละลายโกลด์เตตราคลอไรด์ จากนั้นทำการศึกษาคุณสมบัติของอนุภาคนาโนที่ได้จากกระบวนการนี้โดยใช้กล้องจุลทรรศน์อิเล็กตรอนแบบส่องผ่าน การเบี่ยงเบนรังสีเอ็กซ์ เทคนิคอัลตราไวโอเลตและวิซิเบิลสเปกโทรสโกปี และฟูเรียร์ทรานสฟอร์มอินฟราเรดสเปกโทรสโกปี ทำการเพาะเมล็ดข้าวในอนุภาคนาโนที่สังเคราะห์ได้ที่ความเข้มข้นต่าง ๆ (0 10 100 500 1000 2000 มิลลิกรัมต่อลิตร) เป็นเวลา 7 วัน ประเมินผลกระทบของอนุภาคนาโนต่อการงอกและรากของข้าวโดยการติดตามการงอก การวัดการตายของเซลล์ การวัดความเป็นพิษต่อพืช การวัดระดับเมลอนไดออกไซด์ และระดับไฮโดรเจนเปอร์ออกไซด์ในเนื้อเยื่อ พบว่า ข้าวในชุดทดลองมีอัตราการงอกที่สูง (95-98.38%) ถึงแม้จะพบว่ามีความยาวรากและยอดต่ำกว่ากลุ่มควบคุมเล็กน้อย ผลการศึกษาระดับความเป็นพิษต่อพืชแสดงให้เห็นว่าอนุภาคนาโนของทองที่สังเคราะห์โดยใช้สารสกัดจาก *T. triandra* ไม่แสดงความเป็นพิษต่อข้าว พบการตายของเซลล์ที่รากเพิ่มขึ้น ปริมาณไฮโดรเจนเปอร์ออกไซด์ และปริมาณเมลอนไดออกไซด์เพิ่มขึ้นเมื่อเทียบกับกลุ่มควบคุม อย่างไรก็ตามความแตกต่างนี้ไม่มีนัยสำคัญทางสถิติ ($p \leq 0.05$) การทดลองทั้งหมดในการศึกษานี้แสดงให้เห็นอย่างชัดเจนว่า อนุภาคนาโนของทองที่สังเคราะห์โดยใช้สารสกัดจาก *T. triandra* ไม่

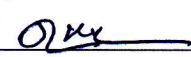
เป็นพืชต่อเมล็ดข้าว และผลการทดลองยังแสดงให้เห็นว่าอนุภาคทองคำยังมีความปลอดภัยต่อ
สิ่งแวดล้อม



สาขาวิชาชีววิทยา

ปีการศึกษา 2559

ลายมือชื่อนักศึกษา 

ลายมือชื่ออาจารย์ที่ปรึกษา 

NJI TSI : GOLD NANOPARTICLE EFFECT ON RICE GERMINATION AND
ROOTS. THESIS ADVISOR : ASST. PROF. DUANGKAMOL MAENSIRI,
Ph.D. 117 PP.

PHYTOTOXICITY/ PLANT-MEDIATED NANOPARTICLE SYNTHESIS/

TILIACORA TRIANDRA

Nanoparticles are now widely used in a range of applications and in fields such as medicine, cosmetics and in agriculture. Gold nanoparticles, for example, have potential applications in medicine, biotechnology and electronics. Like with every growing technology, there is the need to invest in efforts to cut back associated risk. Plant-mediated synthesis as an alternative, aligns with such a goal. This research seeks to monitor the effect of gold nanoparticles, on the roots of rice seedlings at various concentrations as well as its phytotoxicity. In this study, plant leaf extracts of *Tiliacora triandra* were used to synthesized gold nanoparticles from an aqueous mixture of gold tetrachloride. The nanoparticles particles obtained from this process were characterized by use of transmission electron microscope, X-ray diffraction, UV-vis spectrophotometer and Fourier Transform infrared spectroscopy. The rice grains were exposed to the biosynthesized nanoparticles at different concentration (0, 10, 100, 500, 1000, 2000 mg/L) for a period of seven days. The effects of these nanoparticles on rice germination and roots were assessed by several experiments such as germination measurements, cell death evaluations, phytotoxicity, the extent of the effect of incubation and soaking on root length, Malondialdehyde (MDA) and hydrogen peroxide (H₂O₂) tissue levels. Germination percentages were high (95 to 98.38%), though a slight decrease in root and

shoot lengths relative to the control was observed. Phytotoxicity results proved that *T. triandra* synthesized gold nanoparticles were of minimal toxicity to rice seedlings. Incubation was found to hamper root elongation more than soaking. Increases in root cell mortality, hydrogen peroxide and MDA amounts in root and shoot tissues with respect to the control were observed. These increases were not statistically significant ($p \leq 0.05$). All experiments conducted in this research proves beyond reasonable doubt that *T. triandra* synthesized gold nanoparticles are non-toxic to rice grains. This study suggest that the nanoparticles synthesized are environmentally benign.



School of Biology

Academic Year 2016

Student's Signature _____

Advisor's Signature _____

CHAPTER I

INTRODUCTION

1.1 Background/Problem

The term nanotechnology refers to the ‘ability to observe, measure, manipulate, and manufacture things at the nanometer scale’ (Mongillo, 2007). The emergence of nanotechnology is linked to its potential to be used in diverse fields and applications to complement or enhance their current status quo. The implication of the rise of nanotechnology is, more manufacturing will be able to be accomplished on a nanoscale (Logeswari *et al.*, 2015). Given the diverse nature of our subject, this discussion will be primarily centered on metal nanoparticles.

Though a number of physicochemical methods abound in the synthesis of nanoparticles, there is a growing disposition towards approaching synthesis by methods that environmentally benign. An added appeal to nanoparticles manufactured under such circumstances is that being contamination free, they make good candidates for medical applications (Mittal *et al.*, 2013). The biosynthetic method carries within it such dividends. The biosynthetic method puts to use microorganisms such as bacteria and fungi or plant extracts. As far as the use of plants go in synthesis, whole plants, plant tissue, fruits and marine algae have been used in the production of nanoparticles (Luangpipat *et al.*, 2011, Basavegowda *et al.*, 2013). For synthesis to be successful, the corresponding metal salt of the nanoparticle in question is needed in

the biosynthetic process. Typically, the process of synthesis commences when aqueous plant extract reacts with the aqueous solution of the suitable metal salt. Copper, lead, palladium, platinum, silver and gold are examples of metals whose nanoparticles have been successfully synthesized with the use of plant extracts. A lot more publications are available on gold and silver nanoparticle synthesis owing to their status as noble metals. This follows from their application in sensors, detectors and as antibacterial agents. The ancient healing science of Ayurveda utilized gold in some of its treatment (Swarna Bhasma) on a nano-level to treat tuberculosis, anemia and cough (Isaac *et al.*, 2013). The potential of gold nanoparticles' in a modern context vis-à-vis the health sciences and other domains cannot be dismissed.

Tiliacora triandra is a flowering plant native to Southeast Asia. It is known locally as *Yanang* in Thailand. It is used in the cuisines of Northeast Thailand, Laos, Cambodia and Vietnam. *T. triandra* is known to contain Vitamin A, beta-carotene, minerals such as calcium and iron, phosphorus, polyphenols, flavonoids and alkaloids. The leaves of this plants have been demonstrated to be rich in condensed tanins, triterpenes, flavonoids and saponins (Kaewpiboo *et al.*, 2014). The use of this plant is not solely limited to culinary purposes. In traditional Southeast Asian medicine, it is used to reduce pain, fever, reduce sugar levels in diabetics, and as an antibacterial and antioxidant etc.

In this research, an environmental friendly and low cost approach was used to synthesize gold nanoparticles using the leave extracts of *T. triandra* for the first time. The effects of these green synthesized gold nanoparticles on rice seedlings were investigated, with special emphasis on germination and root growth. Ultimately, this study seeks to add to ever-growing list of plants with the capability of biosynthesis. In

addition, investigations relating to its interaction with an economical important plant such as rice, will contribute towards settling safety concerns, and shedding light on the darkness of uncertainty that often hovers over growing technologies.

1.2 Research objectives

1. To find a plant with the potential to reduce and stabilize gold nanoparticles.
2. To establish an eco-friendly protocol for the synthesis of gold nanoparticles.
3. To monitor the effect of these synthesized gold nanoparticles on germinating rice.
4. To assess the effect of gold nanoparticles on rice root at varying concentrations and possibly offer an explanation to the mechanism of uptake.

1.3 Research hypothesis

At higher temperatures and concentration of the plant extract, gold nanoparticles are expected to be spherical and monodispersity is high. The green synthesized gold nanoparticles are assumed to be biologically compatible because of the biological material that envelopes them. It is expected that there will be no adverse effects on germination and rice roots even at high concentrations. As to the mechanism of uptake, there are no expectations.

1.4 Scope and limitation of the study

In this study, green synthesized gold nanoparticles at different concentrations were exposed to germinating rice grains and observations made. Morphological and

microscopic studies were carried out exclusively on rice roots that had been affected significantly following exposure to gold nanoparticles. Physiological investigations were conducted to determine changes pertaining to exposure at cellular levels. Findings from the aforementioned study were used to provide insight on the mechanism of gold nanoparticle uptake.

1.5 Expected results

It was expected that this study would provide information pertaining to:

1. Gold nanoparticle morphology upon exposure to plant extract under varying conditions.
2. Gold nanoparticle effect on rice germination and root from a microscopic and physiological perspective.
3. The phytotoxicity of gold nanoparticles on rice and pinpoint the step at which adverse effects are most exacerbated.
4. The mechanism of gold nanoparticle uptake by rice plants.

CHAPTER II

LITERATURE REVIEW

2.1 Nanomaterial importance and application

The term nanomaterial refers to materials that have been intentionally designed to have dimensions that fall within the range 1-100 nm (Kregling *et al.*, 2010). As earlier mentioned, materials at such a scale possess numerous physico-chemical properties missing in their bulk counterparts. These unique properties are due to the increased relative surface area, high surface energy, and quantum effects (Arivalagan *et al.*, 2011; Michala *et al.*, 2013). Certain of these important properties are thermal conductivity, electrical and mechanical properties which are higher in nanomaterials due to the insignificant presence of flaws in their structures.

These novel properties are taken advantage of in the fields of medicine, agriculture, environmental remediation and in the cosmetic industry amongst others. For example, nanoparticles are used as drug delivery agents as well as in skin care products such as sunscreens (Salata, 2004).

Size though of great significance, is not the only factor known to contribute to the unique properties and consequent utilization of nanomaterials in several applications. The particles morphology, composition, surface charge and moiety are of importance as well (Jasiorski *et al.*, 2014). For example, spherical shaped nanoparticles or colloids in which they might be suspended in are thermodynamically more stable than other morphologies (Elaissari, 2008).

Besides being engineered, nanoparticles could be incidental or natural. Examples of naturally occurring nanoparticles are volcanic ash, forest fire smoke and lunar dust etc. Incidental nanoparticles are the by-products of human activities such as from welding fumes and coal combustion. Engineered nanomaterial can be further classified into four groups namely composites, dendrimers, carbon based and metal based materials (Monica and Cremonini, 2009). Nanoaluminum, nanozinc, nanogold and nanoscale metal oxides are some examples of metal based material.

2.2 Green synthesis of metal based nanoparticles

Given that the field of nanotechnology is still in its budding years, it is necessary to develop environmentally benign methods of synthesis. Thus, the push for green synthesis should be treated with urgency.

The process of nanoparticle synthesis falls under two categories: top-down or bottom-up approach (Figure 2.1). The top down approach involves successively disintegrating bulk material to obtain nano-sized particles. The bottom up approach on the other hand refers to assembling nano-sized materials by use of atoms or molecules as building blocks. Both approaches are of immense importance to industrial applications and in the field of nanotechnology. For example, the top down approach is commonly used in the field of microelectronics to produce very tiny computer chips. Both approaches have their strengths and weaknesses. Some of the disadvantages of the top down approach include the risk for internal stress, surface defect and contaminations. The bottom up approach makes up for the limitations of the top down approach in that nanostructures fashion by this method tend to have less

defects and are more chemically homogenous. The chemical and biological synthesis of nanoparticles can be approached by the bottom-up and top-down strategy. Green synthesis chemistry focuses on the complete exclusion or reduction of toxic substance generation or use in synthetic processes (Wang *et al.*, 2012). On the other hand, conventional methods of synthesis such as Laser ablation, pulse wire discharge method, radiolysis and photochemical are expensive (require vacuum, specialized equipment and high temperatures) and utilize hazardous chemicals (Umer *et al.*, 2012; Aromal *et al.*, 2012). These toxic agents serve the purpose of reduction and/or stabilization of these nanoparticles (Mervat and Eisa, 2014). This is of course not healthy to the environment as a whole, should these substances or products that contain them make their way into it. Additionally, it is not a hidden secret that the health risk associated with nanoparticle exposure still remains poorly understood (Varma, 2012).

Silver, gold, copper, cobalt, platinum and pallidum nanoparticles have been synthesized using cell cultures, algae, diatoms and plants (Narayanan and Natarajan, 2012). Synthesis of metal nanoparticles by these options is both cost-effective and eco-friendly. However, plants make excellent candidates in the green synthesis of metal nanoparticles over the other options. Reason being that, they not only dominate terrestrial life, but constitute a sustainable resource. The use of microbial cultures to synthesize these nanoparticles is a put off when compared to ex situ synthesis using plant extracts. This is because it is tedious maintaining these cultures (Sujitha and Kannan, 2013).

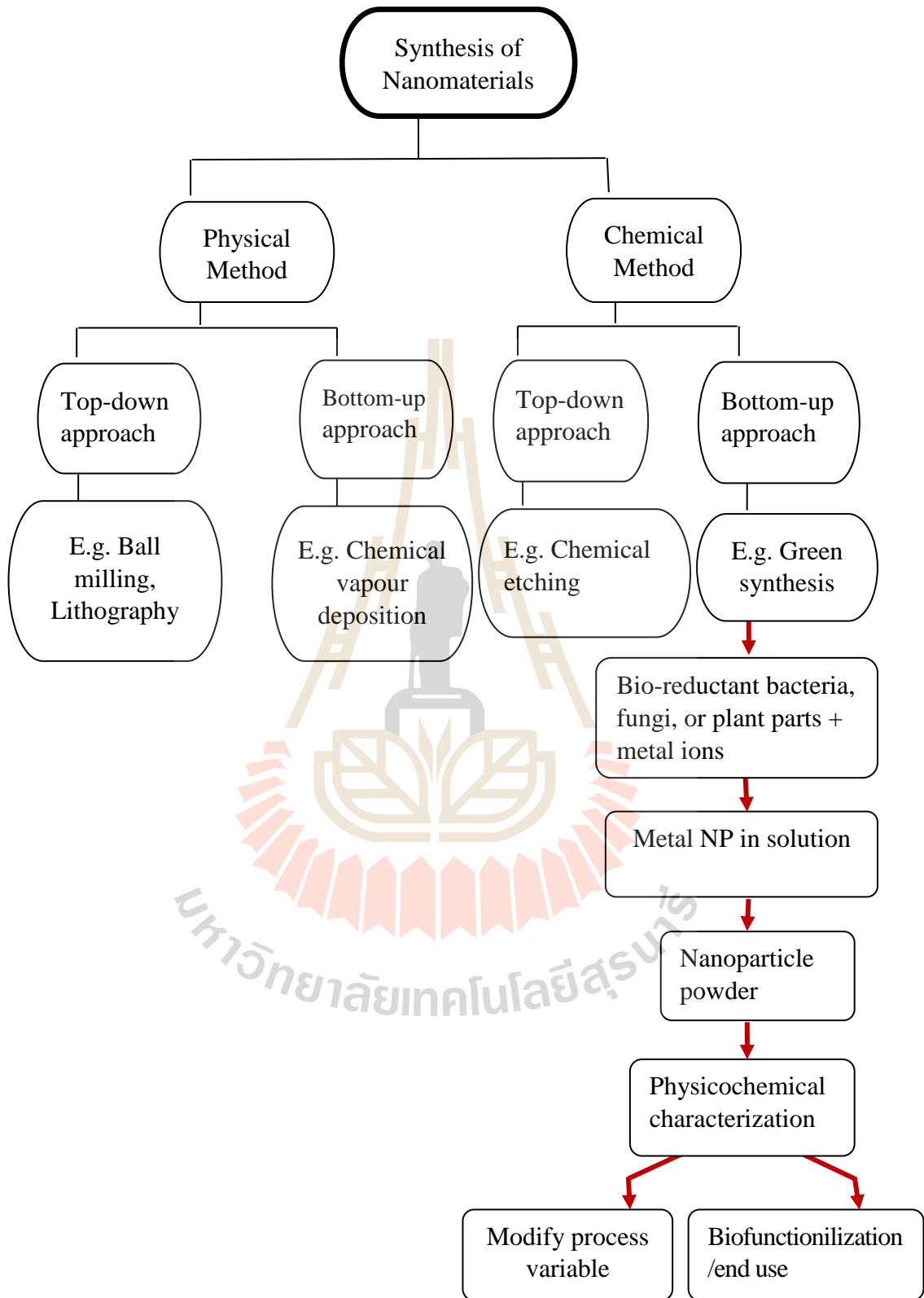


Figure 2.1 Generalized flowchart for nanoparticle syntheses approach with emphasis on nanobiosynthesis (modified from Salam *et al.*, 2012).

2.3 Green synthesis of gold nanoparticles using plants

Gold is among the many noble metals and its historical importance cannot be overemphasized. Nanometer-sized gold particles too are of great importance in chemistry, physics and biology (Geethalakshmi and Sarada, 2013). For instance, they are used for drug delivery, labeling, sensing, water purification, catalysis and in optoelectronics. Comparatively to other metallic nanoparticles as far as the field of biology is concerned, they are preferred over other metallic nanoparticles because of their biocompatible and non-cytotoxic nature (Sujitha and Kannan, 2013).

Interest in plant mediated synthesis of nanoparticles is on the rise. This is because of the simplicity and ecofriendly nature of this method which makes it possible for nanoparticles of varying shapes and sizes to be produced (Mervat and Eisa, 2014). Furthermore, the high diversity and vast potential of chemical compounds in plants is an added appeal. Plant extracts of the plants *Aloe vera*, *Magnolia kobus*, *Magnifera indica*, *Cinnamomum camphora*, *Rosa hybrida*, mushroom, neem, and pear fruit etc. have been used to synthesize metal nanoparticles such as gold and silver (Noruzi *et al.*, 2011).

In plant mediated synthesis of gold nanoparticles, the gold substrate often used is Gold (III) Chloride hydrate (HAuCl_4), otherwise known as Hydrogen tetrachloroaurate (III) hydrate ($\text{HAuCl}_4 \cdot 3\text{H}_2\text{O}$). From this substrate, a gold colloidal solution can also be prepared. A colloid is defined as a system of microscopically small particles, typically in the range of 100 to 10 000 Å evenly dispersed throughout another material (White, 1999). The substrate is subjected to reduction by use of plant extracts. The biologically active components of plants serve as reducing agents in this process. Unlike in conventional chemical reduction procedures where steric stabilizers

are added in the recipe to ensure stabilization, it is common place to have these biological materials double as stabilizing agents or capping agents (Elaissari, 2008; Kumar *et al.*, 2012).

The reaction conditions of the gold substrate and the plant material can be varied to yield different outcomes. By varying the temperature of the reaction, the reaction time, volumes of plant extract, the concentration of the plant extract/gold substrate and the pH of the reaction, differing end results can be reached. Morphology and size are the targets of such modifications in case of reaction condition alterations (Kharissova *et al.*, 2013).

A change in temperature has the potential to speed up or slow down the reaction process. An increase in temperature as expected will accelerate the reaction rate and vice versa. At higher volumes of the plant extract, reaction rates are faster and vice versa. This is because the biological substance responsible for reduction is present in sufficient amounts (Sujitha and Kannan, 2013). At higher concentrations of either the plant extract or gold substrate, the process of gold nanoparticle synthesis is faster. The pH of the reaction has a bearing on the reaction outcome. Gold nanoparticles sizes were reported to be larger at acidic pH than at basic pH in an experiment mediated by tansy fruit extracts (Dubey and Sillanpaa, 2010).

There are morphological implications to changing the reaction conditions of gold synthesis as for other metal nanoparticles synthesis by using plant extracts. At lower temperatures, reaction mixtures have been reported to contain nanoparticles of varying shapes existing side by side (Song *et al.*, 2009). For example, triangular, pentagonal, hexagonal and spherical-shaped nanoparticles (Figure 2.2). At higher temperatures, spherical-shaped nanoparticles dominate the aqueous mixture. The

concentration of the plant extract has been linked to the shape of gold nanoparticles. Song *et al.* (2009) reported that at high concentrations of leaf broth, gold nanoparticles were observed to be spherical in shape. Size is an important feature that is affected by altering the reaction condition of temperature and concentration of the plant extract utilized. Small-sized nanoparticles are associated with higher temperatures. The reason being that when reaction rates are high, gold ions are consumed in the formation of nuclei. This event halts the secondary reduction process on the preformed nuclei surface (Song *et al.*, 2009). However, this is not always the case. In the synthesis of gold nanoparticles using palm oil mill effluent, Au nanoparticle sizes increased with increasing temperatures (Gan *et al.*, 2012). The authors explained that because reduction rates increase at higher temperatures, the capping process is hindered leading to the aggregation of Au nanoparticles.

The formation of gold nanoparticles transitions through the stages of gold substrate reduction by the plant extract, metallic gold nucleation and the growth of individual nuclei. Growth of individual nuclei is achieved as the reaction proceeds with the accumulation of metallic gold on the surface of preformed nuclei. The formation of gold nanoparticles in reaction mixtures is accompanied by an observable change in colour, a phenomenon known as surface plasmon resonance. Surface plasmon resonance is the cumulative excitation of conducting electrons induced by the interaction of electromagnetic fields (Suman *et al.*, 2014). The Surface plasmon resonance of gold nanoparticles is unique and very often lies between 500-550 nm (Shankar *et al.*, 2004).

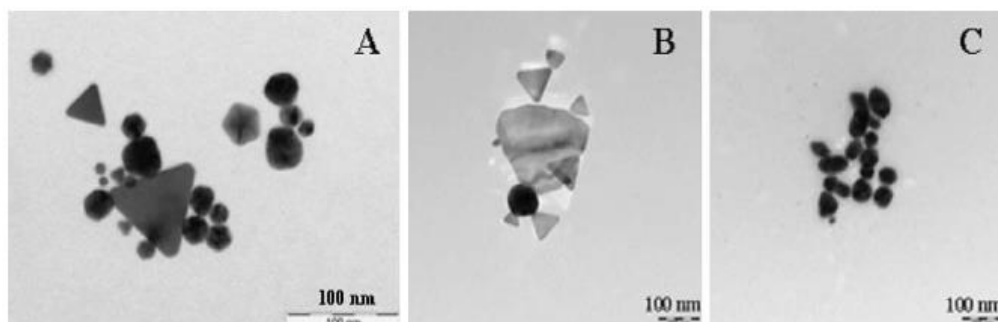


Figure 2.2 TEM images of gold nanoparticles of varying shapes synthesized using Magnolia leaf broth at temperatures of (A) 25°C (B) 60°C (C) 95°C (Song *et al.*, 2009).

As earlier mentioned, nanoscale changes of certain elements such as gold and silver are often accompanied by a visible change in the colour of the colloid. In bulk form and particle sizes of up to a 100 nm, gold metal appears shiny yellow. Colour dynamics set in when particle sizes are further reduced. For example, bright red is associated to a particle size of 30 nm. On the other hand, the colour purple is linked to particle sizes smaller than 30 nm, and a brownish hue, to an even smaller size (Mongillo, 2007).

2.4 Morphology and importance of the rice plant

The rice plant (*Oryza sativa* or *Oryza glaberrima*) from which rice seeds are obtained is an annual plant. However, it is not uncommon for it to subsist as a perennial. *O. sativa* is the Asian species of rice, while *O. glaberrima* is the African species of the grain. It is a monocot and belongs to the plant family Poaceae. It is a cereal grain and constitutes the staple diet for more than half of the world's population

(Lin *et al.*, 2009). As far as the production of grain is concerned, it is second only to maize. In terms of consumption by humans, it is the most consumed grain. A contributing factor to this is linked to its ability to grow under a broad range of climatic and geographic conditions world over. In addition, the rice plant is the only cultivated cereal suited to growing in flooded and non-flooded soils.

In Thailand, rice production contributes enormously to the economy. It is equally one of the world's biggest exporters of rice (Son *et al.*, 2013). More than half of the agricultural land area and labor is recruited to rice cultivation. For most Thais, it is the primary source of food and nutrition.

The rice plant is a grass and can grow to heights of between 1-5 m (Figure 2.3). This depends on the extent of soil fertility and the species type. Its upright stem consists of series of nodes from which long and slender leaves emanates. It is wind-pollinated with small flowers. The flowers which eventually become the grains following pollination, occur on spikes which appear bent over. The grains which measure 5-12 mm long and 2-3 mm thick is the plant's most economically important part.

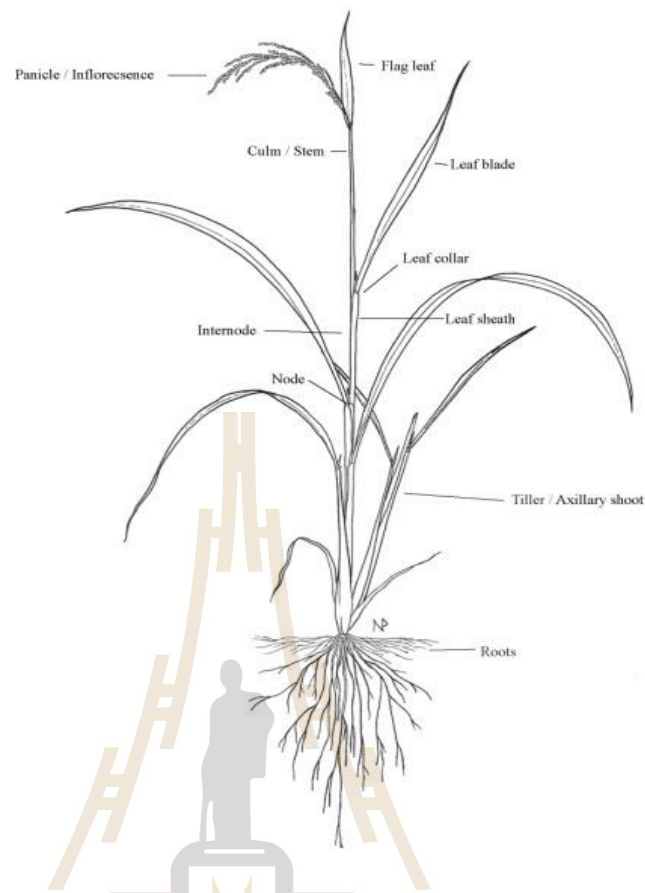


Figure 2.3 Characteristics of rice (*O. sativa*) (Polato, 2013).

2.5 The process of germination

The process of germination is the first step in plant development. Germination is the restoration of an embryo's development and growth following a period of dormancy (Lewis *et al.*, 1998). In eudicots, the embryo moves nutrients in the endosperm to their cotyledons just before germination. Conversely, monocot embryos utilize reserves in endosperm after seed germination comes to completion.

Hypogeal and epigeal germination are examples of germination. A distinctive feature of hypogeal germination is that the cotyledons remain underground. This type of germination occurs in mangos, pea, maize, wheat and rice etc. (Figure 2.4). In

epigeal germination, the cotyledons are raised above the soil and eventually become photosynthetic. Such germination occurs in bean, castor, mustard and sunflower etc.

Imbibition is the physical process that marks the start of germination. It is characterized by the permeation of water into a seed mediated by imbibitional forces within it. The seed's tissue will be enlarged as a result to a point where the seed coat is broken making way for oxygen diffusion. Imbibition helps to kick-start the process of mitosis in dried-out seeds because membrane integrity is restored in the presence of moisture.

Much equally happens at the level of the biochemistry of the seed. The water contained in the tissues of the seed activates the hydrolysis enzymes. These enzymes are responsible for mobilizing the reserves stored in embryonic cells. For example, the starch contained in the cells of endosperm of cereals and grasses are hydrolyzed by α -amylase (Bradbeer, 1988). Sugars are the product of this hydrolysis and are utilized by the meristematic cells of the embryo for growth. The growth process entails cell elongation and division, followed by enlargement, differentiation and maturation respectively.

Germination draws to an end with the emergence of the radicle through the seed coat. The growth of the radicle precedes that of the plumule. In monocotyledons, the growth of radicle is temporary, lasting only through the early stage of development (Dahlgren *et al.*, 1985). Once root and shoot meristems have been formed, germination is irreversible by dehydration without lethal consequences.

By all indication, moisture, oxygen and temperature are important factors of germination. However, the suitable range for each of this factor varies for different plant species.

Seed germination in rice like in other plants, commences with imbibition. The coleorhiza, a sheath that partially envelops the radicle, initially pushes slightly through the seed coat making way for the radicle to emerge through the coleorhiza. The radicle then anchors itself to the soil. This is followed with the elongation of the coleoptile. Radicle emergence precedes that of coleoptile under dry-seeded or aerobic conditions. Under water-seeded or low oxygen conditions, coleoptile emergence may occur ahead of the radicle. Rice seed germination typically occurs within the temperature range of 10°C to 42°C with an optimum temperature of 30.6°C.

In order to ease communication on production practices and research findings on rice production among stakeholders, the rice growth staging system were established (Counce, 2009). The rice growth staging system categorizes and associates the developmental stages of rice based on the distinctive features it progressively exhibits over time. For seedling growth stages, the terms S0, S1, S2 and S3 are used (Moldenhauer *et al.*, 2013). These terms mark the progressive stages of germination to seedling emergence. S0 stands for the dry and unimbibed seed, while S1 marks the emergence of the coleoptile. In cases where the radicle emerges before the coleoptile, the term S1 can be rightly ascribed as well. This term applies to both scenarios provided either of them emerges alone. While the emergence of the radicle is attributed to S2, the emergence of prophyll from coleoptile is linked to S3. Beyond the seedling growth stage which is part of the vegetative phase, the rice growth staging system equally encompasses the reproductive phase.

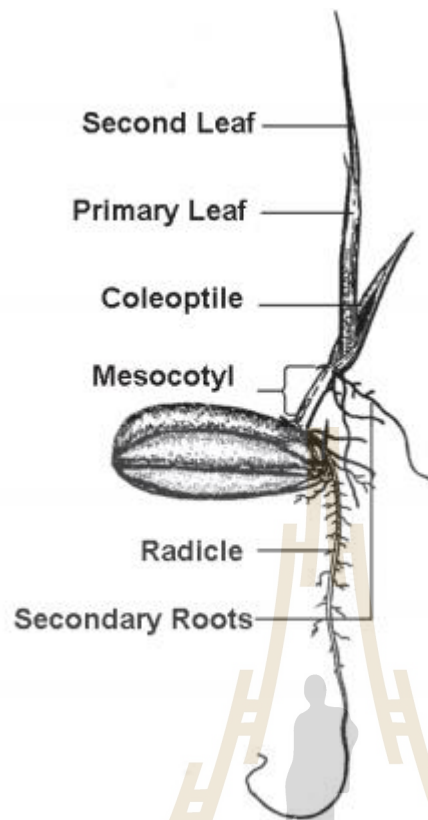


Figure 2.4 Parts of a germinating rice seedling (Moldenhauer *et al.*, 2013).

2.6 Plant root morphology and mechanism of root uptake

The morphological construction of this underground part of plants begins in the seed during germination. The main function of roots is uptake of water and dissolved minerals (Figure 2.6). They equally serve for anchorage and sometimes as storage organs.

Two kinds of root systems exist namely taproot and fibrous root systems. Tap root systems consist of a primary root which developed from the radicle along with lateral branching. This kind of root system is associated with the eudicots. In fibrous root systems, the primary root is replaced by adventitious roots which emanate from

the base of the stem. Lateral roots of identical proportions eventually develop from the adventitious roots. Monocots like rice and maize have fibrous root systems.

Root structures such as the root cap, epidermis, cortex and vascular cylinder are all descended from cells of the root apical meristem (Campbell *et al.*, 1997). At the root apical meristem mitotic division is high. The root apical meristem lies behind the root cap – a thimble-shaped mass of cells that protects the delicate root tip. Other important regions of the root are the zone of elongation and maturation. The root epidermis is the plant's absorptive surface. The area of absorption is greatly increased by root hairs formed from specialized cells of the epidermis (Figure 2.5)

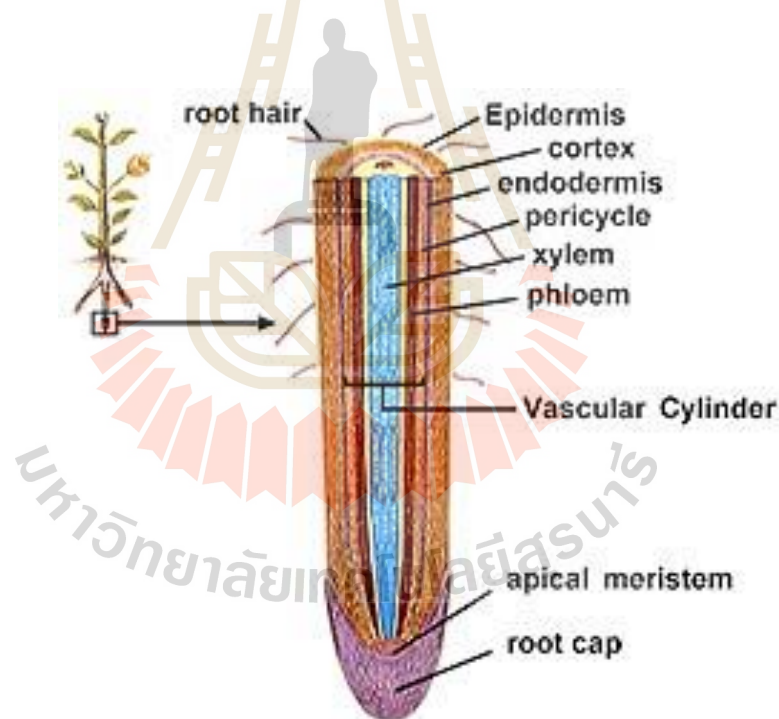


Figure 2.5 Plant root structure (<http://www.desktopclass.com/>)

In plant roots the vascular cylinder serves as the conductive tissue. The vascular cylinder in monocots divides the ground tissue into the cortex and pith. The pericycle,

a layer of parenchyma cells encloses the vascular cylinder. Lateral roots erupt out of the cells of the pericycle through the cortex and epidermis.

Following diffusion of mineral-rich water into plant roots, the vascular cylinder of the roots can be arrived at in either one of two ways: by movement through the cytoplasm, or diffusion across the cell wall (Figure 2.6). These mechanisms are referred to as the symplastic and apoplastic pathway respectively (Sheoran *et al.*, 2013). In the symplastic pathway, water enters the cytoplasm by means of diffusion across the plasma membrane of a cell in the root epidermis or cortex. Movement of water between cytoplasm continues via the plasmodesmata until the endodermis is reached. Water passes through the cytoplasm of endodermal cells to reach the vascular cylinder from where they are moved to different parts of the plant. By means of the apoplastic pathway, water/substances make it all the way to the endodermis via intracellular spaces and cell wall. However, they are unable to reach the vascular cylinder in the same fashion. This is because the overlapping endodermal cell walls of the endodermis which separates the root cortex from the vascular cylinder has walls impregnated with waxy substance which forms Casparian strips. The Casparian strip prevents water from seeping through the cell wall of endodermal cells (Teresa *et al.*, 2009).

Water and the dissolved minerals that take this path can only enter the vascular cylinder via the cytoplasm of an endodermal cell.

Mineral ions dissolved in soil water that crosses the plasma membrane of root endodermal cells prior to entry into a vascular cylinder is regulated by receptors, transport proteins and channels. Transport proteins not only control the type of mineral ions but the quantity suitable for uptake into plant body.

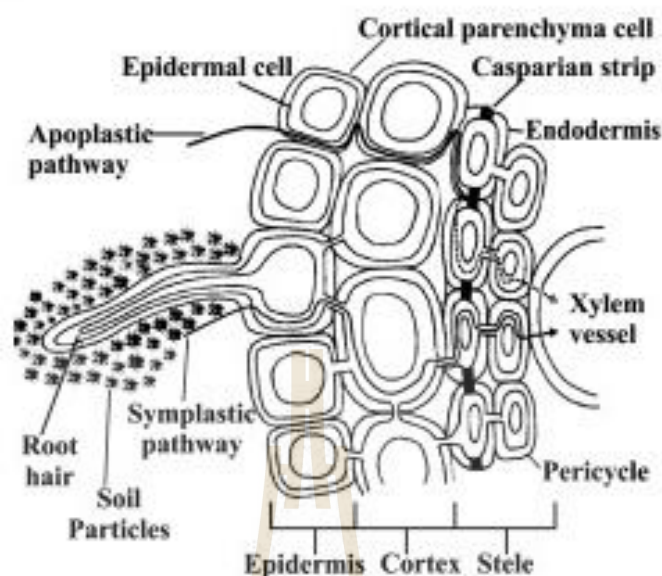


Figure 2.6 Depiction of pathway of water/substance uptake in plant roots (Sheoron *et al.*, 2013).

2.7 Metal nanoparticle effect on germination and uptake

Plants are important components of the ecology and the chances that they may become exposed to nanoparticles are extremely high. One of the reasons being that, nanoparticle use in numerous products and applications have seen a surge in recent times. To that effect, numerous experiments have been carried out to gain a better understanding of their effect on plants. Developmental stages of plants such as seed germination and root growth are often exploited in such experiments (Lin *et al.*, 2009). It is not uncommon for conflicting results to be obtained.

Germination is an important stage in plant development. Seed germination of most seeds exposed to suspensions of metal nanoparticles is hardly ever inhibited.

This is especially true for plants with seeds with thick protective seed coats which offer some form of protection to the embryo against toxicity (Boonyanitipong *et al.*, 2011). Boonyanitipong *et al.* (2011) reported that rice, rye, corn, cabbage and soy bean germination was not affected by suspensions of nano-ZnO and nano-TiO₂ upon exposure. In line with this experiment, seed germination of *Arabidopsis thaliana* exposed to silver nanoparticles has also been reported unaffected (Qian *et al.*, 2013). This has led some to conclude that determining phytotoxicity by relying exclusively on the germination index is misleading given that is a less sensitive approach (Garcia *et al.*, 2011).

In comparative terms, radish seed germination rates have been reported higher than in their control upon exposure to glucoxylian-mediated green synthesis of gold and silver nanoparticles (Iram *et al.*, 2014). The authors offered no explanation as to this case in point. According to Kumar *et al.* (2013), who experimented with gold nanoparticles effect on *A. thaliana*, germination rates were increased because gold nanoparticles enhanced water uptake capacity of the exposed seeds.

Though the germination of seeds exposed to nanoparticles might be successful, that is rarely the case for root growth and development especially when parameters such as the time of exposure and concentration of nanoparticle suspension factors in. In the study carried out by Iram *et al.* (2014), higher concentrations (27 µg/ml) of Ag nanoparticles inhibited root length while lower concentrations (13.5 µg/ml) of the nanoparticle improved root growth. The authors attributed this occurrence to the sterilizing ability of Ag nanoparticles to encourage root growth at lower concentrations and inhibit growth at higher concentrations due to its toxicity. This experiment clearly demonstrates the “hormesis effect” (Ma *et al.*, 2010); a dose

response phenomenon wherein low doses stimulate a response and high doses inhibit that response. In the same experiment, glucoxyylan-mediated gold nanoparticles showed no significant effect on the plants under investigation; an indication the particles are non-toxic to radish.

Plant uptake of nanoparticles is either by the apoplastic or symplastic pathway along with water and dissolved nutrients. Silver nanoparticles as large as 40 nm have been reported to be taken up by *A. thaliana* roots, and transported to the shoots (Ma *et al.*, 2010). However, a majority of the nanoparticles adhered to the root cap. In a report by Krishnag *et al.* (2012), there was a slight change in root and shoot anatomy of *Bacopa monniera* plant exposed to biologically synthesized silver nanoparticles following uptake. Roots lacked their characteristic air chambers and partition filaments.

Nanoparticle distribution in plant tissue is related to the surface charge of the nanoparticle in question. For example, Au nanoparticle distribution in tissue of rice root varied with the surface charge in short and long term treatments (Koemel *et al.*, 2013). In short term treatments, Au concentration in rice roots was highest in plants treated with positively charged gold nanoparticle, followed by neutrally charged and negatively charged gold nanoparticles respectively. The authors of the study explained that the concentration of positively charged gold nanoparticles was highest in the root organ because, its active site binds strongly to the carboxyl group of pectin that makes up the root cell wall. Hence, it is not easily moved to the shoot like in the case of negatively charged gold nanoparticles.

As earlier stated, there are no clear cut expectations as to the outcome. In a nutshell, uptake and translocation of nanoparticles across the root cell depends on the

type and concentration of metal ions and the plant species involved (Krishnag *et al.*, 2012).

2.8 Relationship between plant stress and hydrogen peroxide

Plants are subjected to stress when a deviation in the optimal conditions under which they thrive occurs. Under such circumstances, plant growth, development and productivity may be hampered. This is an indication that changes are effected at the functional levels of the organism. Stress can be abiotic or biotic in origin; in addition, it can be sporadic or permanent. Examples of abiotic stress include water logging, drought, ozone, excessive soil salinity and inadequate mineral nutrients amongst others. In addition to the above widely-known stressors, many metals have been associated to the elevation of reactive oxygen species (ROS) production in plants (Shamar *et al.*, 2012).

Superoxide dismutase breakdown of superoxide radicals will yield H_2O_2 and O_2 . Hydrogen peroxide along with other reactive oxygen species have been linked with numerous plant environmental responses and signal transductions (Cheeseman, 2006). Hydrogen peroxide's occurrence in plants therefore goes beyond stress response to include typical aspects of plant development such as growth and development. However, its tissue levels might be raised during ripening, lignification, suberization, photo-oxidation reactions, potassium cyanide inhibition of endogenous catalase, ozone-induced, excessive salinization and heat stress etc.

Under adverse conditions, hydrogen peroxide tissue amounts might be raised to unsafe levels. At unsafe amounts, there is the risk of lipid peroxidation. Lipid peroxidation is the breakdown of lipids, especially tri-unsaturated fatty acids by

oxidants such as hydrogen peroxide and other inorganic peroxides (Ayala, 2014); proteins and other cellular components may be oxidatively damaged as well. Malondialdehyde (MDA) generation is a norm following the degradation of the tri-unsaturated fatty acids. Little wonder, there existence of numerous protocols to assess lipid oxidative damage by the quantification of MDA.

However, plants like countless other organisms are endowed with the ability to combat oxidative stress. In fact, a plant's ability to control oxidant levels is inextricably linked to stress tolerance. To protect against the damage brought about by oxidative stress, plants make use of both enzymatic and non-enzymatic antioxidant defense systems (Habibi, 2014). Superoxide dismutase, ascorbate peroxidase, catalase and glutathione reductase are among the arsenal of enzymes belonging to the enzymatic defense system. Non enzymatic defense system on the other hand makes use of ascorbic acid, phenolic compounds, vitamin E and non-protein amino acids among others.

2.9 The Future of Nanotechnology and Agriculture

Man's scientific explorations over time have paved the way for the perception of his environment in ways that were once deemed impossible. Among them is nanotechnology, whose future holds plenty of promises. These promises are as numerous as the exponential possibilities that come with working on the increased surface area associated with materials on such a minuscule scale. According to expert projections, the market of nanotechnology based products is expected to increase to over a trillion dollars in 2015 from 146 billion USD in 2007 (Adams and Barbante, 2013). However, Market and Research, a market research platform, estimates the

global nanotechnology industry will reach 75.8 billion USD by 2020 (Research and Market, 2015). Such contradicting projections only point to the growth potential of this industry and monumental task involved collecting data in such a wide field to make good enough estimates. Simply put: It is arguably science's next big frontier.

The reach of opportunities nanotechnology offers extends into the food and agricultural industries. These applications target the different stages of the food production chain, which ranges from primary production through processing to disposal. A notable example at the level of primary production are nanoscale carriers which can be used for the efficient delivery of fertilizers, pesticides and plant growth regulators amongst others. As a consequence, the bioavailability of intended active ingredient will be increased, and chemical runoff scaled down. Key to the efficient functioning of agrochemical deliveries/ slow release are mechanisms such as the geometry of the nanoscale carriers, encapsulation, surface ionic and weak bond attachments (Moore *et al.*, 2011; Dasgupta *et al.*, 2015). In addition to agrochemical deliveries, plant pathogen detection with the aid of nanomaterials is equally feasible.

At the level of food processing nanoparticles are currently being used as food supplements to increase the bioavailability of trace elements such as iron, as antimicrobials to boost preservation of foodstuffs and for the detection of foodborne pathogens etc. Due to the broad spectrum antimicrobial action of silver/silver nanoparticles, their incorporation into certain food packaging materials has been reported to extend shelf-life and decrease the microbial count of foods with these packaging (Duncan, 2011).

With a growing population expected to hit 9 billion by 2050, a surge in nanotechnology research and development with respect to agriculture is expected

(Yada and Chen, 2011). More effort will be needed to be channeled towards discerning the consequence of the presence of nanoparticles in the food production chain and the environment at large. The sustainability of nanotechnology as a tool in complementing current farming practices will be hugely dependent on the information generated from such findings.



CHAPTER III

MATERIALS AND METHODS

3.1 Synthesis of gold nanoparticle

3.1.1 *Tiliacora triandra* leaf extract aided synthesis

Synthesis of the nanoparticles was preceded by cleaning all glassware with freshly prepared aqua regia (HCl: HNO₃/ 3:1, v/v) to get rid of potential impurities that may interfere with the ensuing rounds of synthesis (Daroudi *et al.*, 2011). To prepare the plant leaf broth, 5 g of thoroughly washed and finely cut leaves of the plant were blended, its extract sifted and volume made up to 100 mL with sterile distilled water in a 300 mL Erlenmeyer flask. The broth was then stored at 4 °C for use within a week.

The reduction of Au³⁺ ions was achieved by the addition of 10 mL of the leaf broth to 190 mL of 1 mM aqueous HAuCl₄ solution. To study the effect of temperature on rate of synthesis and particle size/shape, gold nanoparticle preparations were carried out on hot plates at varying temperatures (25°C, 65°C and 80°C).

Leaf broth concentrations were varied between 50% and 100% (50%, 80% and 100%) along with extracts volume variations (6 mL, 8 mL and 10 mL) and the effect monitored on gold nanoparticle synthesis rate and morphology. This was carried out at a temperature of 65°C and HAuCl₄ concentration of 1 mM.

Reduction of the gold substrate coincides with a change in colour of the solution. Heat supply was discontinued fifteen minutes following this observable change in colour. The resulting gold nanoparticle solution was purified by repeated centrifugations at 12000 rpm for duration of 60 minutes ensued by redispersion of pellet in deionized water (Song *et al.*, 2009). The suspensions were stored in the refrigerator at temperatures of 4°C in the absence of plans in place for further processing right away.

3.1.2 Synthesis of gold nanoparticles with gelatin and gelatin-glucose mixtures

For comparative purposes, gold nanoparticles were synthesized with the help of gelatin and gelatin-glucose mixtures. This experiment was modeled after an earlier experiment but for the use of HAuCl_4 (aq) (Daroudi *et al.*, 2011). Moreover, the choice of reagents used in this experiment was due to them being common laboratory chemicals. Gold nanoparticles were synthesized separately with mixtures of gelatin and gelatin-glucose. In these reactions, gold tetrachloride is reduced to gold ions which eventually become gold nanoparticles by gelatin and glucose under temperatures of 28°C, 40 °C and 60°C.

The gelatin-based reaction was carried out by dissolving 2 g of gelatin in 190 mL of sterile water followed by the addition of 10 mL of 10 mM AuCl_4 . The gelatin-glucose reaction varied from the gelatin-based reduction procedure only in the addition of 20 mL of 2 M glucose. The reaction mixtures were thoroughly stirred in all instances. All reactions without exception lasted for duration of 48 hours. A red wine colour was observed for reactions at 60°C for both gelatin-based and gelatin-

glucose reactions. However, this colour grows fainter at lower temperatures of synthesis.

3.2 Gold nanoparticle characterization

3.2.1 Transmission Electron Microscope

The transmission electron microscope is an essential tool for studies conducted in the material sciences. By using a beam of electrons instead of light, the fine features of specimens such as crystal structure, grain boundaries, shape and size can be observed. A resolution several magnitudes better than that of a light microscope is owed to the much smaller wavelength of electrons. In this experiment, the transmission electron microscope was used for the analysis of the shape and size of the developed nanoparticles. About 3 μL of the gold colloidal samples were placed on carbon-coated copper grids and spread thin (Dubey *et al.*, 2010). It was then left to dry at oven temperatures of 60°C for about 15 minutes prior to analysis.

3.2.2 UV-vis spectroscopy

UV-visible spectrophotometers exploit a molecule's ability to absorb ultraviolet or visible light. Different molecules will absorb radiation of different wavelengths. For this reason, absorption spectra that result from the interaction of photons and analyte molecules possess absorption bands which can be linked to specific structural groups within the molecule. Uncentrifuged gold colloid was characterized using UV-visible spectroscopy. This technique amongst others is used in determining with certainty the formation and stability of metal nanoparticles in aqueous solutions (Kasthuri *et al.*, 2009). The optical properties of the samples were

recorded on a Cary 300 UV-vis spectrophotometer. The reduction of gold ions to gold nanoparticles under different conditions was determined by measuring the UV-visible spectra. Analyses were done in the wavelength range of 400 to 700 nm operating at a resolution of 1 nm (Sujitha and Kannan, 2013). Deionized water was used as blank.

3.2.3 X-ray diffraction analysis

X-ray diffraction analysis, as its name suggests, is an x-ray based analytical approach used in characterizing materials usually in powdery form. X-ray beam interactions with the atoms of different materials yields unique ‘fingerprints’ used for material identification. In this research, XRD analysis was carried out to furnish information on the crystalline size and crystallinity of the gold nanoparticles synthesized under the different conditions (Nadaf and Kanase, 2016). The gold colloids were centrifuged (12000 rpm, 25°C) for 60 minutes and washed several times with distilled water prior to being dried in metal dishes in an oven dryer at temperatures of 60°C (Dubey *et al.*, 2010).

The X-ray diffraction pattern of the dry nanoparticle powder was obtained using Bruker D2 X-ray diffractometer with Cu K α radiations ($\lambda = 1.5406 \text{ \AA}$).

3.2.4 FTIR spectroscopy

FTIR measurements were carried out to identify the biological groups bound to the surface of gold nanoparticle, involved in gold substrate reduction and stabilization. Sample preparation is somewhat identical to that for XRD analysis. The gold colloids synthesized under varying conditions were centrifuged (12000 rpm, 25°C) for 45 minutes and washed several times with distilled water (Noruzi *et al.*,

2011) Subsequently, all samples along with pure plant extract of *T. triandra* were freeze dried and subjected to FTIR analysis in the range 40 – 4000 cm^{-1} .

3.3 Gold nanoparticle effect on rice

3.3.1 Seed preparation, germination and root development

The rice variety KDML 105, preferably stored in dry conditions, was used in the experiment. This was done in the hopes to guarantee high germination rates. Furthermore, the germination rates of the plant seeds were established prior to treatments with the nanoparticles by carrying out a germination test. Ahead of the experiment proper, rice seeds were sterilized by immersion in 2.5% of sodium hypochlorite for 15 minutes (Lin and Kao as cited by Boonyanitiong *et al.*, 2011). It was later rinsed thrice with distilled water prior to being soaked in nano-gold suspensions of varying concentrations (10, 100, 500, and 1000 mg/L). Gold nanoparticle suspensions were prepared by suspending appropriate amounts of the nanoparticles in distilled water and dispersion was achieved by ultrasonic vibrations (100W, 50/60 Hz) for 45 minutes. The pHs of the suspensions were measured following dispersion with the help of a pH meter. The soaking period lasted for 4 hours in an incubator at ambient temperatures. At the end of the soaking period, 16 seeds from each of the suspensions were transferred into labeled petri dishes containing Whatman filter paper number 1. To each of these petri dishes, 4 mL of distilled water (Control) or nanoparticle suspension was dispensed accordingly, followed by incubation for a period of 7 days. The distilled water or nanoparticle suspension introduced into the petri dishes was evenly dispensed to ensure all grains had equal access to moisture. Thus growth disadvantage was minimized. Germination

based on root length emergence stood at lengths of >1 mm or >5 mm (Lin and Xing, 2007). However, only seeds with coleoptile longer than 2 mm were considered to have germinated in this study. The germination percentage, root and shoot length were measured. The germination percentage was obtained by dividing the number of germinated seeds by the total number of seeds incubated/planted. The formula is expressed as:

$$\text{Germination percentage} = \frac{\text{Number of germinated seeds}}{\text{Number of incubated seeds}} \times 100$$

To obtain relative root elongation, the sum total of the average of the root length of grains treated with nanoparticle and that of the control was divided and multiplied by a hundred. It is expressed in the formula below:

$$\text{Relative root elongation} = \frac{\text{Mean length of root with NP}}{\text{Mean root length with Ctrl}} \times 100$$

3.3.2 Determination of germinated seedling relative water content

The relative water content of germinated seedlings was determined at the end of the germination period (7 days) according to the method of Barrs and Weatherly (as cited by Mezer *et al.*, 2014). Seedlings from each treatment, 5 in number, were weighed to obtain fresh weight and later floated in distilled water for 24 hours in the dark at 4°C (Tw). These seedlings were subsequently dabbed off excess water prior to weighing to obtain the turgor weight. The dry weight of the seedlings, which is the weight of the seedlings following overnight oven drying at

temperatures of 80°C was equally acquired. Relative water content was determined by use of the equation: $RWC = [(Fw-Dw)] / [(Tw- Dw)] \times 100$; where Fw is fresh weight of seedling, Dw is dry weight of seedling and Tw is turgid weight of seedling.

3.3.3 Cell death evaluation

Following the exposure of the germinated grains to the various concentrations of gold nanoparticle suspension, plant root cell death evaluations were made. Evaluations were made based on the method outlined by Zanardo *et al.* (2009). Both treated and untreated rice roots tips, measuring 3 cm after excision were exposed to 5 mL of Evans blue (0.25% v/v) for a duration of 15 minutes. To get rid of excess and unbound dye, these roots were washed with distilled water; washing lasted for 30 minutes. The root tips were then incubated in 7 mL of N-dimethylformamide at room temperature for a duration of 50 minutes in the dark. Using N-dimethylformamide as blank, the released Evans blue was measured at a wavelength of 600 nm. Cell death was expressed as the absorbance of treated roots in relation to untreated roots or the control.

3.3.4 Determination of the effects of seed soaking and incubation on root elongation

To determine the effects of seed soaking and the process of incubation on root elongation, three treatments were setup. A single concentration of 2000 mg/L nano-gold suspension was used. In the first treatment, all seeds were soaked in the said concentration for 2 hours, rinsed in distilled water thrice and later incubated in distilled water.

In the second treatment, incubation in the said concentration was preceded by soaking in distilled water for a couple of hours.

Both the incubation and soaking stages were carried out in 2000 mg/L nano-gold suspension for the third treatment. Just as in the aforementioned treatments, soaking lasted for two hours.

At the end of the experiment which lasted for seven days, gold nanoparticles were thought of as being of minimal toxicity on the rice plant if its effect was determined to be null at such high concentrations (USEPA guidelines as cited by Ma *et al.*, 2010).

3.3.5 Hydrogen peroxide and lipid peroxidation estimation

Hydrogen peroxide levels were estimated based on the method of Mukherjee and Choundhuri (1983). Root and shoot tissues (0.5 g) were separately homogenized in 5 mL of 0.1% (w/v) TCA (Trichloroacetic acid). All homogenates were centrifuged at 6,000 rpm for 15 minutes and 2 mL of the supernatant was added to 2 mL of 10 mM K-phosphate buffer (pH 7.0). Subsequently, 4 mL of 1 M KI was added to the mixture. The intensity of the yellow colour of the supernatant due to the addition of KI was measured at 410 nm using a UV-vis spectrophotometer (extinction coefficient = 0.28). The blank used in the experiment was 0.1% TCA. A standard curve was established to calculate the tissue content of H₂O₂ and expressed as $\mu\text{mol g}^{-1}$ FW.

Lipid peroxidation levels were estimated as indicated by Heath and Packer (as cited by Nair and Chung, 2014). Seedling root (0.1 g) and shoot (0.2 g) tissues from both the control and those treated with gold nanoparticles were

homogenized in 10 mL of 5% (w/v) TCA. The homogenized samples were centrifuged at 4000 g for 10 minutes and its supernatant (3 mL) mixed with 3 mL of 0.67% (w/v) thiobarbituric acid (TBA). The mixture was boiled at 90 °C for 30 minutes and cooled after centrifugation. Absorbance of the resulting supernatant was read at 532 nm and 600 nm using a UV-Vis spectrophotometer. The amount of Malondialdehyde (MDA) in tissue samples employed in the experiment was determined by use of the formula:

$$\text{MDA} = \left[\frac{\text{Absorbance(Abs)} \times \text{Volume of extraction (mL)}}{\text{Extinction coefficient } (\epsilon) \times \text{light path (b)} \times \text{Weight of plants (g FW)}} \right] \times 1000$$

Where $\Delta\text{Abs} = \text{Abs}_{532} - \text{Abs}_{600}$

$$\epsilon = 155 \text{ mM}^{-1}\text{cm}^{-1}$$

$$b = 1 \text{ cm}$$

FW = fresh weight of plant

$$\text{Units} = (\mu\text{g}/\text{FW})$$

3.4 Statistical analysis

All treatments were carried out in replicates of three and results were presented as mean standard deviation. The means of the treatments were compared by one-way ANOVA and Tukey's multiple range tests ($p < 0.05$). Analyses were performed with the SPSS 18.0 program (SPSS Inc., Chicago, USA).

CHAPTER IV

RESULTS AND DISCUSSION

4.1 Characterization of gold nanoparticles from *T. triandra*

In order to confirm the success of the plant extract employed in the ex situ synthesis process, characterization was carried out. Characterization not only confirms presence or absence of a nanoparticle but helps to shed light on the particles nature and the possible mechanism of synthesis. In this light, characterization in this experiment was perform on such basis.

4.1.1 TEM studies for *T. triandra* aided synthesis AuNP

To carryout TEM studies, the shape and size of nanoparticles were studied as functions of temperature, concentration and volume of *T. triandra* leaf extracts. By varying temperature of the reaction, as seen in Figures 4.1 – 4.3, nanoparticle size and shape composition is altered. At ambient temperatures (25°C), nanoparticles are mostly spherical-shaped along with plate structures (e.g. triangles, hexagon and nonagon). Gold nanotriangles might have resulted from rapid reduction, assembly and room temperature sintering of spherical shaped gold nanoparticles (Philip, 2009). At higher temperatures, plate structures tend to be fewer; meanwhile, spherical and pseudo-spherical structures tend to be the most dominant. Figure 4.1 – 4.3 shows the corresponding size distribution histograms of Figure 4.8A – C. While size distribution in all cases was very wide, the size of the nanoparticles in the majority increases with

rising temperatures. For example, particle sizes in the majority for ambient, 65°C and 80°C are 10, 20 and 60 nm, respectively. Gold nanoparticle average sizes were equally observed to increase with increasing temperatures (Table 4.1). This trend can be related to the Ostwald ripening – a thermodynamically-driven spontaneous process (Byravand and Kharat, 2014). It is a phenomenon wherein, molecules on the surface of particles in solution, due to being energetically unstable are dissolved and deposited on larger particles. Deposition comes into the fore when the solution is supersaturated with the said particles. The end result is an increase in the average particle size.

At different concentrations of the synthesis reaction, the temperature was kept constant. Spherical and pseudo-spherical structures were present in all synthesis process and constituted the majority (Figure 4.9A – C). Plate structures existed alongside spherical and pseudo-spherical shaped nanoparticles. Nanoparticles synthesized with a plant extract concentration of 50% had the least average size in comparison with other nanoparticles synthesized by varying concentration. The nanoparticle yield under this condition was very low owing to the presence of smaller amounts of biomolecules responsible for the process of reduction. Particles synthesized with plant extract concentrations of 80% had the largest average size in this category (Table 4.1). A close examination of size distribution graphs for both conditions equally reveals that the predominant particle size tends to increase across the board; that is 20 nm and 60 nm respectively (Figure 4.4 – 4.5). At 100% of the plant extract, the primary particle size is 20 nm (Same condition as Figure 4.1B). The absence of trend under this category makes it hard to explain the mechanism at play here.

Spherical and pseudo-spherical shaped nanoparticles were observed in all synthesis processes that entailed varying the volume of the plant extract (Figure 4.10A – C). A few plate structures were seen at plant extract volumes of 10 mL. At plant volume synthesis of 6 mL, clumping is observed, in addition to the particles not having clearly defined edges. This is because the quantity of the plant extract utilized did contain insufficient amounts of biomolecules to prevent aggregation (Khali *et al.*, 2010; Philip, 2009). The presence of sufficient biomolecules, as is the case in higher volumes of the plant extract, would have rendered stronger interactions between the protective/stabilizing biomolecules and the surfaces of the nanoparticles. The gold nanoparticle average size was largest under this condition, and least when plant volume extracts were kept at 8 mL (Table 4.1). The principal nanoparticle size for the synthesis conditions of 6 mL and 8 mL was 90 nm and 20 nm, respectively (Figure 4.6 – 4.7).

Electron diffraction patterns provide crystallographic information on the nature of a material. For example, it can be used to determine if a material is amorphous, single crystalline or polycrystalline. SAED (selected area diffraction pattern) analysis performed on the synthesized nanoparticles, revealed four bright circular rings of Bragg's reflections corresponding to the crystalline face-centered-cubic nature of gold nanoparticles (Figure 4.11). This ring pattern is associated with polycrystalline materials. As a matter of fact, ring patterns are created when nanoparticles are formed (Asadabad and Eskandari, 2016).

In the overall synthesis of nanoparticles in the current research, gold substrate metal reduction typically resulted to spherical or pseudo-spherical shaped nanoparticles being the principal shape. This is because the sphere is the lowest-energy shape (Sajanlal *et*

al., 2011). By varying experimental parameters like the concentration of the reactants (metal salt and or plant extract), reducing agents and reaction conditions such as temperature, the shape of nanoparticles can be tuned. However, the exact role these parameters play in influencing the morphology of nanoparticles is not entirely understood.

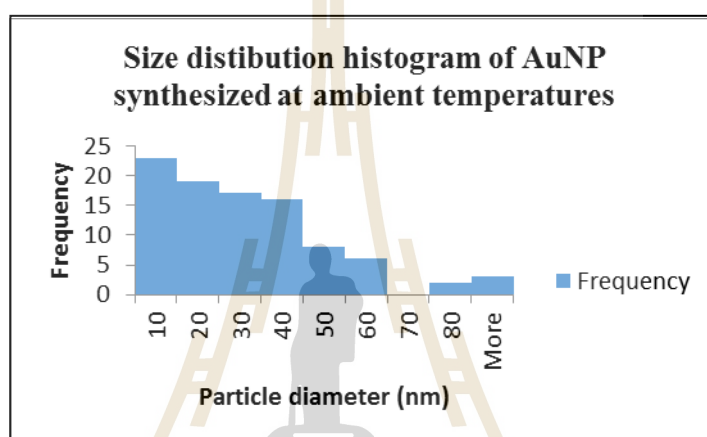


Figure 4.1 Size distribution histogram at ambient temperatures.

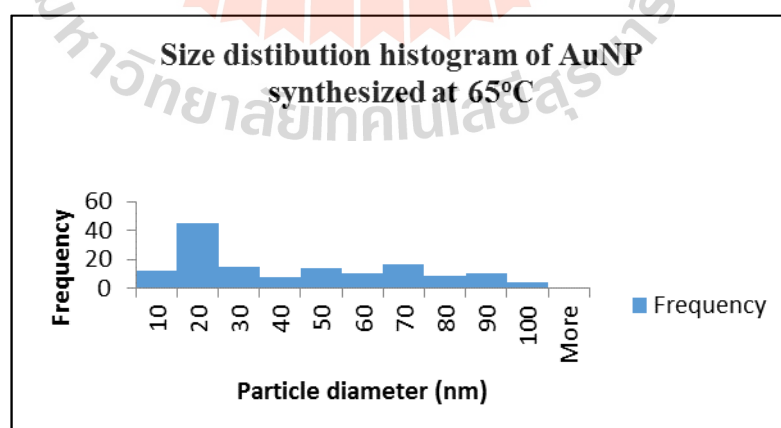


Figure 4.2 Size distribution histogram of AuNPs synthesized at 65°C.

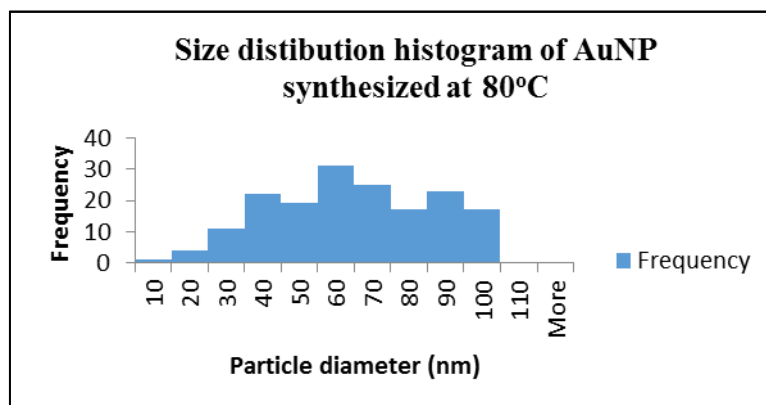


Figure 4.3 Size distribution histogram of AuNPs synthesized at 80°C.

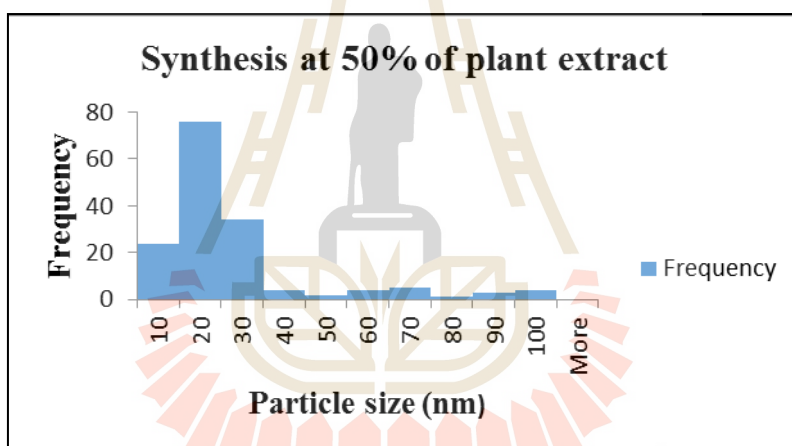


Figure 4.4 Size distribution histogram of AuNPs synthesized with 50% plant extract.

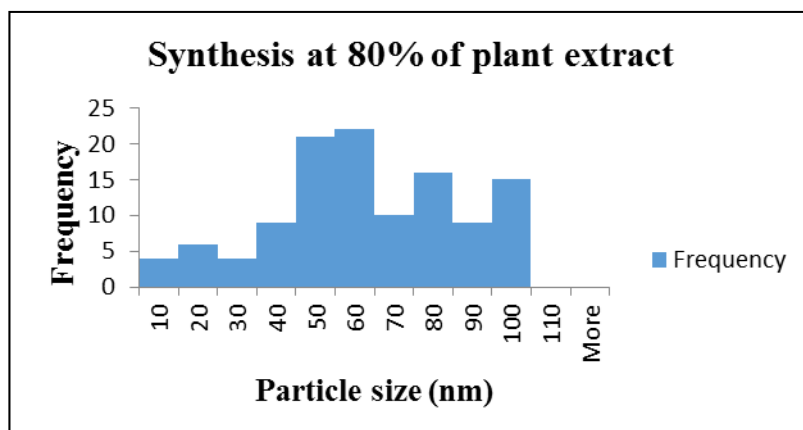


Figure 4.5 Size distribution histogram of AuNPs synthesized with 80% of plant extract.

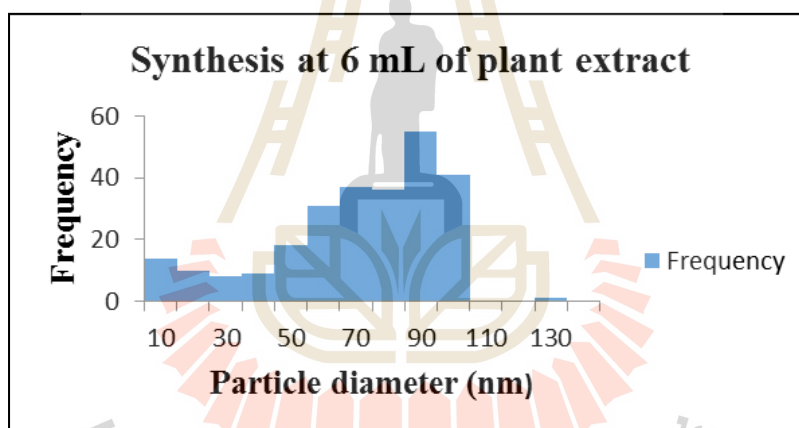


Figure 4.6 Size distribution histogram of AuNPs synthesized with 6 mL of plant extract.

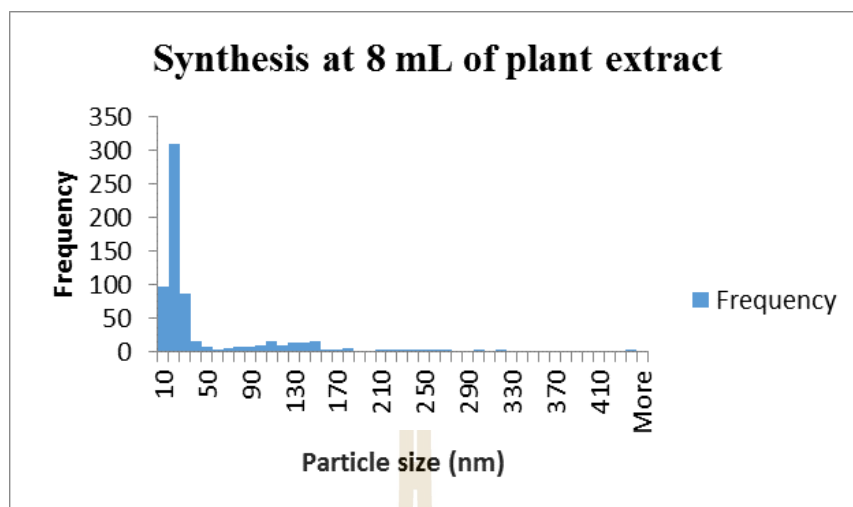
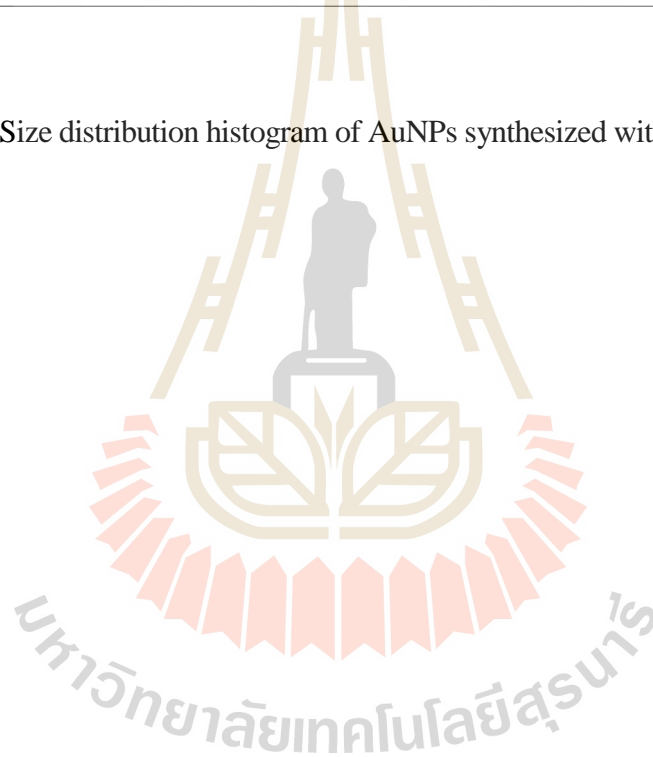


Figure 4.7 Size distribution histogram of AuNPs synthesized with 8 mL of plant extract.



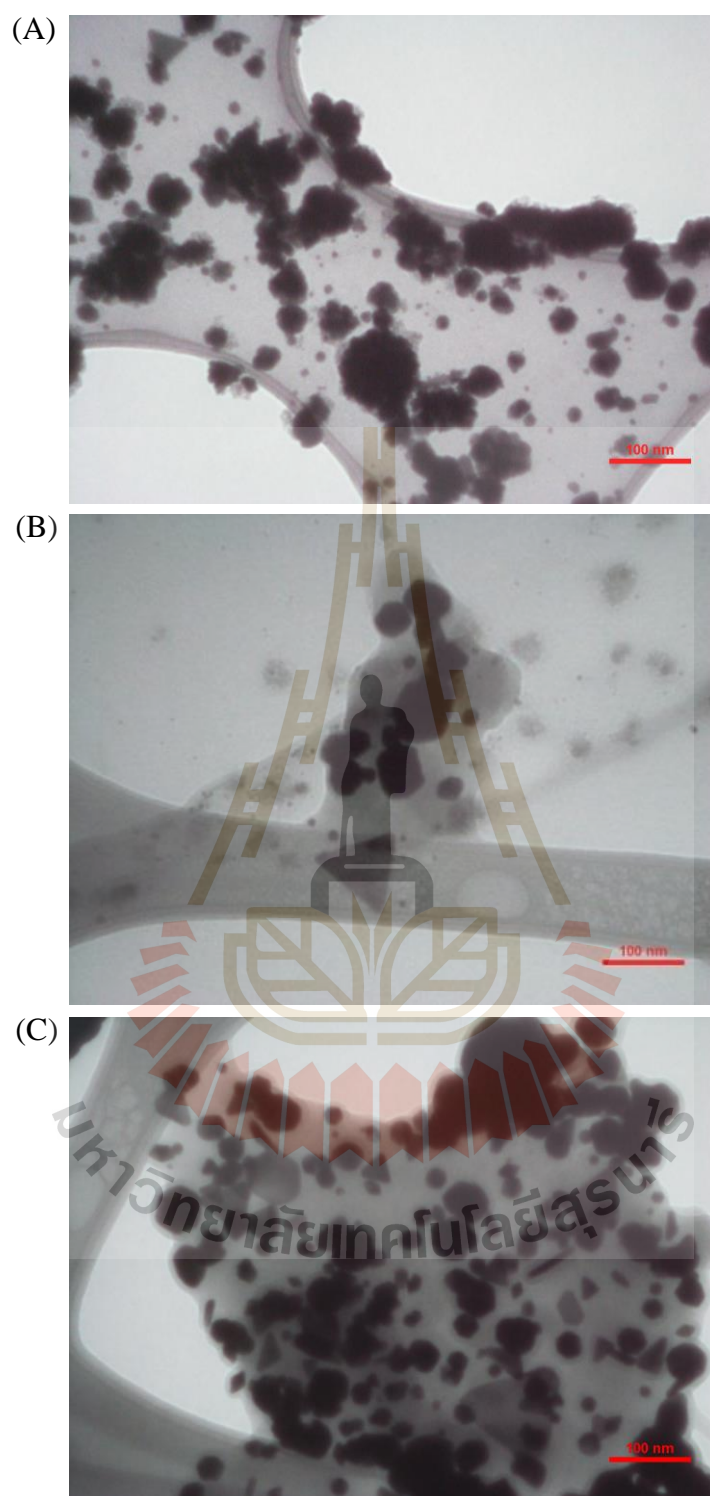


Figure 4.8 TEM images of AuNPs of varying shapes synthesized using *T. triandra* leaf extracts at temperatures of (A) 25°C (B) 65°C (C) 80°C.

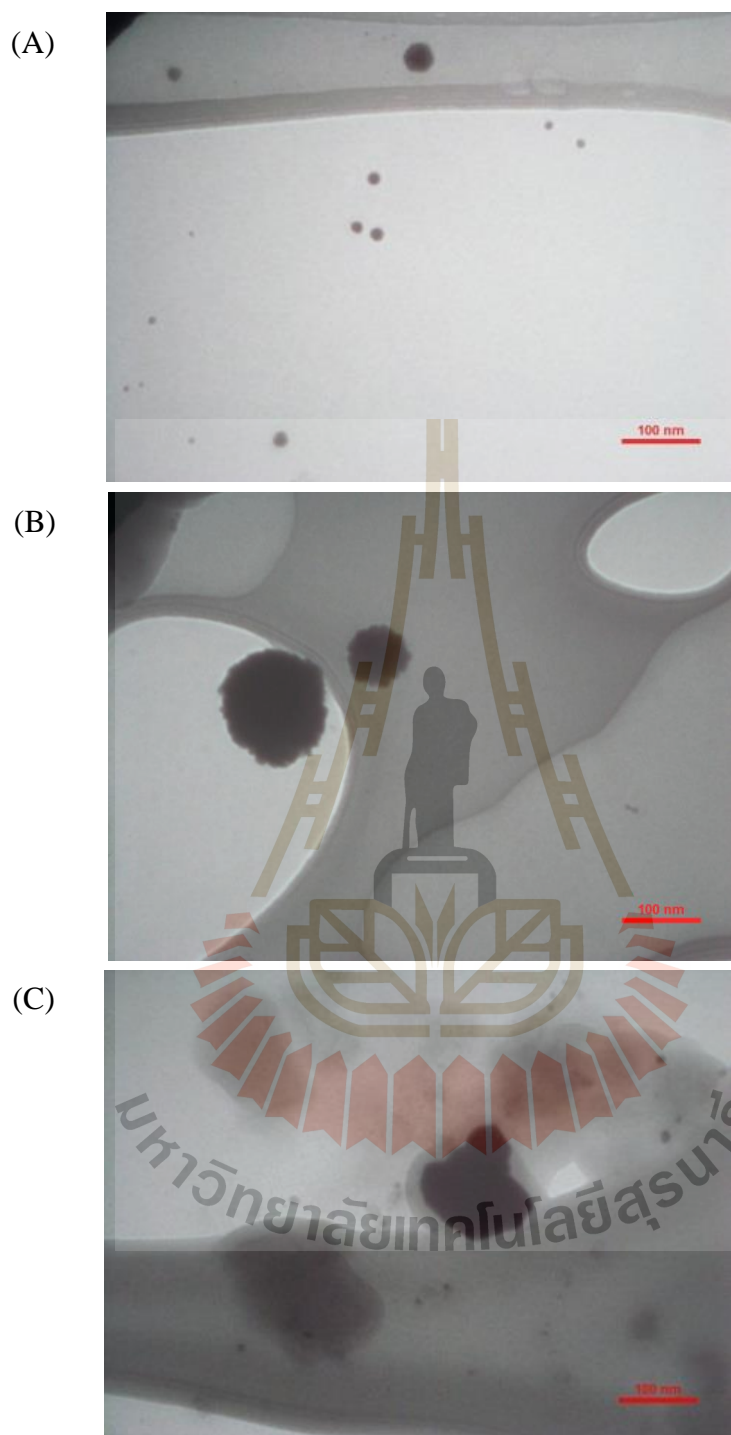


Figure 4.9 TEM images of AuNPs of varying shapes synthesized using *T. triandra* leaf extract concentrations of (A) 50% (B) 80% (C) 100%.

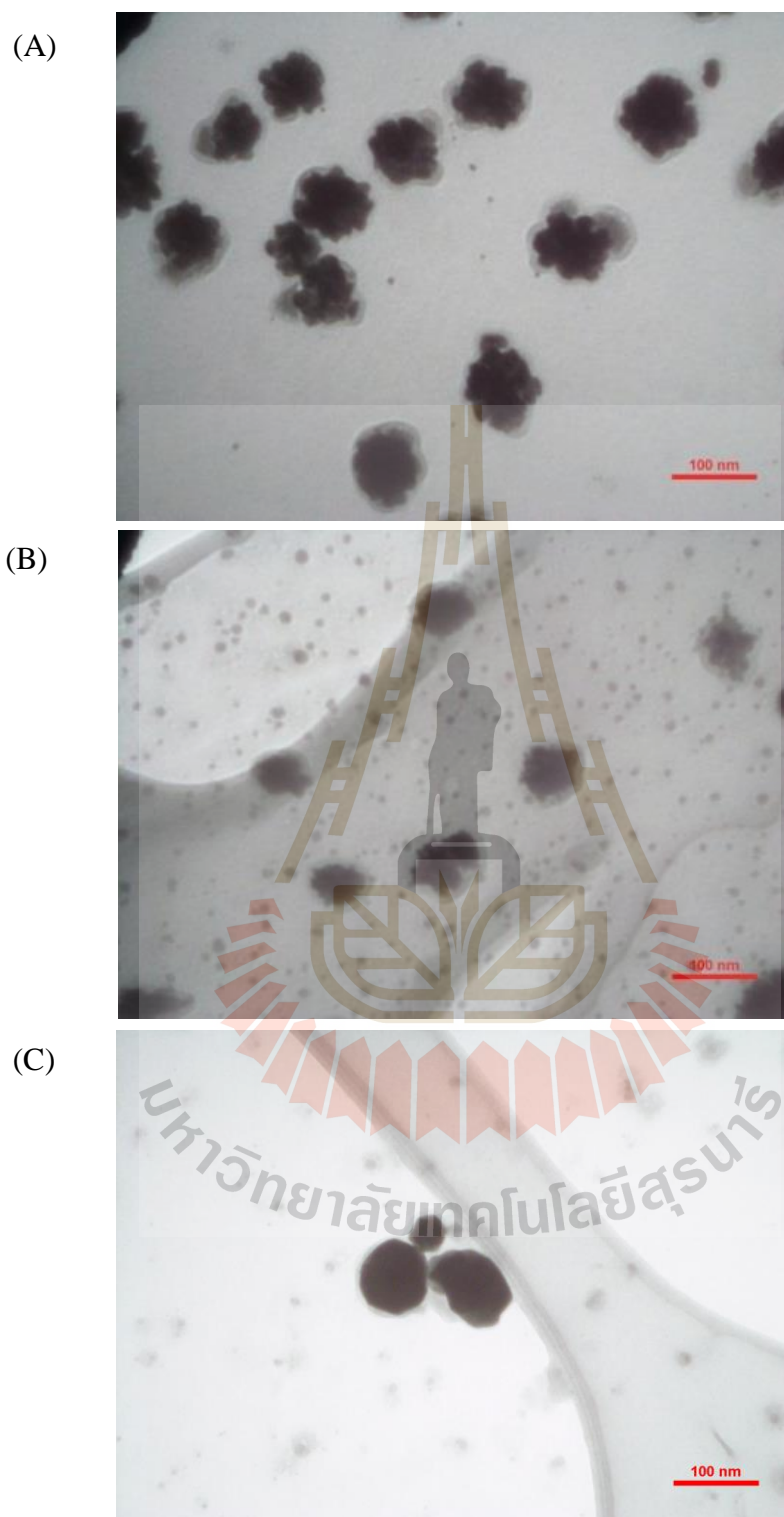


Figure 4.10 TEM images of AuNPs of varying shapes synthesized using *T. triandra* leaf extract volumes of (A) 6 mL (B) 8 mL (C) 10 mL.

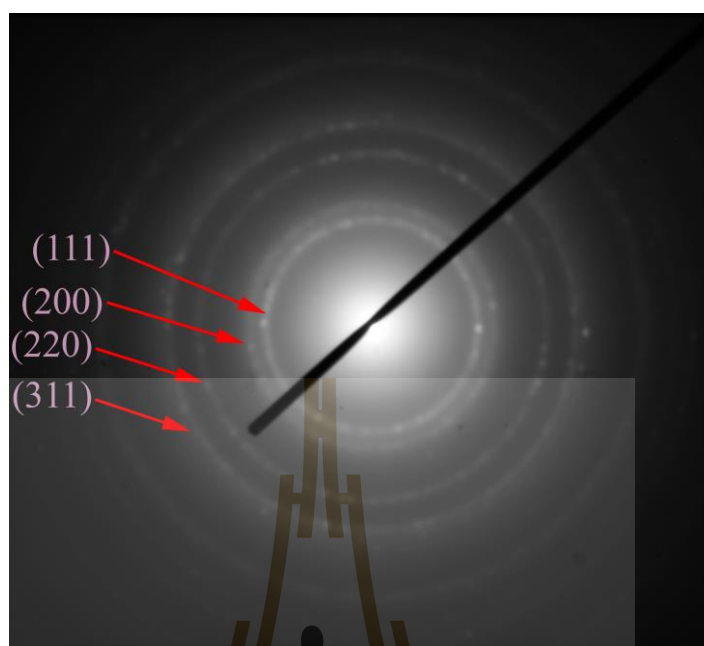


Figure 4.11 SAED pattern of *T. triandra* synthesized AuNPs.

Table 4.1 Average TEM size of AuNPs synthesized under different condition.

Synthesis condition	Average TEM size in nm
Ambient (25°C)	31.96±27.25
65°C	38.64±26.37
80°C	59.92±22.23
50%	22.92±20.50
80%	59.92±24.31
100%	38.64±26.37
6 mL	65.87±25.78
8 mL	20.19±18.96
10 mL	38.64±26.37

4.1.2 XRD patterns of gold nanoparticles synthesized with plant extract

Figure 4.12, 4.13 and 4.14 shows XRD patterns of gold nanoparticles synthesized by plant leaf extracts of *T. triandra* after complete reduction of Au^{3+} to Au^0 . The prominent Bragg reflections present can be indexed on the basis of the face centered cubic (fcc) structure of gold. The diffraction peaks at 38° , 44° , 64° and 77° correspond to the (111), (200), (220) and (311) planes of crystalline gold, respectively, indicating an fcc structure (JCPDS: 04-0784). The most intense peak corresponds to (111) plane, an indication, it is the most predominant orientation. These results are very much in line with previously mentioned SAED patterns (Aromal and Philip, 2012). The lattice parameter of gold nanoparticles synthesized under the various conditions fell within the range 4.0778 \AA to 4.0813 \AA (Table 4.2). The lattice constant or parameter is a property of crystal lattices. It is a measure of the length or angle of the physical dimensions of the unit cell of a crystal lattice.

The XRD peaks are found to be broad, an indication of gold nanoparticle formation (Jayaseelan *et al.*, 2013). Using Debye-Scherrer's equation, the average crystallite size was calculated by determining the width of the (111) peak. It was found to range between 39.9 ± 27.8 to 58.0 ± 29.3 nm (Tab 4.2). However, these values happen not to be in accord with particle size values obtained from TEM images. The difference in particle size value is owed to the instrumentation and particle structure. TEM estimates particle size, while XRD estimates crystallite region by means of the Scherrer's equation. Because a particle may consist of a single or several domains which is equivalent to a crystallite(s), agreement in measurements are only likely when particles each consist of single crystallites.

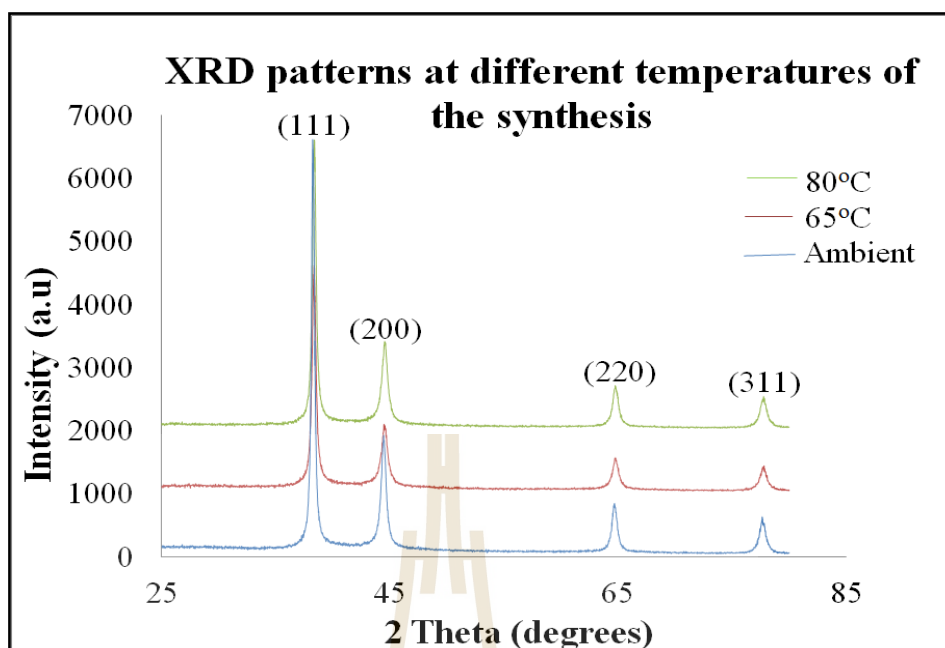


Figure 4.12 XRD patterns at different temperatures of synthesis.

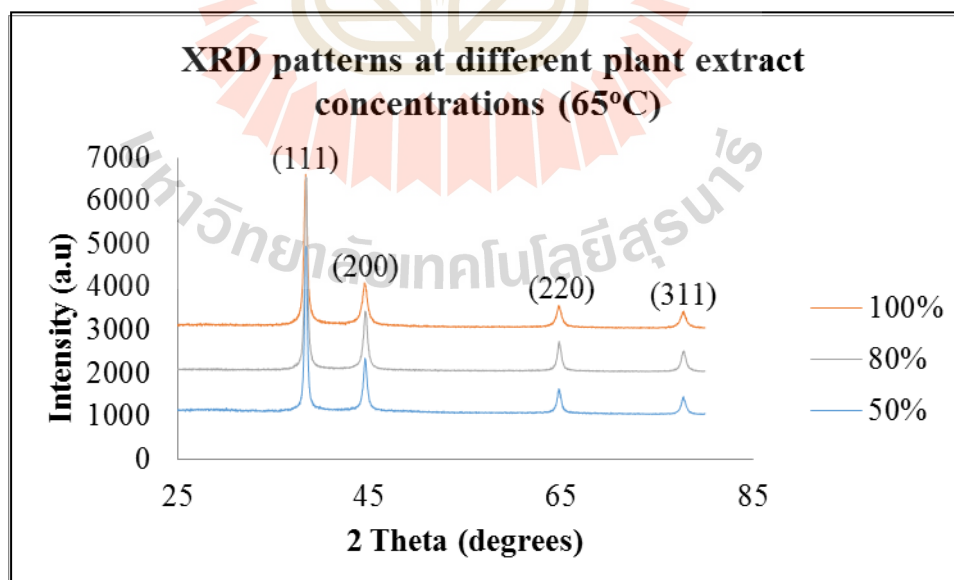


Figure 4.13 XRD patterns at different plant extract concentrations.

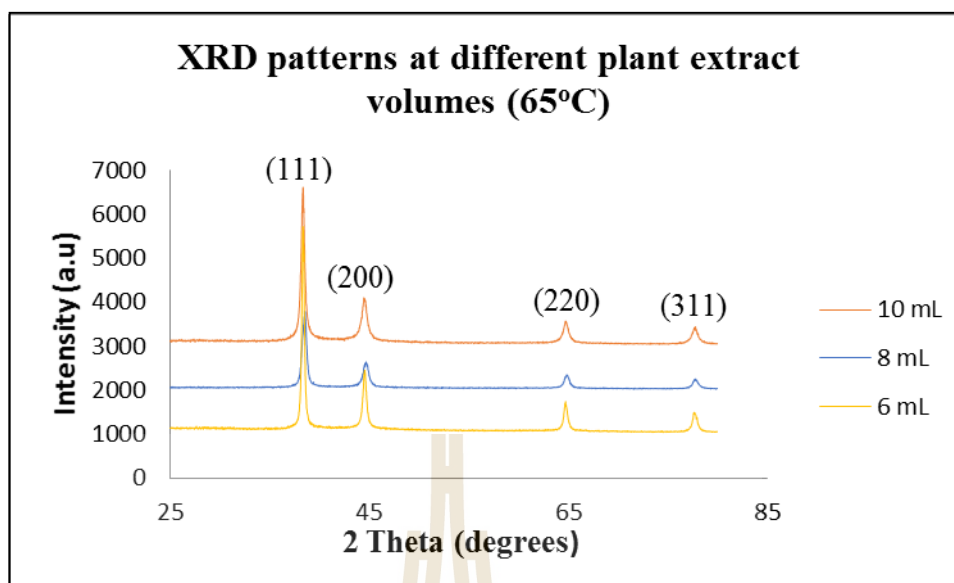


Figure 4.14 XRD patterns at different plant extract volumes.

Table 4.2 Lattice parameter and crystallite size of AuNPs synthesized under different conditions.

Synthesis condition	Lattice parameter/ Å	Crystallite size/ nm
Ambient (25 °C)	4.0778	47.18±18.28
65°C	4.0796	42.28±26.38
80°C	4.0813	39.93±27.77
50%	4.0808	43.13±21.31
80%	4.0814	43.74±18.77
100%	4.0796	42.28±26.38
6 mL	4.0813	58.00±29.34
8 mL	4.0855	43.29±18.21
10 mL	4.0796	42.28±26.38

4.1.3 FTIR spectra for *T. triandra* extract mediated synthesis

The FTIR spectra of *T. triandra* leaf extract did not show significant changes prior to and after bioreduction under the different conditions of synthesis. The FTIR spectrum of the leaf extract shows a number of prominent bands at 3279, 2363.7, 1643.7, 1551.2 and 1039.5 cm^{-1} (Figure 4.15). The intense and broad band observed at 3279 cm^{-1} is characteristic of the O-H stretching vibration which can be found in flavonoids, terpenes and ascorbic acid extracts (Aromal and Philip, 2012). The peak at 1643.7 cm^{-1} can be assigned to the amide I band which springs from the carbonyl stretch vibrations of the proteins and/or the N-H bending of the primary amines (Jayaseelan *et al.*, 2013; Patra *et al.*, 2016). This comes as no surprise since *T. triandra* is known to contain protein (Sriket, 2014). The bands at 1551.2 and 1039.5 cm^{-1} corresponds to the nitro (N-O) and cyano (C-N) groups, respectively. The C-N stretching vibration may be of the aliphatic amines or alcohol/phenols. The weak band at 2916.46 cm^{-1} corresponds to asymmetric stretching of C-H groups (Silverstein *et al.*, 1998) or amine II (Song *et al.*, 2009). The absorption band at 1250 (1234) cm^{-1} is characteristic of the amide III bands of polypeptides or protein (Shankar *et al.*, 2003).

Following bioreduction with HAuCl_4 , the bands at 1551.2 and 2363.7 cm^{-1} suppressed – an indication that the nitro functional group along with $\text{H}_3\text{O}^+/\text{C-O}$ group of *T. triandra* might have played significant roles in bioreduction (Hii *et al.*, 2011; Kumar *et al.*, 2014). The band around 2363.7 cm^{-1} can also be associated to the ionic amines $\text{C}=\text{NH}^+$ (Fayazfar *et al.*, 2013). The resulting FTIR spectra of gold nanoparticles showed bands at 535.8, 1031.7, 1234, 1524.9, 1653.9, 1734.89, 2921.28 and 3310.9 cm^{-1} along with other small bands (Figure 4.15). The aforementioned Au nanoparticle bands represent shifts from 522.8 to 535.8, 1039.5 to 1031.7, 1551.2 to

1524.9, 1643.7 to 1653.9, 1759.4 to 1734.9, 2916.46 to 2921.28, and from 3279 to 3310.9 cm^{-1} . The bands at 535.8 and 1031.7 cm^{-1} were identified as alkyl halides and aliphatic amines(C–N), respectively. The IR bands observed at 1524.9, 1653.9, 1734.89, 2921.28 and 3310.9 represents the stretching modes for N–O, C=C/N–H, C=O, C–H and O–H bonds, respectively. Shifts in the position of FTIR bands are attributed to the binding of functional groups derived from phytochemicals from the *T. triandra* leaf extracts to gold nanoparticle surface (Kannan *et al.*, 2013).

It should be noted that the bands of spectra at other conditions not shown were for the most part the same; except otherwise indicated. For example, *T. triandra*, reduced gold spectra is the poster child of all associated conditions in that category.

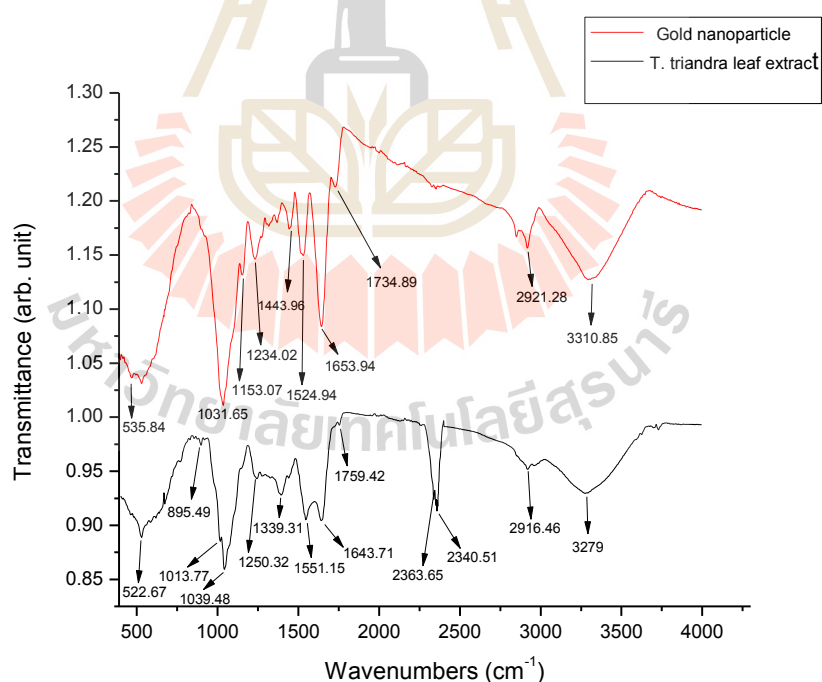


Figure 4.15 FTIR spectrum of pure leaf extract of *T. triandra* and reduced AuNPs.

4.1.4 UV-vis spectroscopy for *T. triandra* synthesized gold nanoparticles

Successful synthesis of gold nanoparticles is accompanied by a colour change. As earlier mentioned, this phenomenon of colour change is attributed to surface plasmon resonance (SPR). *T. triandra* aided synthesis of gold nanoparticle under varying conditions saw changes ranging from dark yellow to various tinges of deep brown colloid. (Figure 4.16). All the colours observed are characteristic of the SPR of the different sizes of gold nanoparticles in the solution.



Figure 4.16 Colour variation of *T. triandra* synthesized AuNPs solutions at (a) ambient temperature (b) 65°C (c) 80°C.

Figures 4.17, 4.18 and 4.19 show the UV-vis spectra of gold nanoparticle colloids at a constant concentration of HAuCl_4 (aq) under different temperatures, concentrations and volumes of the plant extract, respectively. A number of absorptions bands within the range 570 – 593 nm were observed. Figure 4.17 shows the UV-visible spectra of gold colloids synthesized at different temperatures. The SPR band of gold colloids synthesized at the highest temperature (80°C) was

comparatively broader than those synthesized at lower temperatures (25°C and 65°C). Broader SPR bands have been linked to increased particle size (Aromal *et al.*, 2012). Crystalline size measurements obtained from XRD analysis are not in accordance with this observation. However, TEM measurements of size seem to be in line with this position. At reaction temperatures of 25°C, the absorbance peak values were blue-shifted from 585 nm to 578 nm at reaction conditions of 65°C. In reaction conditions of 80°C, a redshift was seen at absorbance peak values of 590 nm. Blueshifts are linked to decreases in particle sizes, while redshifts are associated with increases in particle sizes. Discrepancies in TEM size values between the ambient (25°C) and 65°C condition with respect to the plasmon absorbance peak values were observed though minimal.

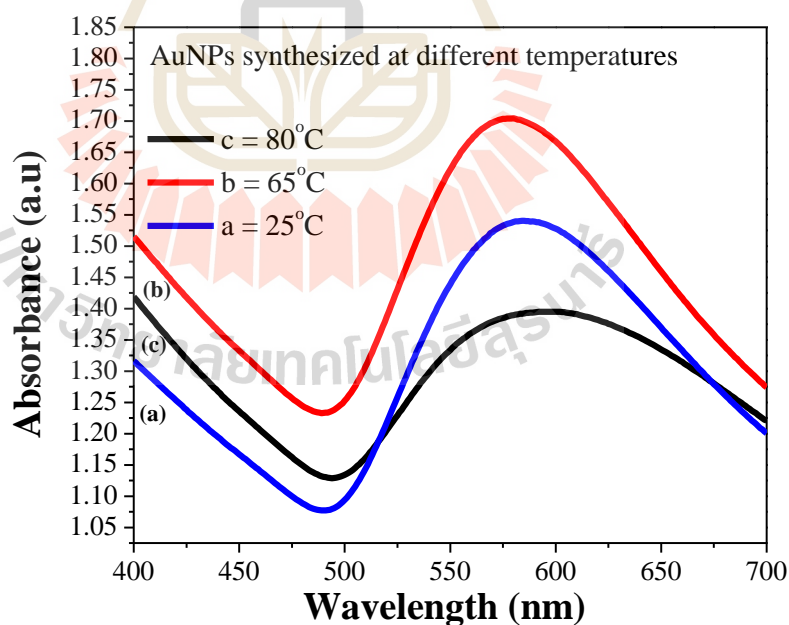


Figure 4.17 UV-vis spectra of *T. triandra* synthesized AuNPs at different temperatures.

A slight shift of the absorbance peak values in the direction of shorter wavelength region is observed with increasing concentrations of the plant extract. For example, absorbance peak values blueshifted from 597 nm through 585 nm to 578 nm for the 50%, 80% and 100% conditions, respectively. This trend is associated with a decrease in particle size. Judging from the spectra in Figure 4.18, lower concentrations of the plant extract is tied to broader SPR peaks. This is probably due to the formation of large anisotropic particles (Aromal *et al.*, 2012). The very blunt peak especially that at a concentration of 50% of plant extract is most likely due to the fact that very few nanoparticles were formed at such low concentrations of the plant extract. Intensity of SPR peaks indicates the extent of the gold ion reduction by plant biocomponents. Linearity between absorption peak and gold nanoparticle concentration, suggesting compliance to Beer-Lambert's law has been reported in the past (Zuber *et al.*, 2016). At such a low concentration of the plant extract, the biomolecules responsible for reducing the gold salt substrate was present in inadequate amounts.

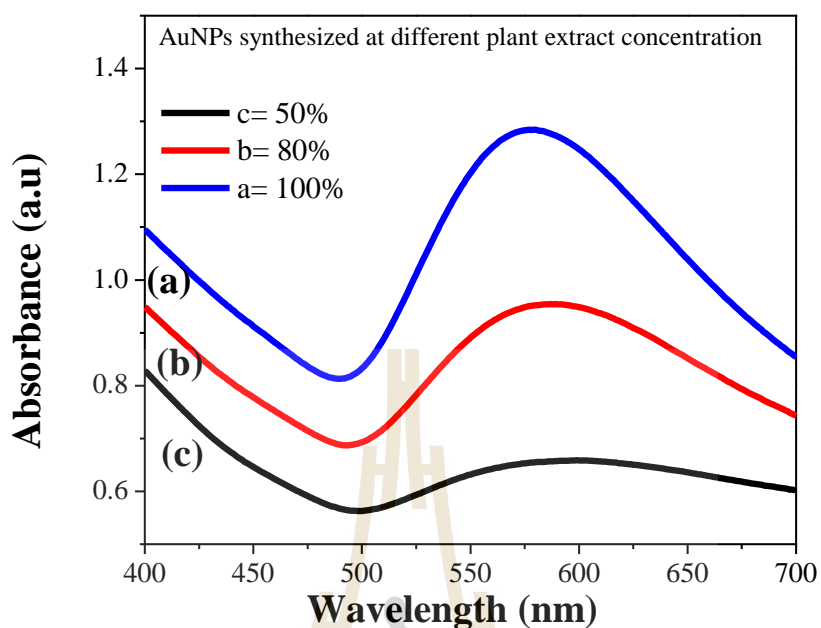


Figure 4.18 UV-vis spectra of synthesized AuNPs at different plant extract concentrations.

When the volume of the plant extract is raised, the SPR band tends to become narrower (Figure 4.19) with the narrowest absorption peak belonging to the 10 mL condition. Narrower peaks tend to be characteristic of almost spherical particles (Aromal *et al.*, 2012). As in the previous synthesis condition of plant extract concentration (50%), the blunt SPR peak of 6 mL is indicative of the degree of gold ion reduction to gold nanoparticles. It was at best minimal owing to absence of sufficient amounts of biological agents responsible for reduction.

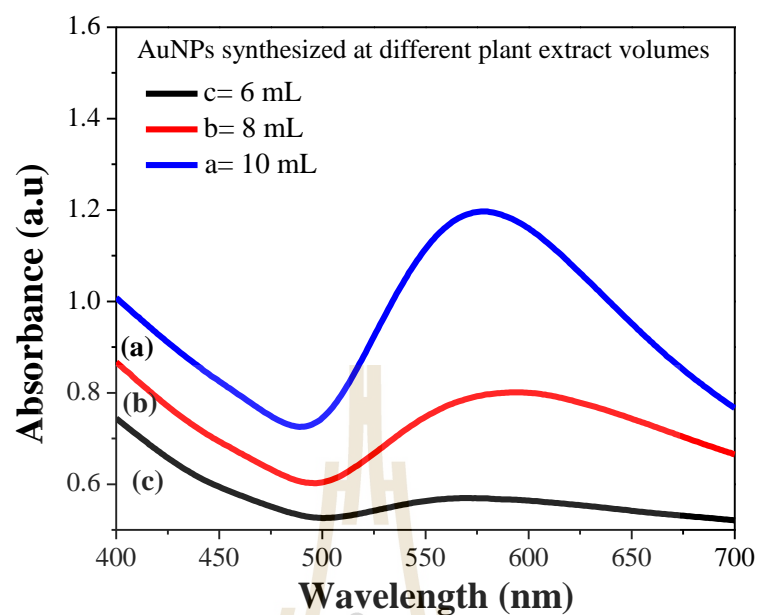


Figure 4.19 UV-vis spectra of synthesized AuNPs at different volumes of plant extract.

The sharper the absorption peak of the spectra, the more spherical the particles in the colloid tend to be. In comparative terms, the colloids synthesized from higher volumes of the plant extract contained more spherical nanoparticles. This is probably linked to the presence of sufficient amounts of biomolecules to support the reduction and stabilization process, essential to synthesis.

4.2 Characterization of gold nanoparticles synthesized from glucose/gelatin-glucose mixture

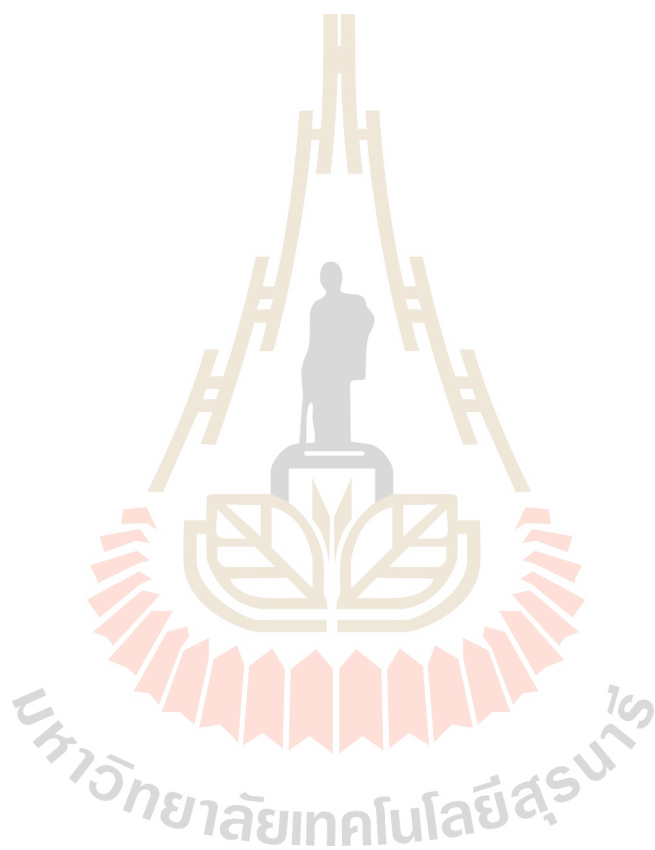
Characterization was equally done on gold nanoparticles synthesized from glucose and gelatin-glucose mixtures. It was done for the same reasons in the plant mediated synthesis case. X-ray diffraction analysis were not determined due to the sticky nature of the colloids and the difficulties encountered with preparing powdered forms of the nanoparticles.

4.2.1 TEM studies for gelatin/gelatin-glucose synthesis of AuNP

All colloids examined no matter the condition of synthesis contained a mixture of spherical, pseudo-spherical and plate structured nanoparticles. However, spherical and pseudo-spherical shaped nanoparticles were in the majority in terms of shapes (Figures 4.20A - C). Although rare, capsule-shaped nanoparticles were seen in micrographs of GR28, GR40 and GGR40.

The temperature effect on particle size of AuNP was also studied. Studies revealed that particle sizes witnessed a decrease with increasing temperatures. Comparatively speaking, particle sizes obtained in gelatin solutions were found to be smaller than those in gelatin-glucose solutions (Table 4.3). As expected, the smallest average sizes for the nanoparticles were obtained from GR60 and the largest for GGR28. The size distribution graph below illustrates the point (Figure 4.22 and 4.23). The reason for this is because reduction reaction rates are greater in gelatin solutions than in gelatin-glucose solutions (Darroudi *et al.*, 2011). Furthermore, gelatin is capable of stabilizing surfaces by forming steric barriers (Akbulut *et al.*, 2008). The benefits of a stabilized surface is the prevention of the agglomeration of nanoparticles.

The effectiveness of this ability might have been slightly compromised in the gelatin-glucose reaction by gluconic acid from glucose. Hence, gelatin-glucose synthesized gold nanoparticles were comparatively larger.



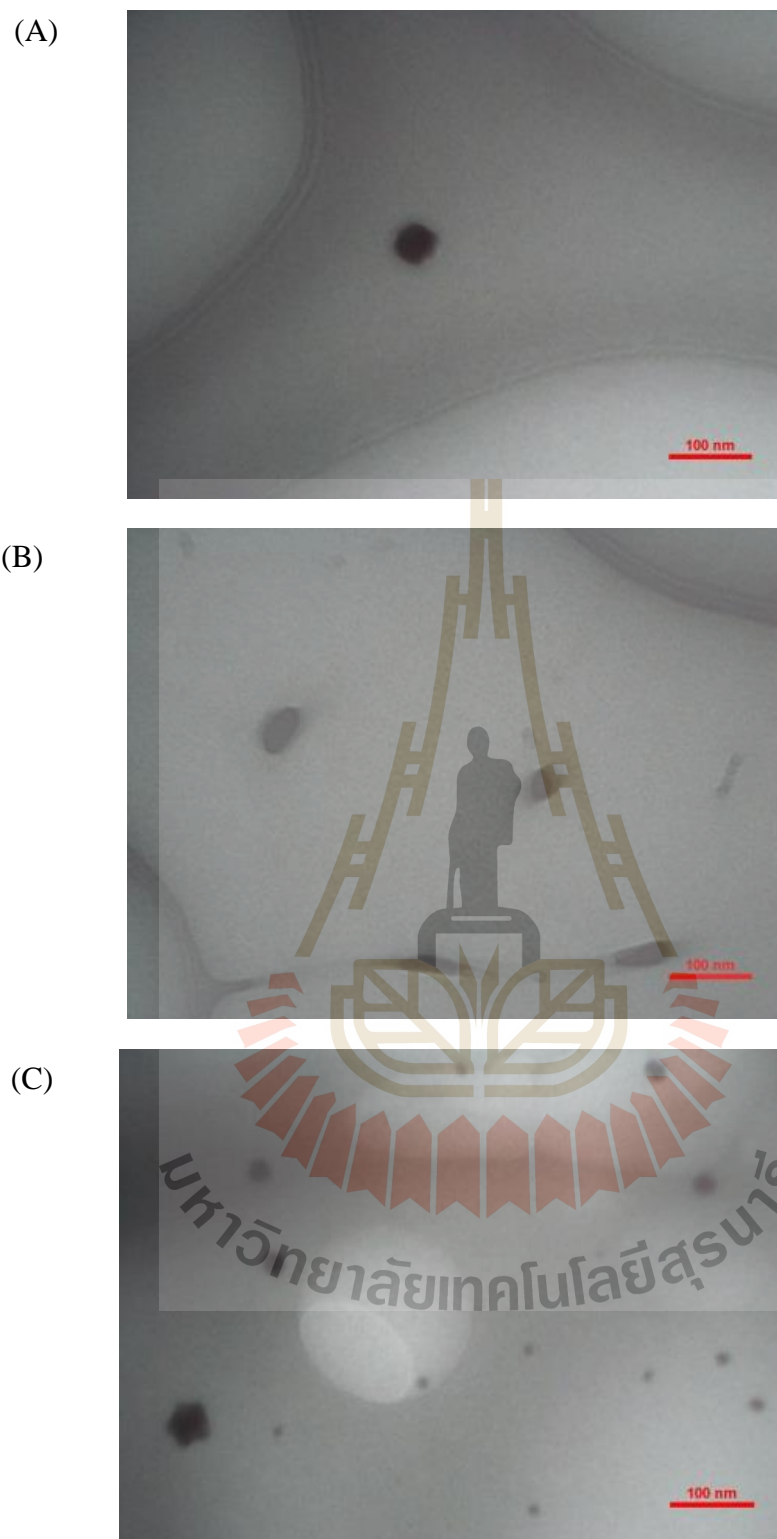


Figure 4.20 TEM images of AuNPs of varying shapes synthesized using gelatin-glucose (GGR) solution at temperatures of (A) 28°C (B) 40°C (C) 60°C.

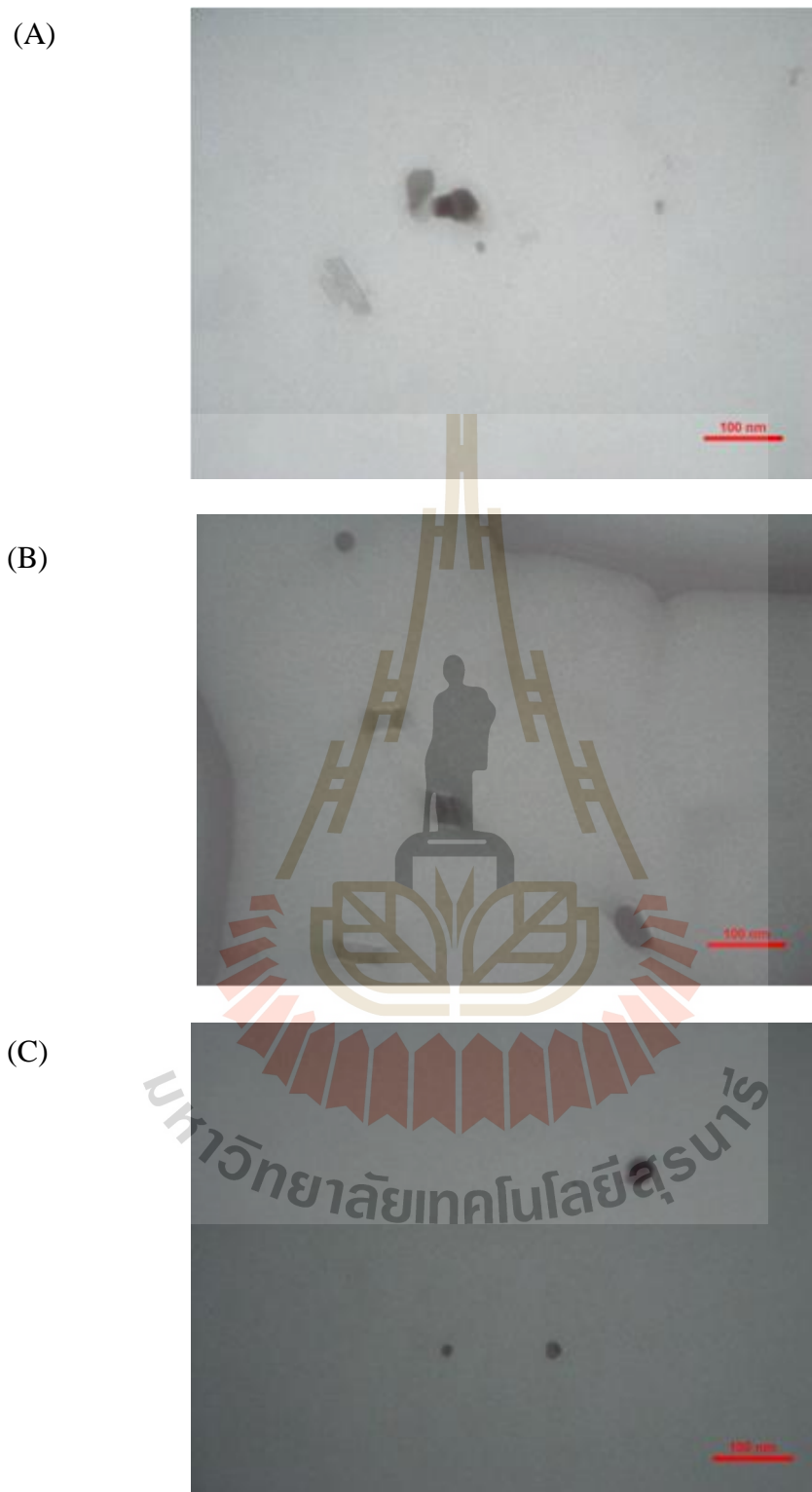


Figure 4.21 TEM images of AuNPs of varying shapes synthesized using gelatin (GR) solution at temperatures of (A) 28°C (B) 40°C (C) 60°C.

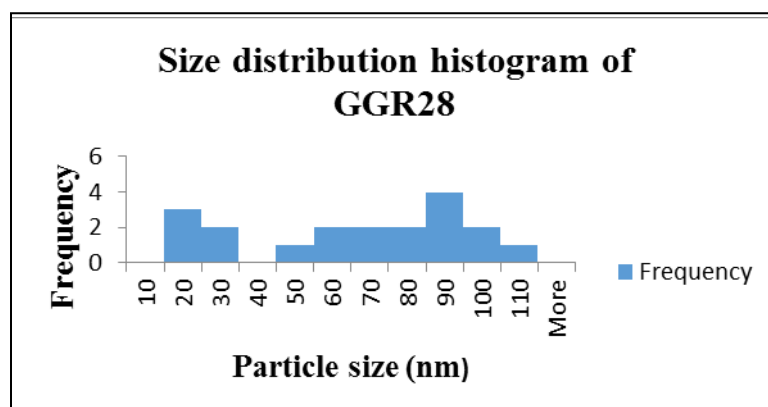


Figure 4.22 Size distribution histogram of gelatin-glucose synthesized AuNPs at 28°C

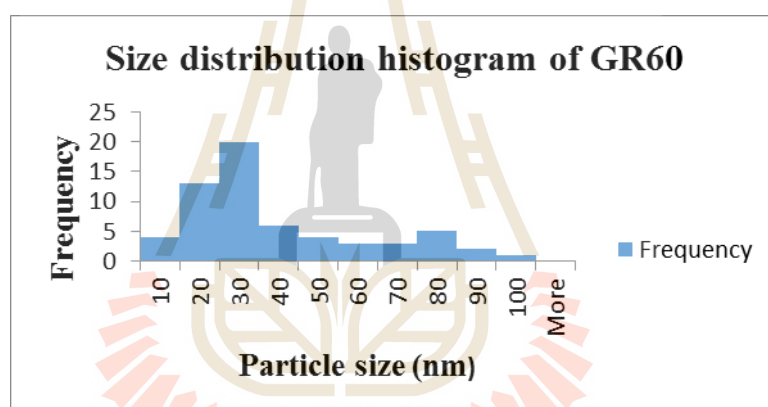


Figure 4.23 Size distribution histogram of gelatin synthesized AuNPs at 60°C.

Table 4.3 Average TEM size of AuNPs synthesized from gelatin/gelatin-glucose mixture at different conditions.

Synthesis condition	Average TEM size in nm
GR28	80.7±94.15
GGR28	119.5±112.84
GR40	64.9±31.80
GGR40	68.4±42.33
GR60	35.0±22.64
GGR60	38.6±26.19

4.2.2 FTIR spectra for gelatin/gelatin-glucose synthesized AuNPs

The FTIR spectra of gelatin/gelatin-glucose colloids showed prominent bands at 3275.4, 1646.4, 1024.1 and 1547.7 cm^{-1} (Figure 4.24 – 4.25). The IR band observed at 3275.4 cm^{-1} is characteristic of the stretching vibration of the -OH bond. The band at 1646.4 cm^{-1} can be assigned to the primary amines and the band at 1024.1 cm^{-1} , to the C–N stretching vibrations of the aliphatic amines or to alcohols /phenols. The band at 1547.7 cm^{-1} resulted from the N–O asymmetric stretch. This is no surprise given that gelatin is a protein derived from collagen.

It should be noted that the bands of spectra at other conditions not shown were for the most part similar; except otherwise indicated. GR40 and GGR60 reduced gold spectra are poster children of all associated conditions in that category. Furthermore, slight variations in the values of IR bands represented in both examples

belong to the same functional group. For example, 3275.48 and 3280 represent the –OH bond.

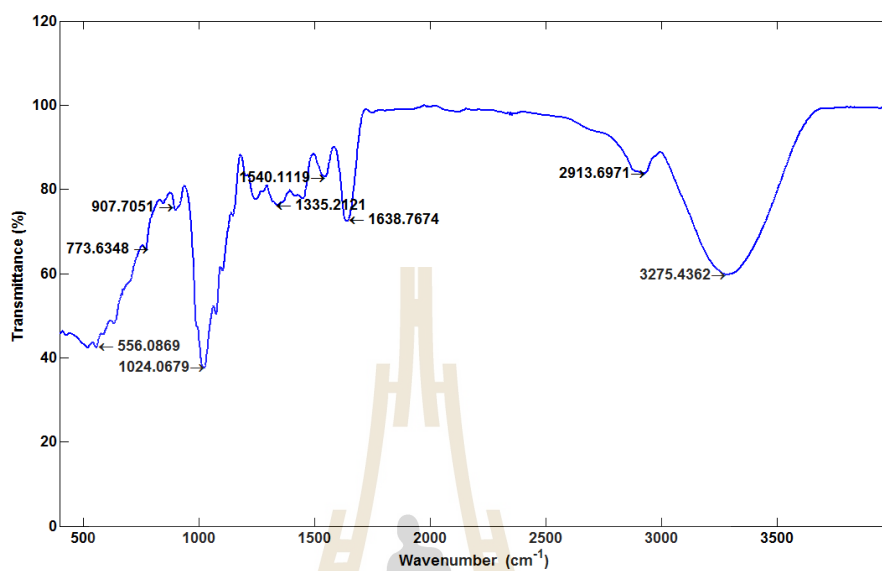


Figure 4.24 FTIR spectrum of gelatin reduced (GR) AuNPs at 40°C.

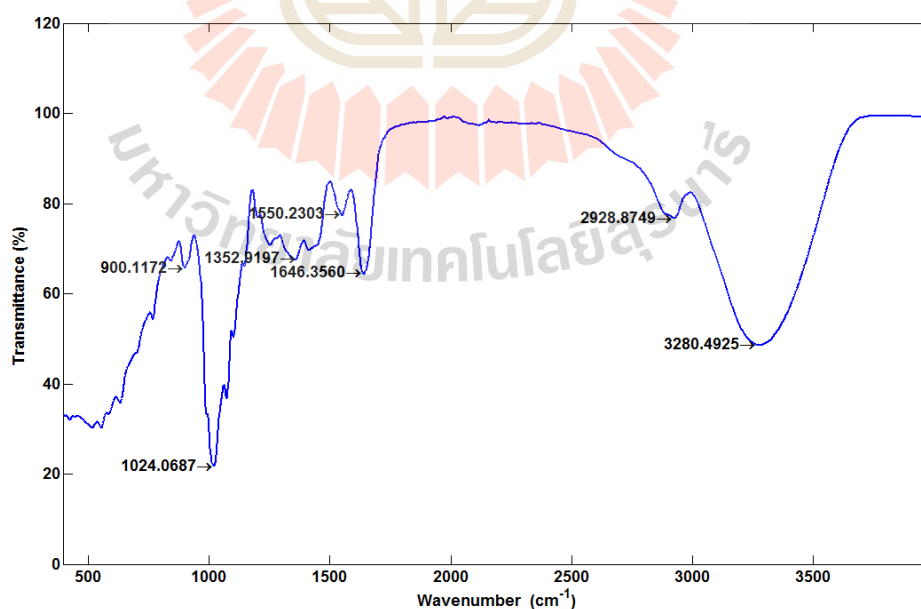


Figure 4.25 FTIR spectrum of gelatin-glucose reduced (GGR) AuNPs at 60°C.

4.2.3 UV-vis spectroscopy for glucose/gelatin-glucose synthesized AuNPs

Successful synthesis of gold nanoparticles is accompanied by a colour change. As earlier mentioned, this phenomenon of colour change is attributed to surface plasmon resonance (SPR). Changes in gelatin/gelatin-glucose synthesis transitioned from colourless, to various shades of wine red colloid upon completion of reaction (Figure 4.26). Only the gelatin/gelatin-glucose gold nanoparticle preparations at 28°C remained colourless throughout the duration of the experiment. While gold nanoparticles may have been formed, it was not sufficient enough to translate to a visible colour change. All the colours observed are characteristic of the SPR of the different sizes of gold nanoparticles in the solution.

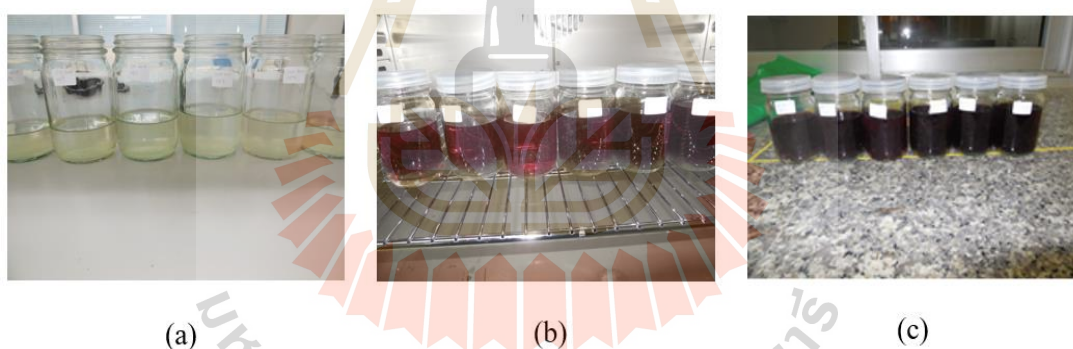


Figure 4.26 Colour variation of gelatin/gelatin-glucose synthesized AuNP solutions at temperatures of (a) 28°C (b) 40°C (c) 60°C.

The absorbance intensity of all SPR peaks increased as the reaction temperature increased for gelatin/gelatin-glucose synthesized gold nanoparticles (Figure 4.27). The increase in intensity indicates more gold ions were reduced; consequently, gold nanoparticle concentration levels were raised (Daroudi *et al.*, 2011). These suggest the existence of a directly proportional relationship between the

densities of nanoparticles in solution to the intensity of the surface plasmon peak (Basavegowda *et al.*, 2014). The Au-NPs obtained following reaction at 28°C showed SPR bands at about 563 nm and 569 nm for GR28 and GGR28, respectively. At reaction temperatures of 40°C, the λ_{\max} values were blue-shifted to 555 nm and 552 nm for GR40 and GGR40, respectively. The λ_{\max} values for GR60 and GGR60 were slightly blue-shifted and red-shifted to 552 nm and 555 nm, respectively. While blue-shifts were accompanied by a decrease in nanoparticle sizes, red-shifts are often linked to increasing particle sizes.

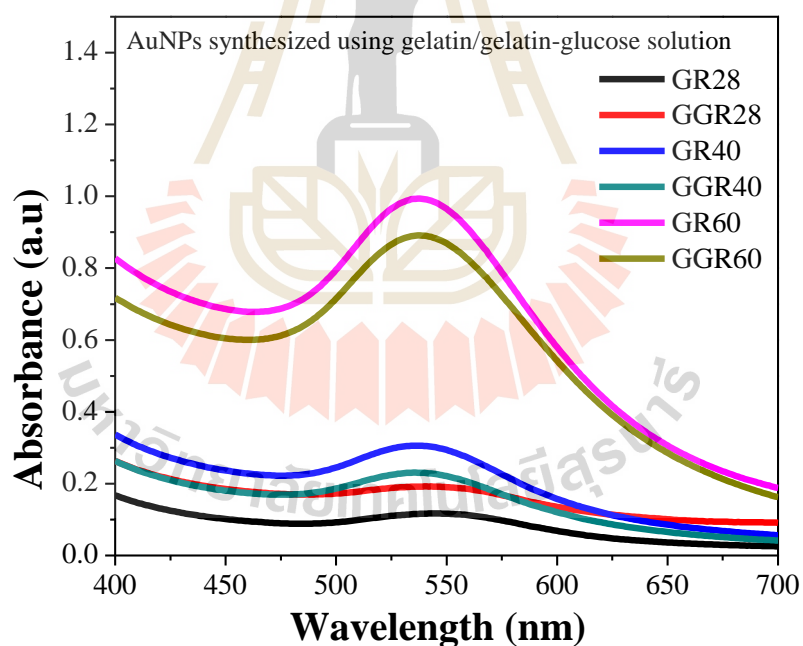


Figure 4.27 UV-vis spectra of gelatin/gelatin-glucose synthesized AuNPs.

4.3 Possible mechanism of gold nanoparticle formation

T. triandra leaf extracts have been reported to contain condensed tannins, triterpenes, flavonoids and saponins alongside other chemical compounds (Phadungkit *et al.*, 2012). The carbonyl functional group/ ionic amines furnished by the flavonoids seems to have made an important contribution to the bioreduction process. In the reduction of gold ions (Au^{3+}) to gold (Au^0) particles, the π -electrons of the carbonyl groups might be used in the absence of a strong ligating agent (Mahakham *et al.*, 2016). The flavonoids and tannins belong to a large class of chemical compounds known as the polyphenols, capable of serving as reducing agents (Aromal *et al.*, 2012). Flavonoids may equally double as stabilizing agents in aqueous medium; in addition they may as prevent agglomeration (Raghunandan *et al.*, 2009). The leaf extracts of *Dracocephalum kotschyi*, which share some phytochemicals with *T. triandra*, such as the flavonoids, terpenoids, saponins and tannins have been used to synthesize gold nanoparticles (Dorosti and Jamshidi, 2016). Terpenoids are an immense and varied class of naturally occurring organic chemicals present in all classes of living things (Song *et al.*, 2009). They might have contributed to chloroaurate ion reduction by oxidation of their alcohol groups to carbonyl groups (Shankar *et al.*, 2003). Besides being capable of reduction, terpenoids have been reported to be able to cap and stabilize biosynthesized gold nanoparticles. Proteins via free amines or cysteine residues in saponins, may have been adsorbed on gold nanoparticle surfaces, adding to stabilization (Arunachalam *et al.*, 2013).

A possible mechanism of gold nanoparticle formation likely involved the carbonyl group in conjunction with several other functional groups provided by bioactive agents in the aqueous extract, initially binds with gold ions (Au^{3+}) to form

gold complexes (Figure 4.28). These complexes are subsequently reduced to seed particles with an oxidation state of zero, i.e. Au^0 . Aggregation of the reduced seed particles then sets in, leading to the formation of clusters which end up serving as nucleation sites. The remainder of the metal ions will eventually build up around these centers which somewhat fosters the reduction process. This later stage is referred to as secondary growth (Krishnaswamy *et al.*, 2014).

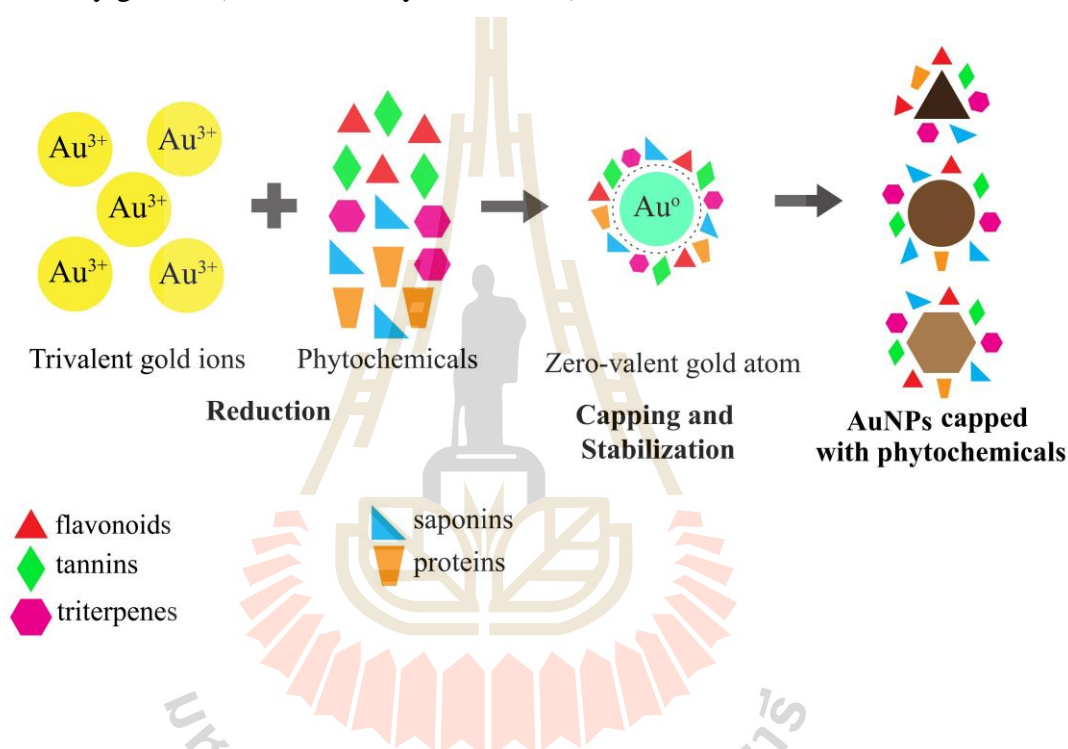


Figure 4.28 Schematic representation of possible mechanism of AuNPs synthesis (modified from Mahakham *et al.*, 2016).

The above described mechanism applies for gelatin/gelatin-glucose synthesized nanoparticles except that the biomolecules that played a leading role in the reduction process varies.

4.4 Gold nanoparticle effect on rice seedlings

T. triandra synthesized gold nanoparticles at temperatures of 80°C were used in the treatment of rice grains. Nanoparticles synthesized under this condition had a size range of 10 – 100 nm. However, the majority of these nanoparticles had a size range of 60 nm. The primary motivation for choosing nanoparticles synthesized under this condition is owed to the rate of synthesis and yield upon completion. Furthermore, nanoparticles synthesized under this condition were predominantly spherical in shape. Hence, are thermodynamically more stable (Elaissari, 2008).

Upon ultrasonic dispersion of the appropriate amounts of gold nanoparticles in distilled water, the pHs of the respective suspensions was determined. Increasing concentrations of gold nanoparticles in the various suspensions were accompanied by a decrease in the pH levels (Figure 4.29). In other words, the acidity of the solutions increased with the concentration of the gold nanoparticle it contained. The least pH recorded, 4.59, was that of concentrations at 1000 mg/L. The control had the highest pH of 6.55.

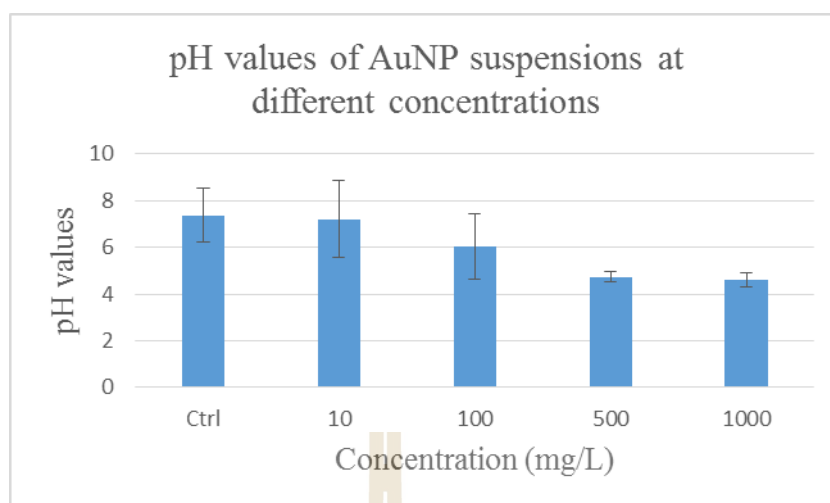


Figure 4.29 pH value of nano-gold suspensions at different concentrations.

Both the root and shoot length of the rice seedlings were determined at the end of the experiment which lasted seven days. The highest average root length recorded, 6.2 cm, was that of the control (Figure 4.30). At 5.6 cm, the average root length of grains grown at concentrations of 500 mg/L was the least. Judging by the nature of plant root response to dose, a non-threshold relationship was observed (Figures 4.30 and 4.31). In non-threshold dose-response relationships, any dose produces a response (Forshier, 2009). A decrease in the overall growth of *B. juncea* seedlings treated with increasing concentrations of citrate stabilize gold nanoparticles has been reported in the past (Gunjan *et al.*, 2014). Drawing from the explanation of the researchers of the said article, the average root length of rice seedlings might have experienced a decline due to the channeling of a portion of the metabolic resources destined for normal growth and development to processes engaged in mitigating toxicity triggered by the likes of gold nanoparticles. Despite the comparative decrease in root lengths upon

exposure to gold nanoparticles with respect to the control, all such differences were statistically insignificant (Table 4.4).

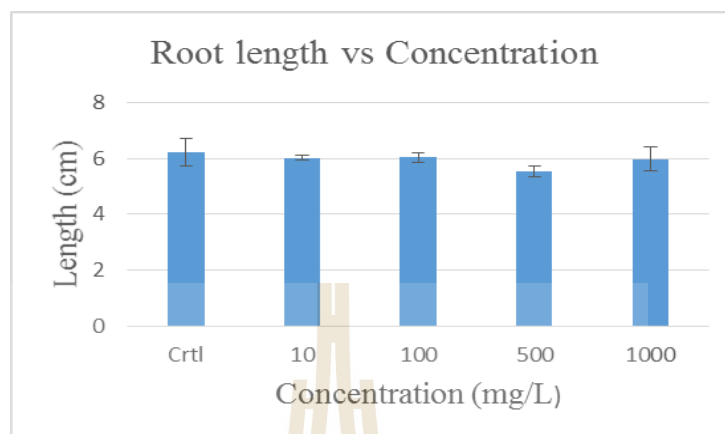


Figure 4.30 Seedling root length upon exposure to AuNPs.

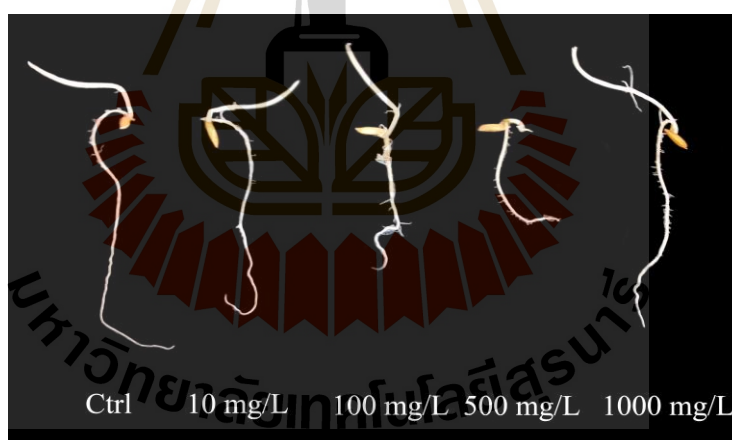


Figure 4.31 Untreated and treated rice seedlings after seven days of germination.

The highest shoot length for rice seedlings recorded was that of the control (Figure 4.32). The concentration of 100 mg/L yielded the least average shoot length of 3.0 cm. The average shoot length for the experimented treatments (excluding

phytotoxicity concentration) fell within a range of 3.0 to 3.41 cm. Much like in the case of root length, a non-threshold dose-response relationship was observed. Differences in shoot length were statistically insignificant as well (Table 4.4).

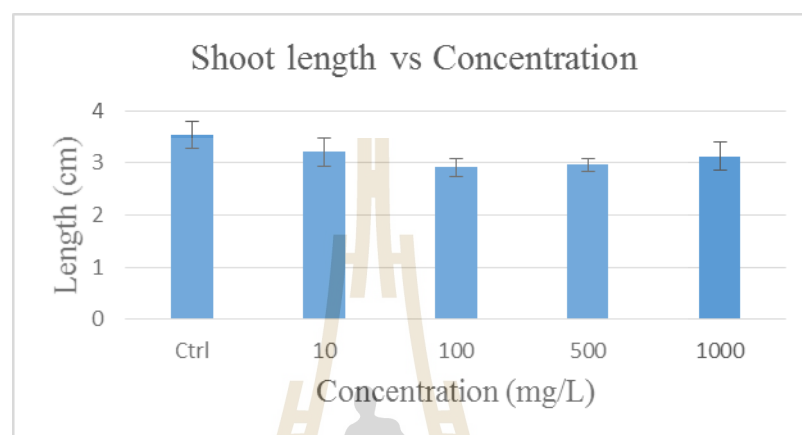


Figure 4.32 Seedling shoot length upon exposure to gold nanoparticles (AuNP).

The percentage germination of rice grains upon exposure to the nanoparticles at various concentrations ranged between 93.09 to 98.08% (Figure 4.33). Despite the acidic nature of certain suspensions, seed germination, shoot length and root length were only subtly affected with respect to the control. Germination of the grains remained high despite the acidic nature of the suspensions at high concentration due to the protection the seed coat affords the embryo and its selectively permeable property (Lin and Xing, 2007). Gold nanoparticles are known to be capable of increasing the permeability of seed coats which could in turn boost the germination process/seed germination and metabolic activity (Gopinath *et al.*, 2014). The germination and metabolic activity increment comes from the easier access to water and oxygen. *Glorosia superba* seeds treated with gold nanoparticles synthesized from

Terminalia arjuna fruit extracts, spherical in shape with a size range of 20-50 nm, benefited from this potential, according to research published by Gopinath *et al.* (2014). A possible reason why rice grains in the present study did not profit from the seed germination boost gold nanoparticles impart might have been due to the combined nature of the nanoparticles and the seed coat. Wang *et al.* (2014) reported similar results of citrate gold nanoparticles having a benign effect on germinating rice seeds. During germination, the radicles of seedlings are known to emerge before the shoots. That amounts to roots being exposed to the toxic effect of the nanoparticles longer. However, relative root elongation values ranged from 90.94% to 100% (Figure 4.34), suggesting the severity of toxicity is very minimal. Contrary to our findings, Wang *et al.* observed citrate synthesized gold nanoparticles inhibit rice root elongation despite being present in comparatively lower concentrations. It therefore stands to reason that, the rate of germination along with other measured parameters, was probably a product of a combination of some of the aforementioned reasons.

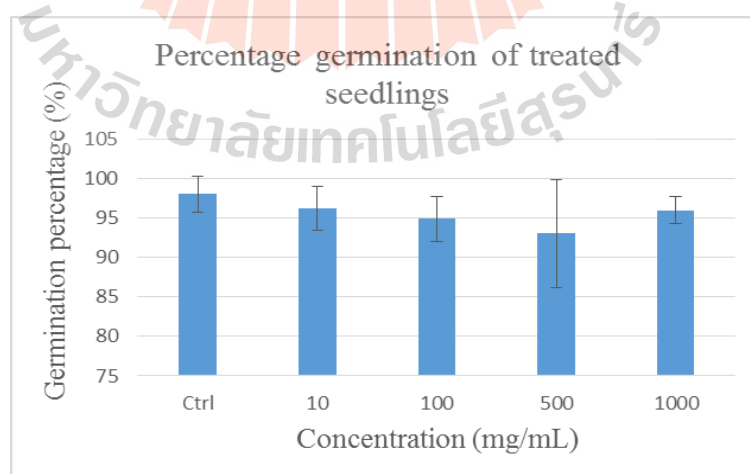


Figure 4.33 Percentage germination of AuNP treated seedlings.

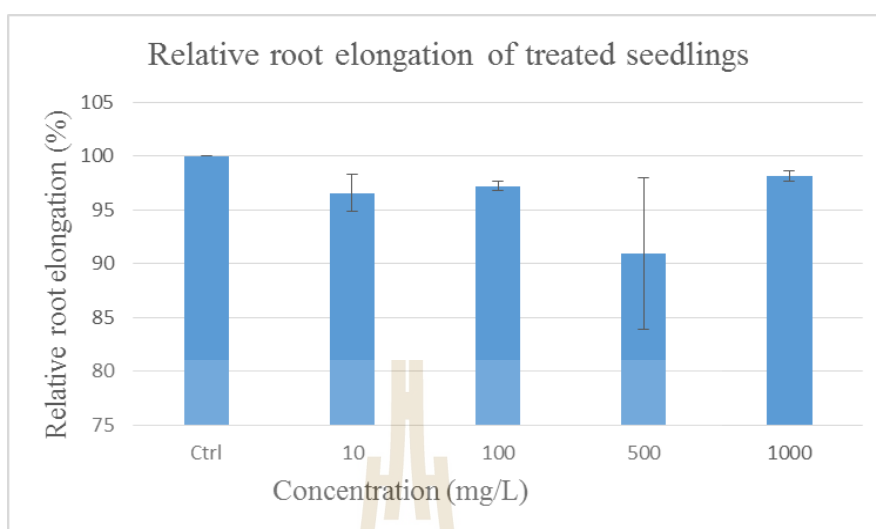


Figure 4.34 Relative root elongation of AuNP treated seedlings.

Table 4.4 Values are means \pm SD (n=3) of germination percentage, relative root elongation, root length and shoot length of rice seedlings under different concentrations of gold nanoparticles. Means with the same letter are not significantly different at Tukey's test ($p \leq 0.05$).

AuNP concentration (mg/L)	Germination percentage (%)	RRE (%)	Root length (cm)	Shoot length (cm)
0	98.08 \pm 2.27a	100 \pm 0a	6.21 \pm 0.49a	3.53 \pm 0.26a
10	96.27 \pm 2.76a	96.54 \pm 1.73a	6.02 \pm 0.08a	3.21 \pm 0.27a
100	94.97 \pm 2.85a	97.20 \pm 0.45a	6.03 \pm 0.17a	2.91 \pm 0.17a
500	93.09 \pm 6.84a	90.94 \pm 7.06a	5.53 \pm 0.18a	2.96 \pm 0.13a
1000	96.02 \pm 1.71a	98.10 \pm 0.48a	5.98 \pm 0.41a	3.13 \pm 0.26a

4.4.1 Determination of germinated seedling relative water content

Formerly referred to as relative turgidity, relative water content is the ratio of plant tissue fresh weight at the time of sampling, to its turgid weight. Plant water status can be assessed by the relative water content technique (Smart and Bingham 1974).

The average relative water content of rice seedlings in this experiment fell within the range of 64.98% to 79.90% (Figure 4.35). The least value for average relative water content belonged to the control. The 500 mg/L treatment had the highest value of 79.90%. While relative water content values for all treatments were comparatively higher than the control, no particular trend was observed (Figure 4.35). Furthermore, these differences in relative water content percentages were proven to be statistically insignificant (See appendix). Increased water uptake capacities of seeds are known to boost seed germination rates (Kumar *et al.*, 2013). It is likely that, the not significant relative water content percentages are linked to the fairly normal relative root elongation values.

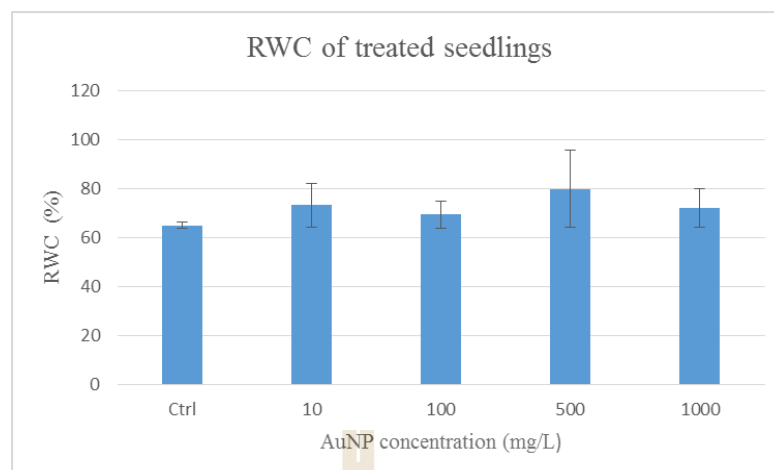


Figure 4.35 Relative water content of AuNP treated seedlings.

4.4.2 Cell death evaluation

Crucial to any plant's development is cell death, which starts off as early as female gametophyte formation (Steffens and Sauter, 2009). Cell death events transcend beyond this early stage to include later stages such as root cap development and the shaping of leaves. In as much as it being a natural order of a plant's existence, abiotic stresses such as heavy metals, heat and ozone can induce cell death. Cell death evaluations are generally performed to assess the outcome of the interaction between biological systems and abiotic stressors (Baker and Mock, 1994).

The spectrophotometric determination of cell death hinges on the ability of dead cells to retain Evans blue stain. Therefore, by measuring absorbance, the extent of cell mortality can be indirectly gauged. Spectrophotometric absorbance was observed to increase in seedlings that had been exposed to greater concentrations of the gold nanoparticles (Figure 4.36). This means, higher mortality of root cells was incurred with increasing concentrations of nanoparticles. In spite of the perceived

differences in the extent of viability and root sensitivity to toxic substances, it was statistically insignificant (See appendix). These results fall in line with the previous proposition that, gold nanoparticles are not harmful.

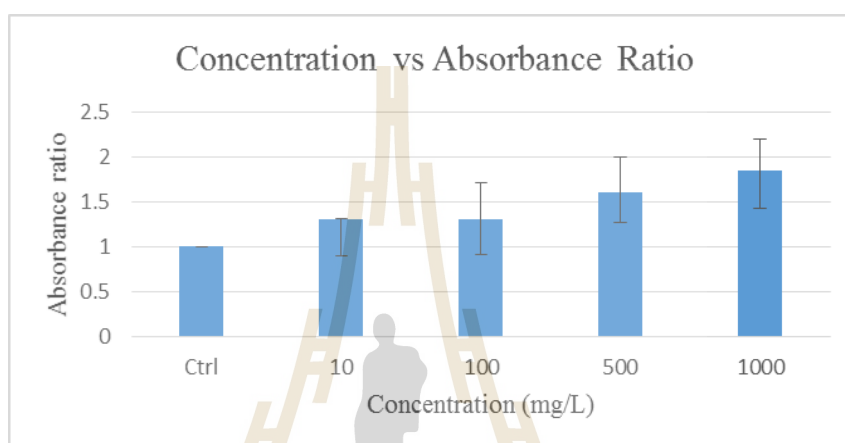


Figure 4.36 Cell viability extent following AuNP treatment.

4.4.3 Determination of the effects of seed soaking and incubation on root elongation

A number of experiments were devised to determine the extent to which the process of soaking and incubation had on root elongation; along with establishing the phytotoxicity of *T. triandra* synthesized gold nanoparticles. The root elongation measurements obtained from rice grains subjected to the first treatment (soaked in AuNPs suspension and incubated in distilled water) proved to be the highest at 6.62 cm (Figure 4.37). This probably is as a result of the minimal trigger/stress brought about by the shorter exposure time to the gold nanoparticles during the soaking

period. This trigger was probably sufficient enough to encourage germination once incubation resumed in distilled water.

At an average root length of 5.29 cm, grains subjected to the second treatment (soaked in distilled water and incubated in AuNPs suspension) threw the least in comparison (Figure 4.37). Perhaps, the longer and sudden exposure to nanoparticles during the incubation period may have set the path for a less than favourable elongation of the plant roots. The abrupt change from soaking in distilled water to incubation in a suspension of gold nanoparticles, allowing little time for adaption, may have contributed to root retardation.

The average root length for grains soaked and later incubated in gold nanoparticle suspensions (third treatment) of the same concentration stood at 6.22 cm (Figure 4.37). By comparison to the control and the two previous treatments, seedlings under these conditions fared well. It would appear that the longer duration of exposure of grains to conditions in the third treatment (soaked and incubated in AuNPs suspension) helped boost plant stress tolerance levels. Conceivably, some form of physiological adjustment may have been prompted timely enough between the processes of imbibition and germination allowing seedlings the ability to accommodate their environment.

Going by the results obtained from the respective treatments, it is safe to point out that seed incubation affects root elongation more adversely than soaking does. Furthermore, *T. triandra* synthesized gold nanoparticles were proven to be of minimal toxicity on rice plants owing to their null effect. Cell mortality in roots was highest in treatment II (B) and least in treatment III (C) (Figure 4.38). All perceived cell viability differences were statistically insignificant even at such high

concentrations (See appendix). Nanoparticle phytotoxicity is greatly influenced by factors such as the plant growth stage, physicochemical properties of nanoparticles and the nature of the exposure medium (Cui *et al.*, 2013). As oppose to agar media which are semi-solid and resemble soil, the medium of exposure used in this experiment minimally impedes nanoparticle bioavailability. In spite of this factor being in its favour, signs of phytotoxicity were not observed.

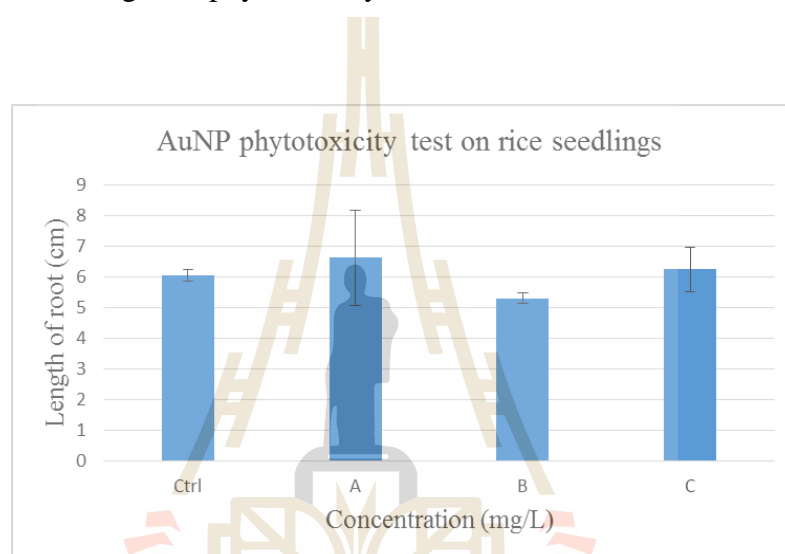


Figure 4.37 Seed soaking/incubation and phytotoxicity test on rice seedlings (A, B and C represents treatment I, II and III, respectively).

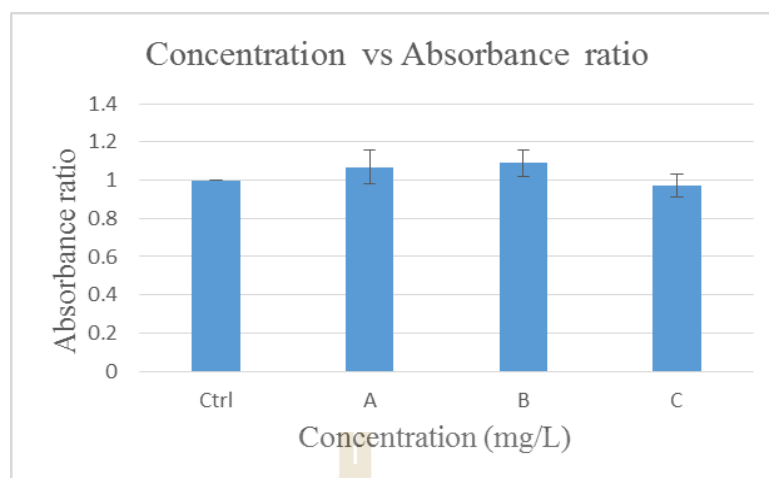


Figure 4.38 Cell viability of roots of seedlings subjected to soaking/incubation and phytotoxicity treatments.

4.4.4 Uptake of gold nanoparticles by seedling roots

The TEM technique was applied in the study of gold nanoparticle uptake in seedling roots that had been exposed to concentrations of 2000 mg/L, at both stages of soaking and incubation. Root samples of this concentration were chosen so as to increase the chances of nanoparticle observation in the plant tissue. Upon examination, gold nanoparticles, visualized as black dots, were observed in root tissue of exposed seedlings (Figure 4.39a and b). The majority nanoparticles spotted were contained in a number of organelles in the plant cell. This suggests the symplastic pathway was the primary route of uptake. The presence of nanoparticles, trapped in the intercellular region, most likely suggests the nanoparticles found their way into plant cells via the apoplastic pathway. It is equally possible that gold nanoparticles suspended in solution can be adsorbed on the root surface, and make its way into the root cell by passively passing through cell wall pores (Li *et al.*, 2016). This is very

likely because plant cell wall pores are estimated to range between 5 and 20 nm. While the average of size of nanoparticles used in the present study exceeds the cell wall pore size range, its size distribution (10 – 100 nm) was wide enough to allow to for possibility of uptake. The sonication process involved in the preparation of nano-gold suspensions equally improves uptake chances. The fact that gold nanoparticles can be taken up by rice plants has been reported (Koelmel *et al.*, 2013).

Plant's ability to take up nutrients/metals effectively is linked to the pH of soil or the medium (e.g. bioavailability in the water phase) in which it finds itself. Age equally affects the ability of roots to absorb ions. In this respect, young plants show great physiological activity than older plants of similar size (Tangahu *et al.*, 2011). The availability of micronutrients such as Zinc and Copper, elements required for certain biological processes, dwindles as alkalinity increases. These elements like gold, are considered transition metals. As transition metals, they share certain chemical properties which likely influences how plants might take up and translocate these elements. It has been reported that gold is taken up by plants in the ionic form by means of metal transporters (Taylor *et al.*, 2014). Many of these metal transporters (cation transporters) are already known to be involved in metal uptake, notably heavy metals. While no plant transporters capable of taking up gold has been found, ITR (Iron regulated transporters) transporters are suspected of being capable of taking up non-essential metal ions of gold (Taylor *et al.*, 2014). This is because these transporters (e.g. ITR1 and ITR2) show activity upon exposure to gold and are able to take up a wide range of metal cations. Tomato plants have been reported to be able to take up gold nanoparticles (Dan *et al.*, 2015). These plants are known to express the proteins LeIRT1 and LeIRT2 specifically in their roots (Hall and Williams, 2003).

This perhaps adds some validity to the presumption that these transporters are implicated in gold/ gold nanoparticle uptake. A variant of this transporter known as OsIRT1 and OsIRT2 is equally chiefly expressed in rice roots (Kim and Guerinot, 2007).

Nano-gold suspensions (2000 mg/L) used in the current research had a pH of 3.92. This decrease in pH might have resulted from the release of gold ions (Au^{3+}) by nano-gold particles owing to their size and immense specific surface area (Reidy *et al.*, 2013). Uptake of gold nanoparticles by rice seedlings in the present research might have been enabled by both the pH of the medium, which favours bioavailability, and age of the seedlings. The severity of toxicity may have been contained, amongst other mechanisms, by storage of the nanoparticles or metal ions in the vacuole (Tangahu *et al.*, 2011). This is evidenced by the presence of a majority of these particles in plant cell compartments (Figure 4.39).

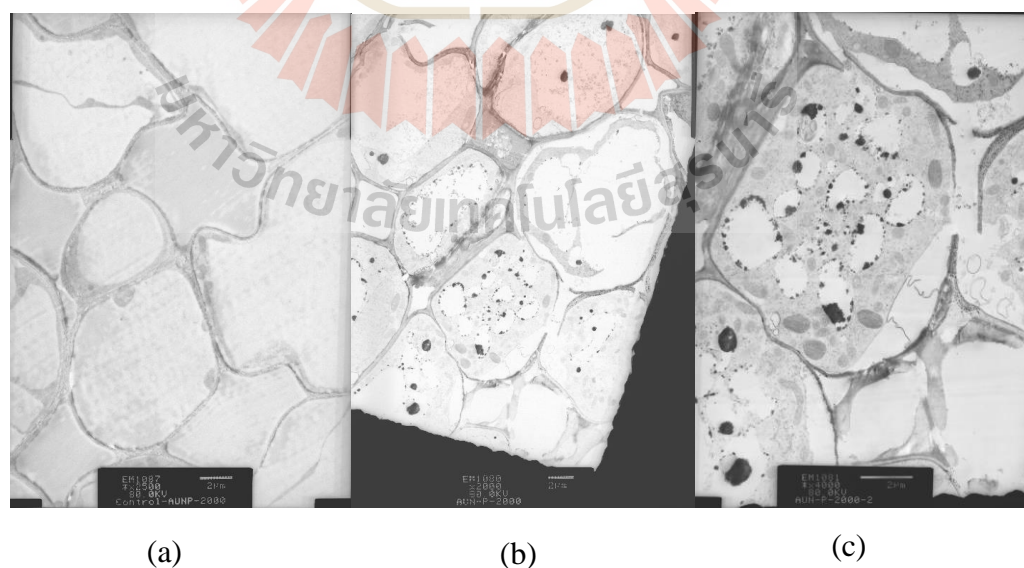


Figure 4.39 Micrograph of (a) untreated root tissue (x2500) (b) treated root tissue (x2000) (c) treated root tissue (x4000).

However, a handful of plant uptake studies involving gold nanoparticles has been carried out with different outcomes. For example, wheat plants exposed to citrate and tannate coated gold nanoparticles (10, 30 and 50 nm) did not bioaccumulate these nanomaterials in their tissues (Judy *et al.*, 2012); however, tobacco plants used in the same experiment bioaccumulated these nanoparticles. Judy *et al.* (2012) in an attempt to explain this phenomenon, established a link between bioaccumulation, aggregation of nanoparticles and the nature of plant root exudates. The gold nanoparticles used in wheat treatment were found to aggregate in the course of the treatment. This no doubt affected uptake of the nanoparticles. The results of another study involving gold nanoparticle uptake in alfalfa plants were in contrast to our findings (Taylor *et al.*, 2014). The authors of the said study reported that alfalfa plants failed to take up nanoparticles in the range 5 – 100 nm. However, gold nanoparticles were observed in plant root tissue upon exposure to a suspension of ionic gold. The researchers hinted that gold taken up in the ionic form, by means of metal transporters, undergoes reduction in the plants to yield gold nanoparticles. It is noteworthy to point out that, the authors acknowledged the soundness of their conclusions were limited to the experimental conditions employed in their study. This conclusion falls in line with the well-established fact that, the uptake of engineered nanoparticles in plants depends on their composition, shape, size and the anatomy of the plant under investigation (Ma *et al.*, 2010).

4.4.5 Hydrogen peroxide and Lipid peroxidation estimation

While hydrogen peroxide has been implicated with numerous signaling cascades in plants, it has equally been known to occur as a response to stress, be it

abiotic or biotic in origin. (Cheeseman, 2007). Aspects of plant development such as xylem differentiation, root/tissue coordination, wall loosening and cross-linking have been observed to raise hydrogen peroxide tissue levels. Furthermore, its importance as a signal molecule, capable of regulating genes engaged in defense response and other physiological processes (as previously indicated), is a reality when the compound is present in low concentrations. Hydrogen peroxide levels might be increased due to environmental stimuli such as salinization, heat stress or ozone induction (Cheeseman, 2006). Stress triggers the production of reactive oxygen species which eventually brings about hydrogen peroxide production. Examples of reactive oxygen species include superoxide anion, peroxide, hydroxyl radical and hydroxyl ion. Oxidative damage to protein, membrane lipids and other cellular components will result, if hydrogen peroxide concentration levels become exceedingly high (Habibi, 2014).

The hydrogen peroxide levels were estimated in root and shoot tissue for rice seedlings that had been exposed to gold nanoparticle at different concentrations. This is because it is widely accepted that nanoparticle toxicity is caused by excessive production of reactive oxygen species (Sharifi *et al.*, 2012). Hydrogen peroxide levels in root tissue increased with increasing concentrations of the gold nanoparticle (Figure 4.40). Hence, the control recorded the least concentration of 3.60×10^{-15} $\mu\text{g/mL}$, and the 1000 mg/L treatment peaked at a concentration of 2.68×10^{-6} $\mu\text{g/mL}$ (see standard curve in appendix). Statistical significance was not observed between the treatments (Table 4.5). This is evidence by the fact that root growth and development was hardly affected. While no particular trend was observed, every treatment had hydrogen peroxide levels greater than control (Figure 4.41). Hydrogen

peroxide levels (4.91×10^{-16} $\mu\text{g/mL}$) were highest in the shoot tissue of seedlings exposed to the 1000 mg/L concentration. However, these existing differences were not statistically compelling.

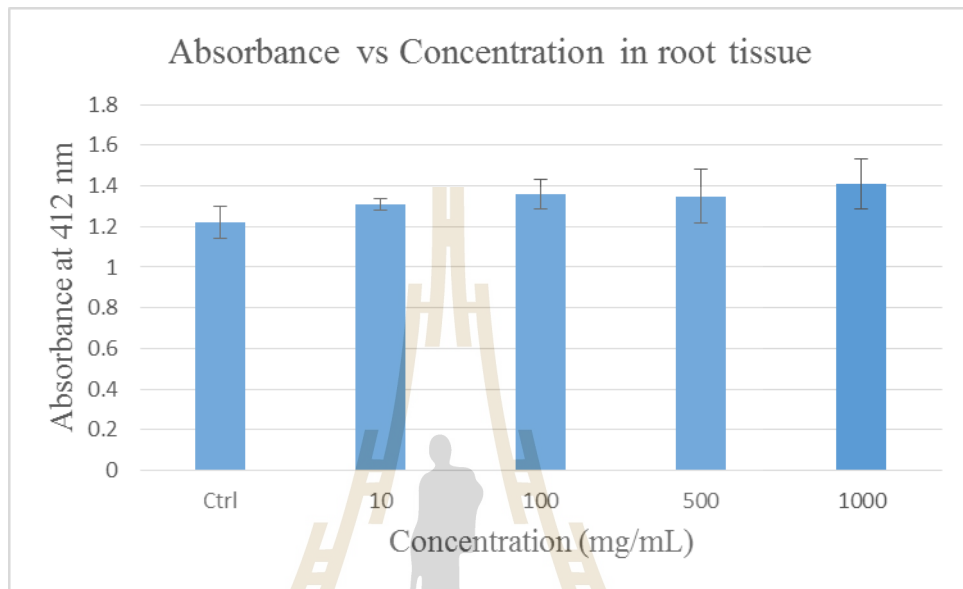


Figure 4.40 Hydrogen peroxide amount in root tissue of treated seedlings.

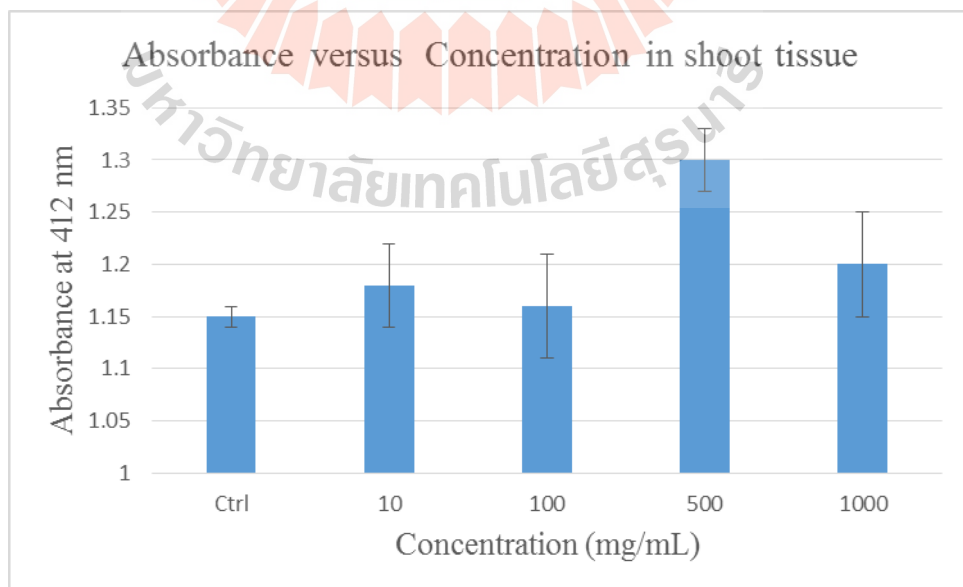


Figure 4.41 Hydrogen peroxide amount in shoot tissue of treated seedlings.

The oxidative degradation of lipids, especially polyunsaturated fatty acids (PUFA), by free radicals is known as Lipid peroxidation (Ayala *et al.*, 2014). During this process, free radicals bring about cell damage if generated in excess or left unchecked, by 'stealing' electrons from lipids in the cell membrane. The extent of damage on membranes can be ascertained by determining the level of lipid destruction under stressful conditions. Hence, by measuring the by-products of lipid peroxidation reactions obtained from polyunsaturated fatty acids such as ketones and MDA, insights on a plant's stress condition can be arrived at (Semsang and Yu, 2013).

To assess lipid peroxidation in seedling root and shoot, Malondialdehyde (MDA) quantification on these tissues were performed. The MDA quantification method employed is referred to as the TBA test. A parallel increase between MDA content of the seedling roots and gold nanoparticle concentrations was observed (Figure 4.42). On the other hand, no clear trend was noted for MDA content levels in shoot with respect to the nanoparticle treatments (Figure 4.43). In a similar experiment conducted by Gunjan *et al.* (2014), they found out that citrate stabilized gold nanoparticles brought about an increase in H₂O₂ and MDA content in *Brassica juncea* seedlings upon exposure. Contrary to the results obtained in this experiment, Arora *et al.* (2012), observed a reduction in Malondialdehyde content with respect to control in *B. juncea* seedlings with increasing concentrations (0 – 100 ppm) of gold nanoparticles. The ability of gold nanoparticles to lessen the oxidative stress of treated seedlings is brought about by improving the efficiency of electron exchange/transport reactions (Joshi *et al.*, 2011). On the other hand, the authors found no significant differences in H₂O₂ content using 10 ppm of gold nanoparticles. Above this

concentration, H₂O₂ content steadily rose, peaking with a 29% increase at a concentration of 100 ppm. In view of the duality of the outcome of plant oxidative index in the present context, the imbalance or balance between ROS generation and detoxification may very well be contingent on the type, size, concentration of nanoparticle, exposure time and the plant species in question (Iannone *et al.*, 2016).

Heavy metal ion release from nanoparticles is crucial to the phytotoxicity of metal-based nanoparticles (Cui *et al.*, 2014). Perhaps release of such gold ions from gold nanoparticles failed to cause significant rise in reactive oxygen species because of the counter effects of reducing substances of plant origin. Perhaps release of such gold ions from gold nanoparticles failed to cause significant rise in reactive oxygen species because of the counter effects of reducing substances of plant origin. In line with this, a possible reason why oxidative stress levels in the current experiment is significantly low might be linked to the antioxidant activity of *T. triandra* leaf extracts (Chaveerach *et al.*, 2016). It is highly probable that the functional groups of chemical compounds responsible for the antioxidant property of the plant might have been attached to the surface of gold nanoparticles in the course of synthesis. Hence, the insignificant increases in oxidative stress levels in root and shoot tissue upon gold nanoparticle interaction in the current experiment.

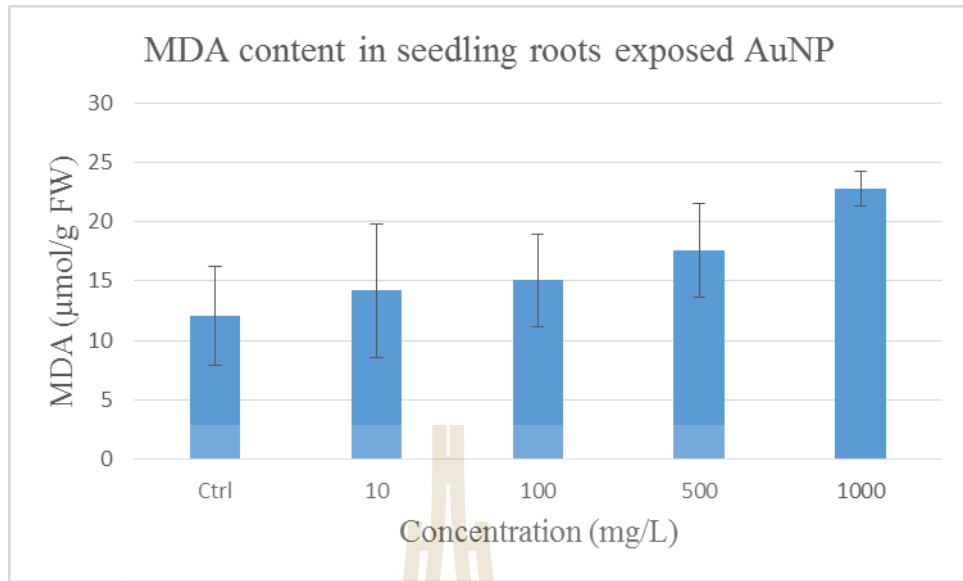


Figure 4.42 MDA content in seedling roots exposed to AuNPs.

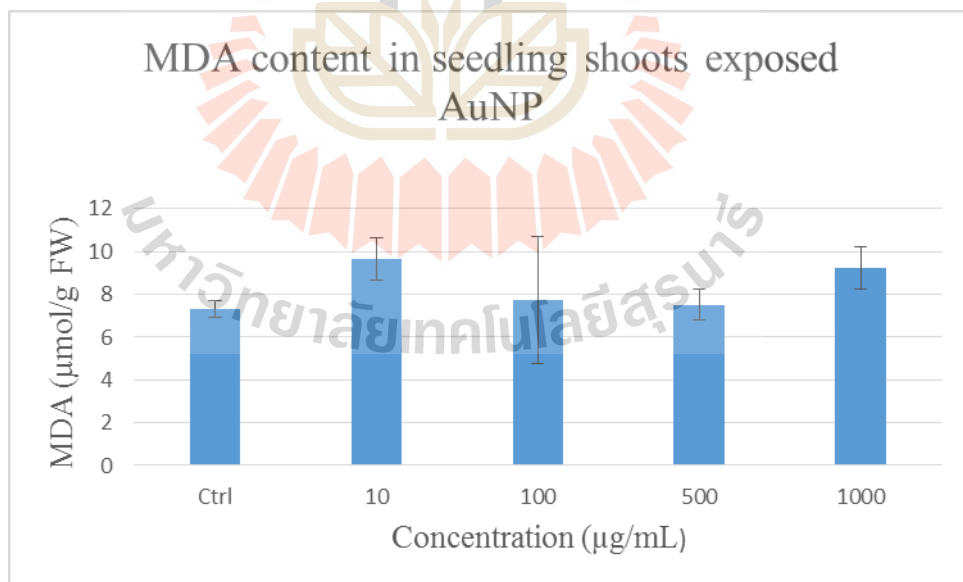


Figure 4.43 MDA content in seedling shoots exposed to AuNPs.

Two different procedures were employed to gauge stress in rice seedlings due to the shortcomings associated with both methods. For example, the unavoidable risk of interference by plant constituents in the assaying of hydrogen peroxide; with regards to MDA quantification, MDA yields from sources other than polyunsaturated fatty acids, the inability of some peroxides to form MDA and its not so specific nature, are among this method's drawbacks (Baryla *et al.*, 2000). Despite the demerits of both methods, results obtained were in accordance.

Table 4.5 Values are means \pm SD (n=3) of hydrogen peroxide and MDA amounts in root and shoot tissue of rice seedlings exposed to different concentrations of gold nanoparticles. H₂O₂ amounts in $\mu\text{g/mL}$ correspond to the absorbance amounts in graphs. Means with the same letter are not significantly different at Tukey's test ($p \leq 0.05$).

AuNP concentration (mg/L)	Root H ₂ O ₂ ($\mu\text{g/mL}$)	Root MDA ($\mu\text{mol/g FW}$)	Shoot H ₂ O ₂ ($\mu\text{g/mL}$)	Shoot MDA ($\mu\text{mol/g FW}$)
0	$3.06 \times 10^{-15} \pm 3.75\text{a}$	$12.04 \pm 2.39\text{a}$	$1.94 \times 10^{-18} \pm 0.42\text{a}$	$7.31 \pm 0.37\text{a}$
10	$5.74 \times 10^{-11} \pm 1.25\text{a}$	$14.19 \pm 3.25\text{a}$	$4.88 \times 10^{-17} \pm 1.67\text{a}$	$9.68 \pm 0.99\text{a}$
100	$1.24 \times 10^{-8} \pm 2.92\text{a}$	$15.05 \pm 2.28\text{a}$	$5.68 \times 10^{-18} \pm 2.09\text{a}$	$7.74 \pm 0.96\text{a}$
500	$4.24 \times 10^{-9} \pm 5.01\text{a}$	$17.63 \pm 3.94\text{a}$	$1.96 \times 10^{-11} \pm 1.67\text{a}$	$7.53 \pm 0.74\text{a}$
1000	$2.68 \times 10^{-6} \pm 4.17\text{a}$	$34.40 \pm 21.60\text{a}$	$4.19 \times 10^{-16} \pm 1.25\text{a}$	$9.25 \pm 0.99\text{a}$

CHAPTER V

CONCLUSION

This study had four main objectives: 1) to find a plant extract with the potential to reduce and stabilize gold nanoparticles; 2) to establish an eco-friendly protocol for the synthesis of gold nanoparticles; 3) to monitor the effect of these synthesized gold nanoparticles on germinating rice; and 4) to assess the effect of these nanoparticles on rice roots at varying concentrations and attempt an explanation to the mechanism of uptake.

The leaf extracts of *Tiliacora triandra*, a plant native to Southeast Asia, was for the first time used to synthesize gold nanoparticles under various conditions of synthesis. No additional reagents were added to assist in the process of reduction and stabilization of aqueous Gold (III) chloride trihydrate to gold nanoparticles. Characterization by use of Transmission electron microscope, UV-vis spectrophotometer, FTIR and X-ray Diffractometer were employed to prove beyond reasonable doubt that the nanoparticles obtained following the plant-mediated synthesis was gold.

Nanoparticles synthesized at temperatures of 80°C were further used to treat rice seeds. This process entailed exposing rice grains to nanoparticles at concentrations ranging from 10 mg/L to 1000 mg/L at crucial stages dubbed, soaking and incubation for a duration of seven days. At the end of the said period, gold nanoparticles were not found to interfere with germination in any way. In fact, percentage germinations lay

between 95 to 98.38%. It is thought the selectively permeable and protective nature of rice seed coat might have played an important role in keeping the germination percentage numbers high.

It is widely known that using germination parameters solely to assess the sensitivity of plants to nanoparticles has the potential for faulty conclusions. In order to avoid such a prospect, the relative root elongations of rice seedlings were determined. This is because root elongation is more sensitive, for example, than germination index, in cases where toxicity directly affects root development. While the root length of the control was the highest, there was statistically no difference when compared to seedling root lengths at different concentrations. By exposing and observing the root response of seedlings to concentrations of the nanoparticles at 2000 mg/L, phytotoxicity was determined. Based on this study, gold nanoparticles were determined to be of minimal toxicity owing to their benign effect on seedling roots.

While physical observations of the seedlings pointed to these plants being healthy, physiological tests needed to be conducted. Though cell viability of the roots of rice seedlings decreased with increasing concentrations, these changes were not out of order upon comparison with the control. Furthermore, stress levels in the seedlings were checked by measuring hydrogen peroxide and Malondialdehyde levels in their respective roots and shoots. Like in the case of cell viability, the stress levels for the various treatments were slightly higher than their controls. These differences were statistically not compelling. All experiments conducted in this study seem to lend credence to the biocompatible nature of gold nanoparticles. Numerous published studies attest to this fact. The use of an eco-friendly method to synthesize the nanoparticles

may have equally gone a long way to ensure their safe nature and mild outcome following interaction with rice seedlings





REFERENCE

มหาวิทยาลัยเทคโนโลยีสุรนารี

REFERENCES

- Akbulut, M., Reddy, N.K., Bechtloff, B., Koltzenburg, S., Vermant, J. and Prud'homme (2008). Flow-induced conformational changes in gelatin structure and colloidal stabilization. **Langmuir**. 24(17): 9636 – 9641.
- Arivalagan, K., Ravichandran, S., Rangasamy, K. and Karthikeyan, E. (2011). Nanomaterials and its potential application. **International Journal of ChemTech Research**. 3(2): 534 – 538.
- Aromal, S.A., Vidhu, V.K. and Philip, D. (2012). Green synthesis of well-dispersed gold nanoparticles using *Macrotyloma uniflorum*. **Spectrochimica Acta Part A: Molecular and Biomolecular Spectroscopy**. 85: 99 – 104.
- Aromal, S.A. and Philip, D. (2012). *Benincasa hispida* seed mediated green synthesis of gold nanoparticles and its optical nonlinearity. **Physica. E**. 44: 1329 – 1334.
- Aromal, S.A. and Philip, D. (2012). Green synthesis of gold nanoparticles using *Trigonella foenum-graecum* and its size dependent catalytic activity. **Spectrochimica Acta A**. 97: 1 – 5.
- Arora, S., Sharma, P., Kumar, S., Nayan, R., Khanna, P.K. and Zaidi, M.G. (2012). Gold-nanoparticle induced enhancement in growth and seed yield of *Brassica juncea*. **Plant Growth Regulation**. 66(3): 303 – 310.
- Arunachalam, K.D., Annamalai, S.K. and Hari, S. (2013). One-step green synthesis and characterization of leaf extract-mediated biocompatible silver and gold

- nanoparticles from *Memecylon umbellatum*. **International Journal of Nanomedicine**. 8: 1307 – 1315.
- Asabadad, M.A. and Eskandari, M.J. (2016). Electron diffraction. In Janecek. M. and Kral, R. (eds.). **Modern electron microscopy in physical and life sciences**. Available: <http://www.intechopen.com/books/modern-electron-microscopy-in-physical-and-life-sciences/electron-diffraction>.
- Audesirk, T., Audesirk, G. and Byers, B.E. (2009). **Life on Earth**. Fifth edition. Pearson Education, Inc.
- Ayala, A., Munoz, M.F. and Argüelles, S. (2014). Lipid peroxidation: Production, metabolism, and signaling mechanisms of malondialdehyde and 4-hydroxy-2-nonenal. **Oxidative Medicine and Cellular Longevity**. 6(360438).
- Boonyanitipong, P., Kositsup, B., Kumar, P., Baruah, S. and Datta, J. (2011). Toxicity of ZnO and TiO₂ nanoparticles on germinating rice seeds *Oryza sativa L.* **International Journal of Bioscience, Biochemistry and Bioinformatics**. 1(4): 282 – 285.
- Bradbeer, J.W. (1988). Seed Dormancy and Germination. **Chapman and Hall**.
- Campbell, N.A., Mitchell, L.G. and Reece, J.B. (1997). **Biology concepts and Connections**. (2nd ed.). The Benjamin/Cumming Publishing Company.
- Chaveerach, A., Lertsatitthanakorn P., Tanee, T., Puangjit, N., Patarapadungkit N. and Sudmoon, R. (2016). Chemical constituents, antioxidant property, cytotoxicity and genotoxicity of *Tiliacora triandra*. **International Journal of Pharmacognosy and Phytochemical Research**. 8(5): 722 – 729.

- Cui, D., Zhang, P., Ma, Y., He, Y., Li, Y., Zhang, J., Zhao, Y. and Zhang, Z. (2014). Effect of cerium oxide nanoparticles on asparagus lettuce cultured in an agar medium. **Environmental Science: Nano**. 1: 459 – 465.
- Counce, P. (2009). Drain rice by growth stages. **Delta Farm Press**.
- Dahlgren, R.M.T., Clifford, H.T. and Yeo, P.F. (1985). The families of the monocotyledons: Structure evolution and taxonomy. **Springer-Verlag Berlin Heidelberg**.
- Dan, Y., Zhang, W., Xue, R., Ma, X., Stephan, C. and Shi, H. (2015). Characterization of gold nanoparticle uptake by tomato plants using enzymatic extraction using followed by single-particle inductively coupled plasma-mass spectrometry analysis. **Environmental Science and Technology**. 49: 3007- 3014.
- Darroudi, M., Ahmad, M.B., Abdullah, A.H. and Ibrahim, N.A. (2011). Green synthesis and characterization of gelatin-based and sugar-reduced silver nanoparticles. **International Journal of Nanomedicine**. 6: 569 – 574.
- Dorosti, N. and Jamshidi, F. (2016). Plant-mediated gold nanoparticles by *Dracocephalum kotschyi* as anticholinesterase agent: Synthesis, characterization, and evaluation of anticancer and antibacterial activity. **Journal of Applied Biomedicine**. 3: 235 – 245.
- Dubey, S.P., Lahtinen, M. and Sillanpaa, M. (2010). Tansy fruit mediated synthesis of silver and gold nanoparticles. **Process Biochemistry**. 45: 1065 – 1071.
- Fabrega, J., Luoma, S.M., Tyler, C.R., Galloway, T.S. and Lead, J.R. (2011). Silver nanoparticles: Behavior and effects in the aquatic environment. **Environmental International**. 37(2): 517 – 531.

- Fayazfar, H., Afshar, A. and Dolati, A. (2013). Controlled growth of well-Aligned carbon nanotubes, electrochemical modification, and electrodeposition of multiple shapes of gold nanostructures. **Material Sciences and Applications**. 4(11): 667 – 678.
- Forshier, S. (2009). **Essentials of radiation, Biology and Protection**. (2nd ed.). Clifton Park, NY: Delmar.
- Gan, P.P., Ng, S.H., Huang, Y. and Li, S.F.Y. (2012). Green synthesis of gold nanoparticles using palm oil mill effluent (POME): A low-cost and eco-friendly viable approach. **Bioresource Technology**. 113: 132 – 135.
- Ganesan, R.M. and Praba, H.G. (2015). Synthesis of gold nanoparticles using herbal *Acorus calamus* rhizome extract and coating on cotton fabric for antibacterial and UV blocking application. **Arabian Journal of Chemistry**.
- Garcia, A., Espinosa, R., Delgado, Casals, E., Gonzalez, E., Puntos, V., Barata, C., Front, X. and Sanchez, A. (2011). Acute toxicity of cerium oxide and iron oxide nanoparticles using standardized tests. **Desalination**. 269(3): 136 – 141.
- Geethalakshmi, R. and Sandra, D.V.L. (2013). Characterization and antimicrobial activity of gold and silver nanoparticles, using synthesized saponin isolated from *Trianthema decandra L*. **Industrial Crops and Products**. 51: 107 – 115.
- Research and Markets (2015). **Global Nanotechnology Market Outlook 2022** [Online]. Available: <http://www.researchandmarkets.com>.
- Gopinath, K., Venkatesh, K.S., Illangovan, R., Sankaranarayanan, K. and Arumugam, A. (2013). Green synthesis of gold nanoparticles from leaf extract of *Terminalia arjuna*, for the enhanced mitotic cell division and pollen germination activity. **Industrial Crops and Products**. 50: 737 – 742.

- Gopinath, K., Gowri, S., Karthika, V. and Arumugam, A. (2014). Green synthesis of gold nanoparticles from fruit extract of *Terminalia arjuna*, for the enhanced seed germination activity of *Gloriosa superba*. **Journal of Nanostructure in Chemistry**. 4: 115.
- Gunjan, B., Zaidi, M.G.H. and Sandeep, A. (2014). Impact of gold nanoparticles on physiological and biochemical characteristics of *Brassica juncea*. **J Plant Biochem Physiol**. 2: 3.
- Hall, J.L. and Williams, L.E. (2003). Transition metal transport in plants. **Journal of Experimental Botany**. 54(393): 260 – 2613.
- Hasna, A.S., Rajiv, P., Kamaraj, M., Jagadeeswaran, P., Gunalan, S. and Sivaraj, R. (2012). Plants: Green Route for nanoparticle synthesis. **International Research Journal of Biological Sciences**. 1(5): 85 – 90.
- Hii, S.L., Estrop, L.L. and Wong, C.L. (2011). Adsorption of reactive blue 4 onto the chemically modified red seaweed *Amphiroa foliacea*: Equilibrium, kinetics and modeling studies. **International Journal of the Physical Sciences**. 6(31): 7171 – 7182.
- Iannone, M.F., Groppa, M.D., Sousa, M.E., Rap, M.B. and Benavides, M.P. (2016). Impact of magnetite iron oxide nanoparticles on wheat (*Triticum aestivum* L.) development: Evaluation of oxidative damage. **Environmental and Experimental Botany**. 131: 77 – 78.
- Iram, F., Iqbal, M.S., Athar, M.M., Saeed, M.Z., Yasmeen, A. and Ahmad, R. (2014). Glucoxylian-mediated green synthesis of gold and silver nanoparticles and their phyto-toxicity study. **Carbohydrate Polymer**. 104: 23 – 33.

- Jayaseelan, C., Ramkumar, R., Rahuman, A.A and Perumal, P. (2013). Green synthesis of gold nanoparticles using seed aqueous extract of *Abelmoschus esculentus* and its antifungal activity. **Industrial Crops and Products**. 45: 423 – 429.
- Joshi, P.K., Saxena, S.C. and Arora, S. (2011). Characterization of *Brassica juncea* antioxidant potential under salinity stress. **Acta Physiol Plant**. 33(3): 811-822.
- Judy, J.D., Unrine, J.M., Rao, W., Wirick, S. and Bertsch, P.M. (2012). Bioavailability of gold nanomaterials to plants: Importance of particle size and Surface coating. **Environ. Sci. Technol.** 46: 8467 – 8474.
- Kannan, R.R., Stirk, W.A. and Staden, J.V. (2013). Synthesis of silver nanoparticles using the seaweed *Codium capitatum* P.C. Silva (Chlorophyceae). **South African Journal of Botany**. 86: 1 – 4.
- Kharissova, O.V., Dias, R.H.V., Kharisov, B.I., Perez, B.O., Victor, M. and Perez, J. (2013). The greener synthesis of nanoparticles. **Trends in Biotechnology**. 31(4): 240 - 248.
- Kim, S.A. and Gueriot, M.L. (2007). Mining iron: Iron uptake and transport in plants. **FEBS Letters**. 581(12): 2273 – 2280.
- Koelmel, J., Leland, T., Wang, H., Amarasiriwardena, D. and Xing, B. (2013). Investigation of gold nanoparticle uptake and their tissue level distribution in rice plants by laser ablation-inductively coupled-mass spectrometry. **Environmental Pollution**. 174: 222 - 228.
- Kregling, W.F., Semmler-Rehnke, M. and Chaudhry, Q. (2010). A complimentary definition of nanomaterial. **Nanotoday**. 5(3): 165 - 168.
- Krishnaray, C., Jagan, E.G., Ramachandran, R., Abirami, S.M., Naha, N. and Kalaichelvan, P.T. (2012). Effect of biologically synthesized silver nanoparticles

- on *Bacopa monnieri* (Linn.) Wettst. plant growth metabolism. **Process Biochemistry**. 47: 651 – 658.
- Khrishnaswamy, K., Vali, H. and Orsat, V. (2014). Value-adding to grape waste: Green synthesis of gold nanoparticles. **Journal of Food Engineering**. 142: 210 – 220.
- Kumar, K.P., Paul, W. and Sharma, C.P. (2011). Green synthesis of gold nanoparticles with *Zingiber officinale* extract: Characterization and blood compatability. **Process Biochemistry**. 46: 2007 – 2013.
- Kumar, V., Guleria, Kumar, V. and Vadar, S.K. (2013). Gold nanoparticle exposure induces growth and yield enhancement in *Arabidopsis thaliana*. **Science of the Total Environment**. 462: 462 – 468.
- Kumav, K.M., Mandal, B.K., Sinha, M. and Krishnakumar, V. (2012). *Terminalia chebula* mediated green synthesis of gold nanoparticles. **Spectrochimica Acta Part A: Molecular and Biomolecular Spectroscopy**. 86: 490 – 494.
- Lee, J., Chatterjee, D.V., Lee, M.H. and Krishnan, S. (2014). Gold nanoparticle in breast cancer treatment: Promise and potential pitfalls. **Cancer Letters**. 347(1): 46 – 53.
- Lewis, R., Gaffin D., Hoefnagels, M. and Parker, B. (1998). **Life**. (5th ed). The McGraw-Hill Companies, Inc.
- Li, H., Ye, X., Guo, X., Geng, Z. and Wang, Z. (2016). Effects of surface ligands on the uptake and transport of gold nanoparticles in rice and tomato. **Journal of Hazardous Material**. 314: 188 – 196.
- Liang, T. B., Yin, Q.S., Zhang, Y.L., Wang, B.L., Guo, W.M., Wang, J.W. and Xie, J.P. (2013). Effects of carbon nanoparticles application on growth, physiological

- characteristics and nutrient application in tobacco plants. **JFAE**. 11(3): 954 – 958.
- Lin, D. and Xing, B. (2007). Phytotoxicity of nanoparticles: inhibition of seed germination and root growth. **Environmental Pollution**. 150: 243 – 250.
- Lin, S., Rappert, J., Hu, Q., Hudson, J.S., Reid, M.L., Ratnikova, T.A., Rao, A.M., Luo, H. and Ke, P.C. (2009). Uptake, translocation and transmission of carbon nanomaterial in rice plants. **InterScience**. 5(10): 1128 – 1132.
- Lisiewska, Z., Kmiecik, W. and Korus, A. (2006). Content of vitamin C, carotenoids, chlorophylls and polyphenols in green parts of dill (*Anethum graveolens L.*) depending on plant height. **Journal of Food Composition and Analysis**. 19(3): 134 – 140.
- Ma, X., Geiser-Leo, J., Deng, Y. and Kolmakov, A. (2010). Interactions between engineered nanoparticles and plants: Phytotoxicity, uptake and accumulation. **Science of the Total Environment**. 408(16): 3053 – 3061.
- Ma, Y., Kuang, L., He, Y., Bai, W., Ding, Y., Zhang, Z., Zhao, Y. and Chai, Z. (2010). Effects of rare earth oxide nanoparticles on root elongation of plants. **Chemosphere**. 78(3): 273 – 279.
- Mahakham, W., Theerakulpisut, P., Maensiri, S., Phumying, S. and Sarmah, A.K. (2016). Environmentally benign synthesis of phytochemicals-capped gold nanoparticles as nanoprimer agent for promoting maize seed germination. **Science of Total Environment**. 537: 1089 – 1102.
- Mezer, M., Turska-Taraska, A., Kaczmarek, Z., Glowacka, K., Swarczewicz, B. and Rorat, T. (2014). Differential physiological and molecular response of barley genotypes to water deficit. **Plant Physiology and Biochemistry**. 80: 234 – 246.

- Moldenhauer, K., Wilson, C.E., Counce, J.P. and Hardke, J. (2013). Rice growth and development. Arkansas rice production handbook. **University of Arkansas Division of Agriculture**. 9 – 20.
- Mukherjee, S.P. and Choudhuri, M.A. (1983). Implication of water stress induced changes in the levels of endogenous ascorbic acid and hydrogen peroxide in *Vigna* seedling. **Physiology of Plant**. 58(2): 166 – 170.
- Nadaf, N.Y. and Kanase, S.S. (2016). Biosynthesis of gold nanoparticles by *Bacillus marisflavi* and its potential in catalytic dye reduction. **Arabian Journal of Chemistry**.
- Nair, P.M.G. and Chung, M. (2014). Physiological and molecular level effects of silver nanoparticles exposure in rice (*Oryza sativa L.*) seedlings. **Chemosphere**. 112: 105 – 113.
- Nair, R., Varghese, S. H., Nair, B. G., Maekawa, T., Yoshida, Y. and Kumar, D. K. (2010). Nanoparticulate material delivery to plants. **Plant Science**. 179(3): 154 – 163.
- Narayanan, K.B. and Sakthivel, N. (2010). Photosynthesis of gold nanoparticles using leaf extract of *Coleus amboinicus Lour.* **Material Characterization**. 61(11): 1232 – 1238.
- Narayanan, K.B. and Sakthivel, N. (2011). Green synthesis of biogenic metal nanoparticles by terrestrial and aquatic phototrophs and heterotrophic eukaryotes and biocompatible agent. **Advances in Colloid Interface Science**. 169(2): 59 – 79.
- Noruzi, M., Zare, D., Khoshnevisan, K. and Davoodi, D. (2011). Rapid green synthesis of gold nanoparticles using *Rosa hybrida* petal extract at room temperature.

International Journal of Bioscience, Biochemistry and Bioinformatics. 79(5): 1461 – 1465.

Patra, J.K., Kwon, Y. and Baek, K.H. (2016). Green biosynthesis of gold nanoparticles by onion peel extract: Synthesis, characterization, and biological activities. **Advance Powder Technology.**

Pettitt, M.E. and Lead, J.R. (2013). Minimum physicochemical characterization requirement for nanomaterial regulation. **Environmental International.** 52: 41 – 50.

Philip, D. (2009). Honey mediated synthesis of gold nanoparticles. **Spectrochimica Acta Part A: Molecular and Biomolecular Spectroscopy.** 73: 650 – 653.

Polato, N. (2013). **Introduction to Rice** [On-line]. Available: http://www.gramene.org/species/oryza/rice_illustrations.htm.

Qian, H., Peng, X., Han, X., Ren, J., Sun, L. and Fa, Z. (2013). Comparison of the toxicity of the silver nanoparticles and silver ions on the growth of terrestrial plant model *Arabidopsis thaliana*. **Journal of Environmental Science.** 25(9): 1947 – 1956.

Questa, K., Avalos-Borja, M. and Castro-Longoria, E. (2013) Biosynthesis and microscopic study of metallic nanoparticles. **Micron.** 55: 1 – 27.

Raghunandan, D., Bedre, M.D., Basavaraja, S., Sawle, B., Manjunath, S.Y. and Venkataraman, A. (2010). Rapid biosynthesis of irregular shaped gold nanoparticles from macerated aqueous extracellular dried clove buds (*Syzygium aromaticum*) solution. **Colloids and Surfaces B: Biointerfaces.** 79(1): 235 – 240.

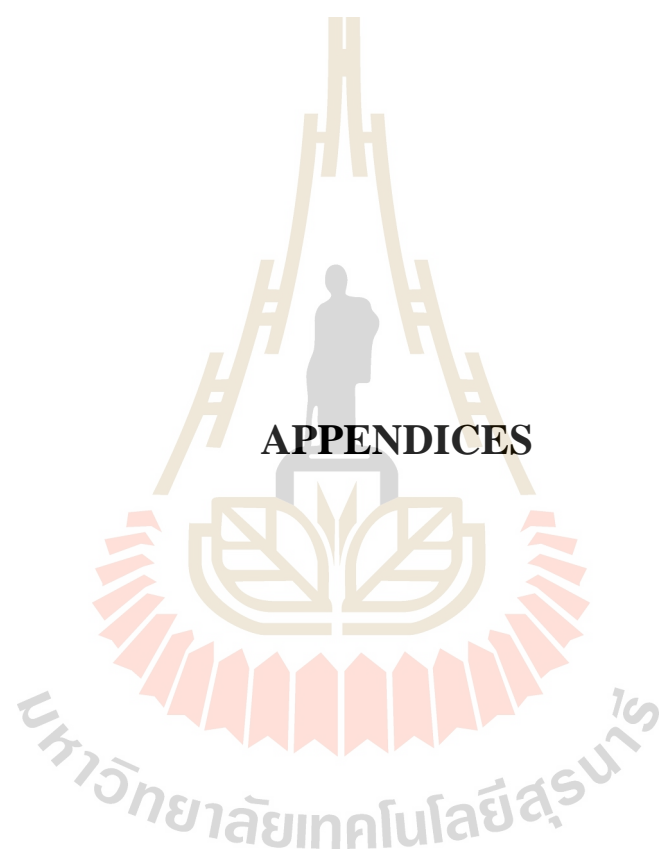
- Reidy, B., Haase, A., Luch, A., Dawson, K.A. and Lynch, I. (2013). Mechanism of silver nanoparticle release, transformation and toxicity: A critical review of current knowledge and recommendations for future studies and applications. **Materials**. 6: 2295 – 2350.
- Sajanlal, P.R., Sreepasad, T.S and Pradeep, T. (2011). Anisotropic nanomaterials: Structure, growth, assembly, and functions. **Nano Reviews**. 2: 5883.
- Shankar, S.S., Ahmad, A., Pasricha, R. and Sastry, M. (2003). Bioreduction of chloroaurate ions by geranium leaves and its endophytic fungus yields gold nanoparticles of different shapes. **Journal of Material Chemistry**. 13: 1822 – 1826.
- Shankar, S.S., Rai, A., Ahmad, A. and Sastry, M. (2004). Rapid synthesis of Au, Ag, and bimetallic Au core-Ag shell nanoparticles using Neem (*Azadirachta indica*) leaf broth. **Journal of Colloid and Interface Science**. 275(2): 496 – 502.
- Sharifi, S., Behzadi, S., Laurent, S., Forrest, M.L., Stroeve, P. and Mahmoudi, M. (2012). Toxicity of nanomaterials. **Chemical Society Reviews**. 14 (6): 2323 – 2343.
- Sharma, P., Jha, A.B., Dubey, R.S. and Pessarakli, M. (2012). Reactive oxygen species, oxidative damage, and antioxidant defense mechanism in plants under stressful Conditions. **Journal of Botany**.
- Sheoran, V., Sheoran, A.S. and Poonia, P. (2013). Phytomining of gold: A review. **Journal of Geochemical Exploration**. 128: 42 – 50.
- Silverstein, R.M. and Webster, F.X. (1998). **Spectrometric identification of organic compounds**. (6th ed.). John Wiley and Sons, Inc.

- Son, N.T., Chen, C.F., Chen, C.R. and Chang, L.Y. (2013). Satellite-based investigation of flood-affected rice cultivation areas in Chao Phraya River Delta, Thailand. **International Society for Photogrammetry and Remote Sensing**. 86: 77 – 88.
- Song, J.Y., Jang, H.K. and Kim, B.S. (2009). Biological synthesis of gold nanoparticles using *Magnolia kobus* and *Diospyros kaki* leaf extracts. **Process Biochemistry**. 44(10): 1113 – 1138.
- Sriket, P. (2014). Chemical components and antioxidant activities of Thai local vegetables. **KMITL Science and Technology Journal**. 14(1): 18 – 23.
- Sujitha, M.V. and Kannan, S. (2013). Green synthesis of gold nanoparticles using citrus fruits (*Citrus limon*, *C. reticulata* and *C. sinensis*) aqueous extract and its characterization. **Spectrochimica Acta Part A: Molecular and Biomolecular Spectroscopy**. 102: 15 – 23.
- Suman, T.Y., Rajasree, S.R.R., Ramkumar, R., Rajthilak, C. and Perumal, P. (2014). The green synthesis of gold nanoparticles using an aqueous root extract of *Morinda citrifolia* L. **Spectrochimica Acta Part A: Molecular and Biomolecular Spectroscopy**. 118: 11 – 16.
- Tangashu, B.V., Abdullah, S.R., Basri, H., Idris, M., Anuar, N. and Mukhlisin, M. (2011). A review on heavy metals (As, Pb, and Hg) uptake by plants through phytoremediation. **International Journal of Chemical Engineering**.
- Taylor, A.F., Rylott E.L., Anderson, C.W.N. and Bruce, N.C. (2014). Investigating the toxicity, uptake, nanoparticle formation and genetic response of plants to gold. **PLoS ONE**. 9(4): e93793.
- Transport of water and salts** (2011) [On-line]. Available: <http://www.desktopclass.com/>.

- Umer, A., Naveed, S. and Ramzan, N. (2012). Selection of a suitable method for the synthesis of copper nanoparticles. **Nano**. 07(05).
- Varma, R.S. (2012). Greener approach to nanomaterials and their sustainable applications. **Current Opinion in Chemical Engineering**. 1: 123 – 128.
- Villagarcia, H., Dervishi, E., Silva, K., Biris, A. and Khodakovskaya, M.V. (2012). Surface chemistry of carbon nanotubes impacts the growth and expression of water channel protein in tomato plants. **Small**. 8(15): 2328 – 2334.
- Wang, A., Ng, H.P., Xu, Y., Li, Y., Zheng, Y., Yu, J., Han, F., Peng, F. and Fu, L. (2014). Gold nanoparticles: synthesis, stability tests, and application for rice growth. **Journal of Nanomaterials**. doi:10.1155/2014/451232.
- Wang, M., Chen, L., Chen, S. and Ma, Y. (2012). Alleviation of cadmium-induced root growth inhibition in crop seedling by nanoparticles. **Ecotoxicology and Environmental Safety**. 79: 48 – 54.
- Wang, T.X., Xu, S.H. and Yang, F.X. (2012). Green synthesis of CuO nanoflakes from $\text{CuCO}_3 \cdot \text{Cu}(\text{OH})_2$ powder and H_2O_2 aqueous solution. **Powder Technology**. 228: 128 – 130.
- Zanado, D.I.L., Lima, R.B., Ferrarese, M.L.L., Bubna, G.A. and Ferrarese-Filho, O. (2009). Soybean root growth inhibition induced by p-coumaric acid. **Environmental and Experimental Botany**. 66: 25 – 30.
- Zayed, M.F. and Eisa, W.H. (2014). *Phoenix dactylifera* L. leaf extract photosynthesized gold nanoparticles, controlled synthesis and catalytic activity. **Spectrochimica Acta Part A: Molecular and Biomolecular Spectroscopy**. 121: 238 – 244.

Zuber, A., Purdey, M., Schartner, E., Forbes, C., Hoek, B., Giles, D., Abell, A., Monro, T. and Ebendorff-Heidepriem, H. (2016). Detection of gold nanoparticles with different sizes using absorption and fluorescence based method. **Sensors and Actuators B: Chemical**. 227: 117 – 127.





APPENDICES

APPENDIX A

CHEMICAL REAGENTS

A.1 Preparation of Aqua regia

Nitric acid 50 mL: Hydrochloric 150 mL

A.2 Preparation of *Tiliacora triandra* broth

5 g of blended *T. triandra* leaves in 100 mL of distilled water

A.3 Preparation of 1 L of 10mM Gold (III) chloride trihydrate

3.9383 g of the gold substrate in 1 L of distilled water

A.4 Preparation of 100 mL of 2.5% sodium hypochlorite

20 mL of 12% w/v NaClO₂ in 80 mL of distilled water

A.5 Preparation of different concentrations of nano-gold (AuNP) suspensions

10 mg/L	0.0005 g
100 mg/L	0.005 g
500 mg/L	0.025 g
1000 mg/L	0.05 g
2000 mg/L	0.10 g

Preparation: Dissolve respective amounts in 50 mL of distilled water and ultra-sonicate for 45 minutes.

A.6 Preparation of 0.25% Evans blue

0.25 g of Evans blue powder in 100 mL in distilled water

A.7 Chemicals for MDA extraction

5% (w/v) Trichloroacetic acid (TCA) 5 g

0.67% (w/v) Thiobarbituric acid (TBA) 0.67 g

Preparation: Dissolve 5 g of TCA and 0.67 g of TBA in distilled water and make up to respective volumes of 100 mL each.

A.8 Chemicals for hydrogen peroxide extraction

0.1% (w/v) TCA 0.1 g

Preparation: Dissolve 0.1 g of TCA in distilled water and make up volume to 100 mL.

10 mM K-phosphate buffer (pH 7.0)

K_2HPO_4 0.348 g

KH_2PO_4 0.272 g

Preparation: Dissolve K_2HPO_4 and KH_2PO_4 in distilled water and make up to a volume of 200 mL.

1 M Potassium iodide (KI)

KI 33.20 g

Preparation: Dissolve KI in distilled water and make up to a volume of 200 mL.

APPENDIX B

CALIBRATION CURVE

B.1 Standard curve of Hydrogen peroxide (H₂O₂)

Prepare hydrogen peroxide standards by diluting down (10^{-2}) 10 $\mu\text{g/mL}$ of the stock with distilled water. The 10 $\mu\text{g/mL}$ stock was prepared by adding 0.8 μL of H₂O₂ to 24.9992 mL of distilled water.

Table B.1 Preparation of hydrogen peroxide standards.

H ₂ O ₂ concentration ($\mu\text{g/mL}$)	Dilution Factor	Distilled water (μL)
0.1	10^{-2}	990
1×10^{-3}	10^{-4}	990
1×10^{-5}	10^{-6}	990
1×10^{-7}	10^{-8}	990
1×10^{-9}	10^{-10}	990
1×10^{-11}	10^{-12}	990
1×10^{-13}	10^{-14}	990
1×10^{-15}	10^{-16}	990
1×10^{-17}	10^{-18}	990
1×10^{-19}	10^{-20}	990
1×10^{-21}	10^{-22}	990

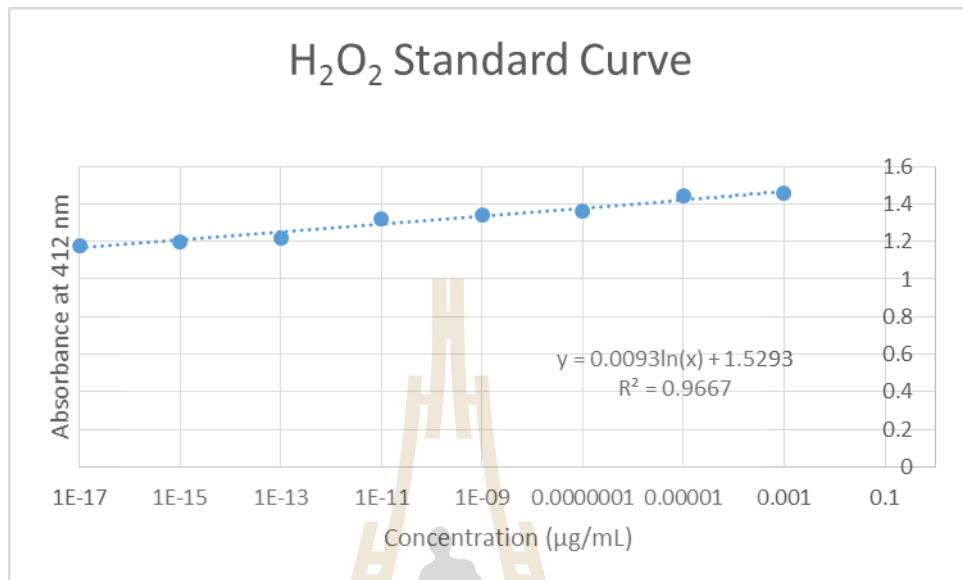


Figure B.2 Standard curve of hydrogen peroxide content.

APPENDIX C

STATISTICAL DATA

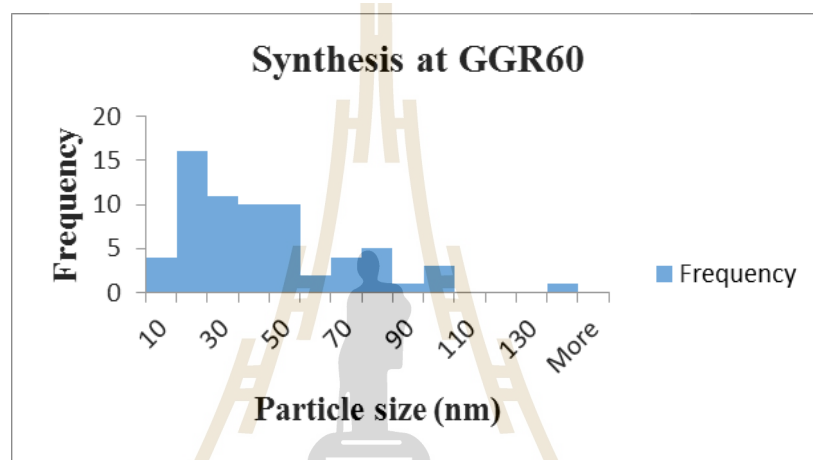


Figure C.1 Size distribution histogram of gelatin-glucose synthesized AuNP at 60°C.

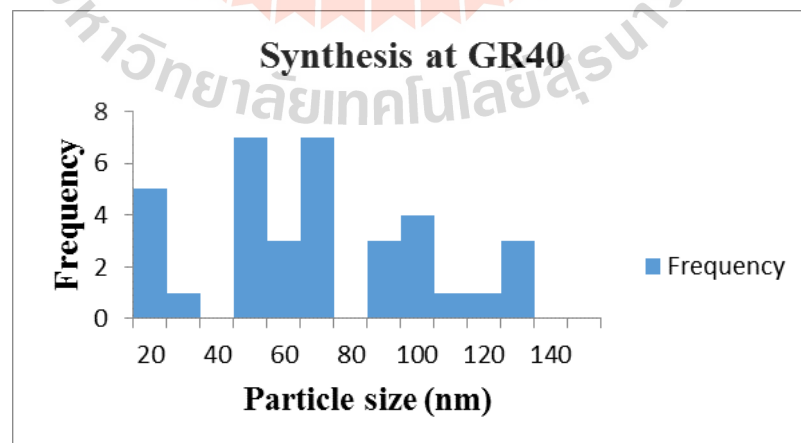


Figure C.2 Size distribution histogram of gelatin synthesized AuNP at 40°C.

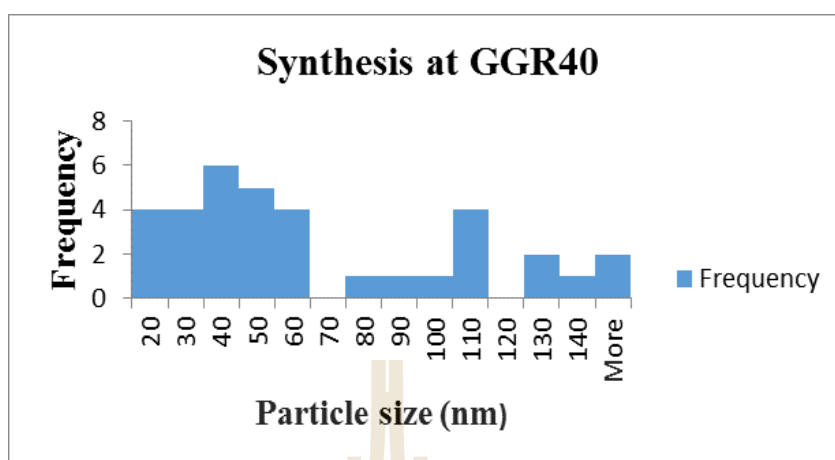


Figure C.3 Size distribution histogram of gelatin-glucose synthesized AuNP at 40°C.

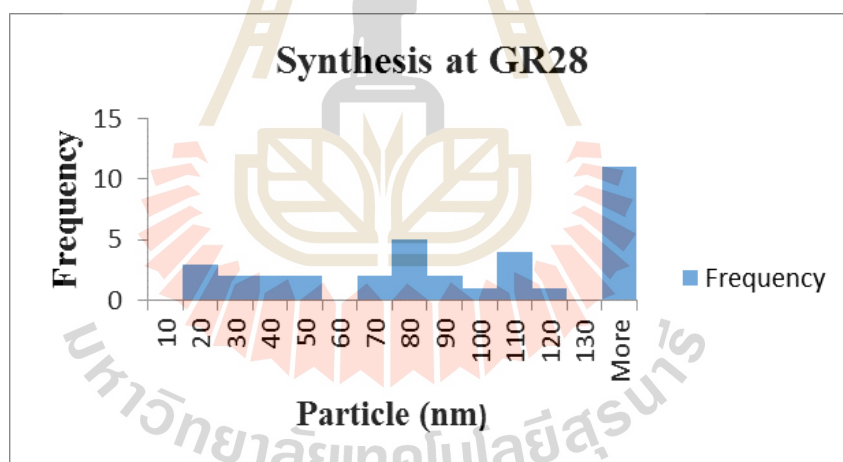


Figure C.4 Size distribution histogram of gelatin synthesized AuNP at 28°C.

Table C.1 Relative water content of rice seedlings exposed to AuNPs at different concentrations.

AuNP concentration (mg/L)	Relative water content (%)
Ctrl	64.98±1.32a
10	73.13±9.12a
100	69.33±5.67a
500	79.90±15.86a
1000	72.01±8.00a

Values are means \pm SD (n=3). Means with the same letter are not significantly different at Tukey's test ($p \leq 0.05$).

Table C.2 Cell viability of rice roots of grains exposed to AuNPs at different concentrations expressed in terms of absorbance ratio.

AuNP concentration (mg/L)	Absorbance ratio
0	1.0±0.0a
10	1.31±0.41a
100	1.30±0.39a
500	1.61±0.34a
1000	1.85±0.42a

Values are means ± SD (n=3). Means with the same letter are not significantly different at Tukey's test ($p \leq 0.05$).

Table C.3 Cell viability of rice roots grains exposed to AuNPs at a concentration of 2000 mg/L under different treatment conditions (A, B, C).

AuNP concentration (mg/L)	Absorbance ratio
Ctrl	1±0.0a
A	1.07±0.09a
B	1.10±0.07a
C	0.97±0.06a

Values are means ± SD (n=3). Means with the same letter are not significantly different at Tukey's test ($p \leq 0.05$).

